Simulating electromigration in atomic contacts

Dissertation submitted for the degree of
Doctor of Natural Science
(Doctor rerum naturalis)

Presented by

Markus Ring

at the

University of Konstanz

Faculty of Sciences

Department of Physics

Konstanz, 2019

Date of the oral examination: 13.12.2019
First referee: Prof. Dr. Peter Nielaba
Second referee: Prof. Dr. Fabian Pauly

Zusammenfassung

Elektromigration und strominduzierte Phänomene umfassen ein weites Feld - angefangen bei der praktischen Frage nach der Stabilität von elektrischen Kontakten und Bauteilen auf alltäglicher Größenskala, bis hinunter zu den Eigenschaften nanoskopischer Konstrukte [1]. Diese breite Palette an Skalen und Anwendungen spiegelt sich auch in den theoretischen Ansätzen wider: Einfache Ingenieurstabellen führen zu komplizierten kontinuierlichen Flussfeld-Modellen [2] und schlussendlich kommen quantenmechanische Eigenschaften der Materie und des Stroms auf nano- und atomaren Skalen hinzu [3].
Diese Arbeit gibt einen Überblick über dieses Thema mit einem starken Fokus auf Modellierung und Simulation von Kontaken auf atomarer Größenordnung. Das Studienobjekt sind dabei metallische Kontakte bestehend aus einigen dutzend Atomen gekoppelt an kristalline Zuleitungen und ihr Verhalten unter Stromfluss. Dieses Modell beinhaltet bereits eine Vielfalt möglicher atomarer Strukturen und Vielteilchen-Elektronen-Wellenfunktionen, sowie die Interaktionen dieser beiden Systeme. Nur im Zusammenspiel all dieser Systeme ergeben sich strominduzierte Strukturänderungen.
Die atomaren Kontakte werden modelliert durch Molekulardynamik (MD) und Dichtefunktionaltheorie (DFT) für die elektronische Struktur und die Elektron-Atom-Interaktion [4]. Die Transporteigenschaften dieser Systeme werden durch Nichtgleichgewichts-Greenfunktionen untersucht. Zu diesen Transporteigenschaften gehören strominduzierte Kräfte auf die Atome, deren Herleitung vorgestellt wird [5, 6]. Diese Kräfte lassen sich in eine Langevin-Gleichung für die Atome zusammenfassen [7], deren Dynamik und Kinetik ebenfalls untersucht wird.
Dadurch werden zwei Mechanismen identifiziert, die zu einem strominduzierten Schalten der Struktur des Kontaktes führen können: zum einen einer Grenzspannung, bei welcher der Strom eine atomare Schwingungsmode destabilisiert, und zum anderen eine effektive Aufheizung durch Streuung der Elektronen.
Diese Modellierung und Konzepte werden an einer Vielzahl von atomaren Kontakten der Metalle Gold (Au), Blei (Pb) und Aluminium (Al) untersucht. Dabei werden experimentelle Werte für elektrische Transmission und Vibrationsspektren gut reproduziert [8]. Die berechneten Grenzspannungen zeigen starke Streuungen, befinden sich allerdings in ähnlichen Bereichen wie experimentelle Schaltspannungen mit sehr guter Vergleichbarkeit für Bleikontakte und Goldkontakte mit kleinem Leitwert.
Schließlich werden die anisotropen Anregungsmoden der Langevin-Gleichung genutzt, um nach weiteren stabilen Kontaktkonfigurationen zu suchen - ein erster Ansatz um strominduziertes Schalten direkt für die Simulation zu nutzen. Damit gibt es jetzt die Möglichkeit elektromigrierte Strukturen in Simulationen zu untersuchen.

Abstract

The topic of electromigration and current-induced dynamics spans a wide field - starting with the practical consideration of contact and circuit stability from everyday appliances down to nano-scale constructs [1]. The theoretical approaches to this problem are similarly diverse. Simple engineering models turn into more complicated continuum flow models [2] and finally it comes down to quantum-mechanical properties of matter and current at the nano- and atomistic scale [3].
This work provides an overview of the topic with a strong focus on the modelling and simulation on the atomistic scale. The framework of this thesis is a metallic contact consisting of several dozen atoms coupled to a crystalline bulk reservoir. This model already provides a complex testbed. There are a multitude of possible atomic structures this contact can take, which is only exacerbated by the addition of electronic degrees of freedom and their interaction with the atomic structure. Current-induced dynamics appear only through the complex interplay of all these systems.
The contacts are investigated with state of the art methods like molecular dynamics (MD) and density functional theory (DFT) for the atomic and electronic structure and their interaction [4]. All of these properties under current are investigated perturbatively with nonequilibrium Green's function methods [3]. Among those properties are current-induced forces [5, 6], whose derivation will be presented. Those forces are modeled in a Langevin equation for the atoms [7], whose dynamics and kinetics are investigated.

First the topic of electromigration will be introduced. The current state of the art in modeling atomic contacts and charge transport will be presented with a special focus on the methods used throughout the thesis, like modeling in DFT and MD as well as nonequilibrium Green's functions (NEGF).

The second chapter will present the models used for the interaction of electrons and atoms and the simulation methods used. Specifically, the current-induced forces acting on the atoms will be derived, their implementation shown, and the resulting Langevin equation will be discussed. Here, we identify two mechanisms possibly leading to a switching of the contact: A runaway voltage at which the system turns unstable in the presence of non-equilibrium transport, and secondly, random impulses from scattered electrons increasing the effective temperature of certain parts of the atomic system.

In the third chapter the simulations applying those models on a sampling of metallic atomic contacts will be presented, and the results investigating three metals (Pb, Au, Al) will be discussed. The calculated runaway voltages are in experimentally relevant ranges [8], indicating that this mechanism has to be at least considered with special relevance for lead and small conductance gold

contacts.

In the foruth and final chapter the Langevin calculation is used to search and find additional stable conductance states - a first approach to simulate current-induced switching extending the possibilities of the simulation to investigate electromigrated structures in addition to the mechanically controlled structures [9, 10] used before.

Contents

Chapter 1

Introduction

Electromigration is the change of a current-carrying structure or contact in response to the electrical current flowing through it. This first chapter serves as an introduction to the topic before the later chapters go in depth into the specific theory and simulations done.

The first section explains the motivation and the current state of the art in experimental investigations and simulations of atomic contacts. In the second section the classical, macroscopic picture of electromigration is presented with a first, more theoretical, introduction to switching phenomena. In the second section the modelling of contacts is presented with short introductions to Density Functional Theory and Molecular Dynamics. In the third section the nonequilibrium Green's function formalism is presented. along with its usage in describing transport processes as scattering events of theoretically arbitrary complexity.

1.1 Motivation

Electromigration has important technological aspects. For one it limits the stability of electronic circuitry and every electronic part has a maximum current it can take[11, 12]. Dealing with this led to the introduction of maximal allowed currents in applications. Circuit breakers and fuses are examples of using electromigration processes for specific purposes.
Understanding the basics of electromigration may allow one to use these processes for other means[1]: To save data [13], maybe to control or to switch[14].

Simulations in the last decades showed the exploration of the transport side - allowing the calculation of electronic transport properties from atomic structures [15] using nonequilibrium Green's function methods [3]. Including the influence of the atomic system on the transport has been the next step in this process [4, 16]. Much progress has been made extending this formalism from electrons to phonons [17, 18].
These simulations are all based on largely static atomic structures with only small deviations treated as perturbation to approximate ground states. The back-action of the electronic transport on the atomic structure proved to be more difficult, for at least two reasons:
The time scale separation of electronic and atomic degrees of freedom. Elec-

tronic dynamics resolve in times of atto- to femtoseconds, while atoms move in pico- to nanoseconds. This separation of at least a factor of 1000 means that one would need to do a prohibitive amount of electronic simulation to get a trajectory.
Secondly, the farther one moves from well separated, local ground states, the worse the used simulation methods become. Especially the Density Functional Theory method mainly used in this thesis is an explicit ground state calculation and any perturbation relies intrinsically on these ground state assumptions for all of its statements.

1.1.1 State of the art

In the last two decades much progress has been made in describing the transport of electrons through structures on atomic and molecular scales [3]. Here the electrons are assumed to move through a fixed atomic structure and the effect of the interaction between electrons and atoms has mostly been dealt with in respect to the change of that electron transport.

To describe electromigration it is necessary to have a theoretical description of the non-equilibrium electrons impacting the atomic structure. The classical picture sees them as a liquid-like bath, whose effect can be subsumed in the known quantities of friction and random forces with the associated Einstein- or fluctuation-dissipation relation connecting the two. From this picture emerges the classical description of electromigration as thermally-activated and current-density driven [2]. This is also the basis for the classical Joule heating of the mechanical system in response to an electronic system out of equilibrium.

Several of these assumptions were challenged with the discovery of non-conservative forces in the theoretical description of atomistic systems [19]. The current induces anti-symmetric terms in the dynamical matrix under bias voltage, which gives rise to forces that can not be integrated into a potential. This led to a waterwheel picture of atomic motion under current, where an atom oscillates in and out of an electron flow, gaining energy through the scattering of the electrons. In the waterwheel picture the wind-force couples more strongly to some of the few modes, resulting in an anisotropy of the dynamics and a mode-specific kinetic energy - decidedly non-equilibrium properties, which are not well described by a uniform temperature and assorted sampling methods.

This picture was further extended by anti-symmetric terms for the friction matrix, due to the Berry-Phase [5]. This paper also introduced a runaway-voltage to that model, where the damping of a specific mode changes its sign, destabilizing the mode in the long run. Under a bias voltage both the dynamical matrix as well as the friction tensor exhibit anti-symmetries and therefore anisotropy of the force and friction, which can be expressed in an effective temperature or excess kinetic energy that is different for different modes [20], depending on how they couple to the electronic motion and to the larger atomic structure.

Simulating the semi-classical generalized Langevin equation [7] underlying this view on the system poses several challenges. As a classical equation it can not reproduce some fundamental quantum-mechanical properties, like quantization and entanglement, while other properties can be approached through appropriate choices of parameters. A suitable choice for the noise terms can re-

produce some of the probability-density nature and uncertainty of the particles and the tunneling effects [7]. Some classical assumption going into the Langevin equation will also naturally fail - the fluctuation-dissipation theorem relating the random force with friction is not valid. Additionally the time scales are below the typical over-dampened approximation, such that ballistic properties have to be taken into account.

Both quantum-mechanical and ballistic effects are stronger for lighter particles. The tunneling probabilities go up, the wavefunctions have greater extent and the trajectories of the lighter particles move further on the same time scale. All of those can act to switch a contact before the runaway-voltage is reached, especially if the electron-vibration coupling is strong, which allows easy pumping of energy into the system, directly increasing the effective temperature.

1.2 Electric contacts

In contrast to normal electronics, where the electric current - the electrons flowing through a system - is determined by the structuring of the system, electromigration is the reverse of that: Electronic current affecting and maybe even changing the structures of the structures of the atomic nuclei.

The atomic contact is the smallest envisionable part of an electronic circuit, consisting of only few atoms with the electrons around them. Far from making the description simpler, this setup emphasizes all the properties that have been integrated out in the many-particle, thermodynamic limit of mesoscopic or even macroscopic circuits. Examples of this are the quantization of the electronic current into single electrons and their transmission channels [21–23]. The concept of conductance G is saved by the Landauer formula [24]

$$G = \mathrm{G}_0 \sum_i \tau_i$$

coupling the macroscopic conductance to the sum of quantized conductance channels with the transmission τ_i and the conductance quantum G_0 [3].
The concept of resistance as an inverse conductance is not valid here. Macroscopic resistance subsumes charge and heat transport and the associated thermalization between systems. In atomic contacts these properties are divided into single scattering events where electrons are scattered back, or transfer energy and momentum to other parts of the system, e.g. into the atomic motion. Similarly the thermodynamic concepts of heat and temperature, which rely on the thermodynamic limit of large ensembles, lose definiteness as well as some properties going together with that, like uniformity and isotropy. Instead of being able to describe one large system with collective properties, in the description of atomic contacts, it turns out to be necessary to describe the interactions of many systems.

These descriptions of the smaller systems are accomplished in simulations. There the individual parts of the atomic contacts, the atoms and the electrons, as well as their interactions are described. The nonequilibrium Green's function methods can then couple those systems perturbatively to reservoirs - sources of charge and energy - of known or calculable properties.

1.2.1 Classical picture

The classical picture of a general contact is often subsumed into Ohm's law

$$V = RI \ .$$

A potential difference V between two areas of a contact leads to a proportional current I, a flow of charge, between those points. Here the resistance R serves as a proportionality constant between current and voltage. The inverse of the resistance is called the conductance $G = R^{-1}$.
This description can be broken down into or derived from electrostatic Maxwell's equation for the charge-density ρ

$$\nabla \mathbf{E} = \frac{\rho}{\epsilon_0}, \quad \mathbf{J} + \epsilon_0 \dot{\mathbf{E}} = 0 \ .$$

Integrating the current density $\mathbf{J}$ over space yields the current I and path integration of the electrical field $\mathbf{E}$ results in the potential difference $V = \int E$. Together these give rise to Ohm's law in the continuous case, coupling the current density with the electrical field through a material-dependent resistivity σ

$$\mathbf{J} = \sigma \mathbf{E} \ .$$

These descriptions break down in the modern picture as described in the following. The continuity of the Maxwell description gives way to the atomic structure of atoms and electrons. Apart from that breakdown of the continuous picture, at least the electrons are also quantized on the scales observed, giving rise to such things as coherent transport, conductance quantization and quantum interference [3].

Discussion

The classical picture of macroscopic electromigration uses tabulated current densities for different materials as indicators for their stability under current. It is doubtful that this also provides a valid criterion at the atomic limit, since the current density as Ampere per area is not that well defined there. Indeed the electron current is split off into conductance channels with their own transmission. Even the simple picture of a cross-section falls apart at the single-atom limit, since the conductance channel have the volume of the underlying wave functions. Not to forget that the contribution of bulk atoms to the structure falls off sharply against the contribution of atoms on the surface of the material.

In the classical picture the energy put into a contact is proportional to the product of the number of charge carriers moving through the contact and their energy $P = I \cdot V$. This equation assumes a full thermalization of that energy, which is valid in macroscopic contacts, but fails in the atomic limit for two reasons. First, one is far from system sizes allowing thermodynamic arguments like temperature for anything but the reservoirs for which it is assumed. Second, the small sizes also mean that most of the transport happens coherently, without the charge carriers scattering or dissipating their energy. So in the atomic limit current density and temperature are difficult concepts to use for electromigration itself.

Direct force and electron wind

From the simple picture of electrons flowing through a crystal of positively charged ions due to an applied voltage, two considerations emerge naturally: One is the direct force of the electrical field acting on the ions; the other is the wind force of the electrons due to them scattering on the atoms. In metals the direct force is often negligible, the electrons are shielding the external field within few nano-meters through surface charges, or more precisely surface polarisation. The field may be much more important in contacts with lower mobile charge density like molecules and tunnel contacts.
The wind force is a more complicated concept in both direction and extent. Since it comes from scattering events its direction is dependent on the charge carriers of the system[1]. These scatterings events are difficult to express as an potential with a fixed energy transfer per distance, instead energy and momentum exchange have to be treated individually and, in the atomistic limit, stochastically. The momentum cannot be transferred that easily into the crystalline lattice of atoms. Even if a direct scattering happens, the moving atom will rebound at the crystalline structure of the other atoms - only part of the momentum and energy transferred stays in the atom, most of it is emitted into the crystal and dissipates, heating up the conducting material. Overall the wind force can add a preferred direction to the electromigration, but the switching process itself is often determined by the directionless energy transfer working on the existing anisotropy of the system.

Structure changes

The effects of electromigration tend to happen at defects and surfaces. In bulk the anharmonic terms of the interatomic forces stabilize the crystalline configuration. This does not necessarily happen at defects and surfaces: A missing atom allows another atom to move in there and movement at the surface is not restricted by the atoms in their crystal. On surfaces the difference between bulk and vacuum or air itself adds an anisotropy to the system that is used in the exploration of the phase space.

Since atomic contacts consist mainly of surface, the typical melting point approach to structure stability also fails. Each atom on the surface has its own barriers for movement and kinetic energy under current, both of which make electromigration in atomic contacts very localized effects.

Early macroscopic investigation of electromigration deals mainly with the electromigration of adatoms on a conductor. Nowadays experiments can resolve structures on atomistic scales [25], although they are often limited to the visible surface. This leads to interesting new questions and options for theory and simulations:

The microscopic atomic and quantized nature of the contacts exhibit properties not possible from the macroscopic description, which require advances and new approaches in the theoretical treatment.

And the small structures allow a treatment with existing atomistic simulation methods, allowing a construction and investigation of those contacts in computers.

Both of these are approached in this thesis.

[1] electrons for metals, electrons and holes in semi-conductors, ions in conducting liquids.

1.2.2 Modern picture

The more modern picture of the electrical contact formulates it as a quantum-mechanical problem based on the Schrödinger equation with a Hamiltonian describing the interacting electrons e and atoms a as:

$$H = H_e + H_a + H_{e-a} \tag{1.1}$$

$$= \sum_i \frac{p_i^2}{2m_e} + \sum_{ij} V_{e-e}(i,j) + \sum_\alpha \frac{p_\alpha^2}{2m_\alpha} + \sum_{\alpha,\beta} V_{a-a}(\alpha,\beta) + \sum_{i,\alpha} V_{e-a}(i,\alpha) \tag{1.2}$$

with the indices i, j and α, β denoting the individual electrons and atoms respectively. The momentum of the electrons and atoms are p_i and p_α, their masses m_e and m_α and their interaction potentials V_{e-e}, V_{a-a} and V_{a-e}. In that formulation the atom-atom interaction V_{a-a} is shielded and mediated by the electrons, so it is often subsumed into the electron-atom interaction V_{a-e}. Any motion of the atoms is often neglected, removing the kinetic part of the atoms and viewing only the electronic Hamiltonian H_e in the potential given by the fixed atom positions $V_e(\alpha)$. This is one step of the Born-Oppenheimer approximation discussed in the next paragraph.

The electronic Hamiltonian H_e is considered more difficult than the atomic potential due to its many-particle nature. In particular the problem is the V_{e-e} - the interaction of the electrons. Since electrons are fermions, it is impossible for two of them to occupy the same state. This means that instead of looking at the lowest energy states, one needs to fill up the Fermi sea; so one has to take into account at least as many states as there are electrons in the system. This is approximated in the exchange functional of density functional theory.

In contrast to atoms, which may be treated as classical particles, the electron mass is so small that they can tunnel easily and have an extended wave function - indeed identifying electrons as particles and waves at the same time is one of the founding experimental proofs of quantum mechanics.

Born-Oppenheimer approximation The Born-Oppenheimer approximation states a full time scale separation of the fast electronic and slow atomic system. In this approximation the electrons react instantly to any changes in the atomic positions and see the atoms as stationary. The atoms on the other hand only interact with a time average of the electrons in form of a electron probability distribution - an averaged electron density $\rho_e(\vec{r})$ over the space $\vec{r}$.

$$H_e = \sum_i \frac{p_i^2}{2m_e} + \sum_{ij} V_{e-e}(i,j) + V_e(\alpha) \tag{1.3}$$

$$H_a = \sum_\alpha \frac{p_\alpha^2}{2m_\alpha} + \sum_{\alpha,\beta} V_{a-a}(\alpha,\beta) + V_a(\rho_e) \tag{1.4}$$

The Born-Oppenheimer approximation allows a separation of the Hamiltonian into an electronic and atomic or ionic part. For the dynamics of the atomic part the electrons are integrated out as a bath with certain properties. The electronic part on the other hand sees the atom positions as fixed and is assumed to be

determined through its minimal energy configuration.

There are obvious limits of that approximation. One example is fast atomic movement as it happens in structure changes, where the electrons may need some time to relax back to their bath nature. This has to be considered especially if it appears together with correlation effects, where the electrons and phonons are coupled very strongly. Even with the time scale separations, some phenomena may not be well represented in the Born-Oppenheimer approximation, e.g. in systems with strong spin-orbit coupling, plasmons or superconductivity.
And of course there are the errors in the separate descriptions of the electronic and atomic system and their interactions, all of which are often perturbative. One example are the perturbative expansions done on the electronic ground state. While the uniqueness of the electronic ground state may be guaranteed, its relevance in comparison to other, excited states, especially with respect to quantum fluctuations or decoherence (coupling to some external system), are not included in most simulational approaches.

There are many cases where the Born-Oppenheimer approximation is not quite valid, nevertheless it provides a good first step, especially when the atomic structure of the contact is more or less constant over longer times. Electromigration itself is a switching process of the atomic system. The switching process itself is the only one where the time scale of the atomic movement can be "visible" to the electrons. So the Born-Oppenheimer states can be developed perturbatively to find conditions and situations where those states are left, after which the approximation is no longer valid.

Ehrenfest dynamics For the atomic system there is the question, which description - quantum-mechanical or classical - is most suitable. While the quantum-mechanical description is the more fundamental description, the classical description has the advantage of being more tractable in calculations - instead of continuous wave functions, one can just integrate differential equations for a finite, discrete number of coordinates describing the state of the system. The Ehrenfest theorem relates the time development of the mean of quantum mechanical position $\hat{x}$ and momentum operators $\hat{p}$ of a particle with mass m to the classical Liouville description with position $x = \langle \hat{x} \rangle$, momentum $p = \langle \hat{p} \rangle$ and potentials $V(x) = \langle V(\hat{x}) \rangle$:

$$m \frac{d}{dt} \langle \hat{x} \rangle = \langle \hat{p} \rangle \, , \; \frac{d}{dt} \langle \hat{p} \rangle = - \langle V'(\hat{x}) \rangle \; .$$

The Ehrenfest theorem is an application of the of the quantum-mechanical commutator relations

$$\frac{d}{dt} \langle A \rangle = \frac{1}{i\hbar} \langle [A, H] \rangle + \langle \frac{\partial A}{\partial t} \rangle \; .$$

The Ehrenfest dynamics are exact for cases where the potential is at most quadratic. The difference between the fully quantum-mechanical and classical description comes down to how well the mean describes the whole system. This is itself related to the quantum-mechanical uncertainty

$$\langle \Delta A \Delta B \rangle \geq \frac{1}{2} \left| \langle [A, B] \rangle \right| \; .$$

For the description with classical mechanics the relevant operators are $A = x$ and $B = p$ and their commutator is $i\hbar$. Since the variation of the momentum still has the mass m multiplied with it and the right side is constant, the quantum-mechanical uncertainty of a particle position and velocity $\dot{x} = p/m$ behaves like an inverse of the mass

$$\begin{aligned} \langle \Delta x \Delta p \rangle &= m \langle \Delta x \Delta \dot{x} \rangle \\ \Rightarrow \langle \Delta x \Delta \dot{x} \rangle &\geq \frac{\hbar}{2m} . \end{aligned}$$

The error one makes with describing the state of massive particles classically with position and velocity drops inversely with the mass. This makes the speed-up of the classical description well worth exploring, especially for systems of many particles, which are not tractable in quantum-mechanical approaches.

1.3 Contact modeling

The potential energy surface in the high-dimensional phase space is one of the central concepts of theoretical solid state physics. Most methods only manage to sample small regions around explicit minima in that surface. From those minima perturbative explorations of the surrounding phase space are started. The minima found depend on the method applied.

Investigating the changes in atomic structure in response to an electronic current requires a description of the non-equilibrium electrons and their coupling to the atoms and their movement. The movement of the atoms can also be described in a quantized picture, in terms of phonons. However, this is only applicable in the harmonic limit for small displacement from a resting position. This approximation is the starting point of the description of the atomic system with a special interest in its breakdown.
So there are three perturbative approaches stacked on top of each other:

- Perturbative coupling of the electron system to non-equilibrium baths using the nonequilibrium Greens function method.
- The approximations of phonons as a valid description in the phase space.
- The perturbative coupling between the electrons and the phonons.

All three of these approaches are investigated in a weak coupling regime, assuming those couplings remain small and their changes tractable with perturbative methods.

1.3.1 Electrons

Electrons are the charge carriers in most solid-state conductors and every single one investigated in this thesis.

Electrons are fermions, so no two electrons can occupy the same state. Together with their small mass, this means that in conductors electrons have large-scale quantum-mechanical properties - instead of localized space positions[2] their wave function is distributed over comparatively large volumes of the conductor.

[2] Those exist for the electrons in the extended core potential.

The electrons fill up their available energy states until there are no more electrons to distribute. Their probability distribution which gives the occupation of the different energy states is the Fermi-distribution

$$n_{\mathrm{F}}(\epsilon) = \frac{1}{\exp(\frac{\epsilon-\mu}{k_B T}) + 1}$$

where ϵ is the energy of the state, μ is the chemical potential or the energy one needs to add one more electron to the system. For fermions this energy is often called the Fermi-energy E_F, which is often considerably larger than the thermal energy scale $k_B T$. In typical metals the Fermi temperature E_F/k_B is at several thousand Kelvin, far beyond the scales in which the atoms remain in a crystalline structure.
Temperature softens the Fermi step function. This has interesting properties for transport and scattering effects, but in comparison to applied bias voltages in ranges of up to several volts[3] the temperature of the electronic system is of reduced importance.

1.3.2 Atoms

The classical description of the system is given in terms of positions x and velocities $\dot{x}$ as well as interactions mediated between the different coordinates often codified in potentials $V(x)$. The study of such systems is much of classical physics and has been codified in the Liouville description of analytic mechanics. A very common, equivalent version are Newton equations for forces $F = m\ddot{x}$ acting on coordinates. These second order differential equations describe many systems well and a standard example is

$$m\ddot{x} = -\frac{dV(x)}{dx}.$$

This can be extended to a 3D-many body description, by reintroducing the indices α, β denoting combined atom number and space dimension, e.g. $\alpha = n, x$ for the x-direction of atom n. The potential will in this case depend on on the position of all atoms $V(x_\alpha)$. System states where there is no force acting are interesting candidates for investigation, since those states have a change to be stable. If the forces can be integrated to a potential, such stable states are minima of the potential energy. Around such a minimum x_0 in that potential a harmonic approximation of the potential is possible $V(x) = k/2\ (x - x_0)^2$ with the full description being

$$m\ddot{x} = -k(x - x_0), \quad H = \frac{p^2}{2m} + \frac{k}{2}x^2\ .$$

The solutions to such harmonic systems are periodic trajectories or vibrations. The quantizations of such vibrations are commonly called phonons.

1.3.3 System interactions

This section presents some methods to describe interacting systems with a special focus of the interaction between the electronic and the atomic system as well

[3] For comparison the energy scale of room temperature is $k_B \times 300\,\mathrm{K} \approx 25\,\mathrm{meV}$.

as the theory used to describe the transport processes. The transport processes are described through scattering processes between electronic states in the lead and contact region. The important system properties of those regions are the distribution of electronic states, Fermi sea, scattering processes and their rates in the contact region.

As already discussed for the Born-Oppenheimer approximation, the time scales of the electrons are much faster than the time scale of the atomic motion, this lends itself to a view of the atomic motion being in a "bath" of electrons. The scattering between those electrons and the atoms gives rise to heating and cooling - thermalization - of the atomic system and hence to the electrical resistance of the material.

Langevin equation

The Langevin equation is a stochastic differential equation capable of describing many processes [7]. In a general form it is an equation for the acceleration of some state coordinate x of a system

$$m\ddot{x} = -\partial_x V(x) - \gamma\dot{x} + f \ ,$$

connecting this state coordinate with its effective mass m to a potential $V(x)$. The additions to the normal Liouville mechanics are the friction terms $\gamma\dot{x}$ and the random force f - those make the system non-deterministic and dissipative by connecting it to some heat bath. This is codified in a fluctuation-dissipation relation relating the force-force autocorrelation with the dissipation γ and the temperature of the system creating the noise

$$\langle f(t)f(t')\rangle = k_B T\gamma\delta(t-t') \ .$$

One of the basic ideas of this thesis is using the Langevin equation to describe the atomic motion by integrating over the electronic system. Here the coupling of the atomic and electronic system is subsumed into the friction term pumping energy in or out of the atomic system depending on its sign[4] together with a random force term taking into account the fundamental stochasticity of the process.

This is similar to the hydrodynamic picture of colloidal particles in a flow. Nonetheless, there are fundamental differences through the quantum-mechanical nature of at least one system with mainly two effects: Quantization far away from the thermodynamic limit and fundamental stochasticity of the scattering process due to the probabilistic nature of the wave function. The electric current is quantized. Since the stochasticity does not come from a large scale limit it has not necessarily the same stochastic properties as gaussian noise - it does not need to be white noise, but can be colored with frequencies specific to the system under investigation.

Adding a coupling to electron baths out of equilibrium poses an interesting extension. The response of the system can be formulated in linear response theory, which adds the nonequilibrium perturbatively to the system, developing it to first (linear) order. The effects of this nonequilibrium can also be integrated into additional forces - direct, frictional and random - acting on the atomic system.

[4] And the difference in average energy between the systems - we assume the electronic system to be at $T = 0\,\mathrm{K}$ compared to the atomic system.

1.4 Switching processes

The transition between stable states of a system requires descriptions different than the typical ones focused on short trajectories and perturbations around stable states. The transition between stable states of different conductance is called switching. Classically such switching is analyzed in statistical mechanics through stochastic processes and Markov chains. These descriptions are extended in quantum-mechanical systems through tunneling.

1.4.1 Switching in conductors

Electromigration can also lead to switching between different contact geometries, changing the electronic transport of a system. Most often these different states have different conductances. The states can be stable over any relevant time scales, metastable with possible changes over the investigated time scales or they are transient states, which are only stable for very short times. Two conductance states close to each other in phase space can exhibit telegraph oscillations - quick oscillations between those states.
Switching as defined in this thesis is the process of changing between stable states of the contact. While experiments found states [26, 27] that change with applied voltage or time, these states are not accessible with the method used in this thesis.
Switching between different structures with different conductance properties can also be induced mechanically - something that is used in both experiment [21] and simulations [15]. The mechanically controlled break junction, where piezos can control the distance of the contact on very small length scales is a standard technique to investigate atomic contacts [23]. Scanning tunneling microscopes [25, 28] use atomic sized tips, which are effectively contacts very similar to those investigated here, although most simulational methods can not deal that well with tunneling effects.
The mechanical control is also very easily implemented in simulations, since it requires only the considerations of atoms and fixing some atoms to appropriate boundary conditions is possible in every setup.

1.4.2 Markov chain switching

Markov chains are a description of stochastic processes, where each step is independent of its history. These are important in theoretical physics due to the ergoden-hypothesis, which states the time-trajectories of the system will in the limit of infinite time reach the history-independent probability distribution given by the statistical ensembles.
Let us assume two stable states of energy E_1 and E_2. Statistical mechanics of the canonical ensemble shows the probability to be in one of those states is proportional to $p_i \propto \exp(-\beta E_i)$ with $\beta = \frac{1}{k_B T}$ being the inverse temperature scale of the system.
The Monte-Carlo method samples that distribution without necessarily going through the time trajectories by setting the switching probability to $p(i \to j) = \min(1, \exp[-\beta(E_j - E_i)])$. Such methods explicitly do not sample the trajectories, which are what happens in reality and experiments - these methods do not have an internal time scale. To illustrate the importance of this, let us assume

a third state of energy E_3 that needs to be visited to switch between E_1 and E_2 - this is the typical picture of a reaction barrier for switching.
This barrier E_3 is visited with probability $\exp(-\beta E_3)$ and through that determines the time it takes for the system to switch out of one of these states to $T_i = \tau_i \exp[-\beta(E_3 - E_i)]$ with τ_i being the time scale of trying the switch. A switching barrier of height E_B over the stable states increases the time needed to realize that switch exponentially.

1.4.3 Tunneling

Quantum-mechanical tunneling changes the switching processes of atoms only slightly. Tunneling enables switching to other states with the tunnel-probability

$$p_T = \exp\left[-\int_{x_1}^{x_2} \sqrt{\frac{2m}{\hbar^2}(V(x) - E)}dx\right].$$

The barrier height $V - E$ only reduces the tunneling as a square-root in the exponential, compared to a pure exponential in the Markov case. Another difference is that the width of the barrier $x_2 - x_1$ decreases the tunneling probability exponentially, while that would be unimportant for the classical case. The behavior for higher energy E is similar to the exponential effect of temperature in the classical case - It decreases the barrier height as well as the width depending on the specific form of the potential.

For a hydrogen atom with a mass $m = 1u$, rectangular potential of height 25 meV and width 1 Å this results in a transmission probability of 10^{-3}. This is low in comparison to an arbitrary macroscopic thermal system crossing the same barrier at room temperature with transmission probability in the order of 1. The different behavior in the exponential is the important part here - using an electron instead of a hydrogen atom would increase the tunneling probability to 0.8, using an iron atom reduces the tunneling probability to 10^{-23}. In the classical Markov chain system, the ensemble method of the last subsection does not care for that difference in mass in its statistical limit. Although the mass has an influence in the ballistic limit and for the time scales when the ballistic motion turns to statistical or diffusive behavior.

1.5 Green's function and transport

The Green's function techniques are a key element for practical perturbation and transport calculations. This will be a short overview over the basics following the textbook "Molecular Electronics" by Cuevas and Scheer [3].

1.5.1 Green's function basics

Starting from a differential equation defined by a differential operator $\hat{O}$ applied on an arbitrary function f

$$\hat{O}f = 0$$

the Green's function $\hat{G}$ is defined as that function that will induce identity

$$\hat{O}(\hat{G}) = \hat{1} \Rightarrow \hat{O}(\hat{G}(f)) = f \ .$$

This makes the Green's function very suited to treat inhomogeneous differential equations as well as boundary and initial conditions. Let us assume an inhomogeneous term g with the corresponding differential equation

$$\hat{O}f = g$$

then the solutions f_{sol} to this differential equation take the form

$$f_{sol} = \hat{G}(g) \Rightarrow \hat{O}(\hat{G}(g)) = \hat{1}(g) = g \ .$$

This is eminently useful for treating perturbations to differential equations as well as boundary and initial conditions.

1.5.2 Green's function in practice

Calculating the Green's function in practice reduces to the inversion of a matrix. To illustrate this, we apply them to the stationary Schrödinger equation

$$\hat{H} \left|\phi\right\rangle = E \left|\phi\right\rangle .$$

Here the Green's function is defined by

$$(E - \hat{H})\hat{G} = \hat{1} \ .$$

If you are working in the eigenspace of the differential operator anyway, calculating with Green's functions is computationally very easy in that the Green's function is just the inverse matrix of the differential operator matrix. Or if we are working in a finite basis ϕ_n with defined effects of the Hamiltonian as a matrix

$$\mathbf{H} = H_{nm} = \sum_{nm} \left\langle \phi_n \right| \hat{H} \left| \phi_m \right\rangle \ .$$

From this we can get the Green's function as an energy dependent matrix of the form

$$\mathbf{G}(E) = [E - \mathbf{H}]^{-1} \ .$$

Close to the eigenvalues of the Hamiltonian we find the problem that the matrix to invert turns singular, which is resolved by shifting the singularity a vanishing distance in the complex plane through

$$\mathbf{G}^{\pm}(E) = \lim_{\eta \to 0} [E - \mathbf{H} \pm i\eta]^{-1} .$$

This $\eta > 0$ also broadens the singularities, effectively coupling them to some infinite bath. The Green's function obtained in that way in the basis of the eigenfunctions of the Hamilton operator $|\phi_n\rangle$ is

$$\mathbf{G}^{\pm}(E) = \sum_n \frac{|\phi_n\rangle \langle\phi_n|}{E - \epsilon_n \pm i\eta} .$$

The Green's function is connected to the density matrix of a quantum mechanical system through the density of states $\rho(E) = \sum_n \delta(E - \epsilon_n)$ by the Cauchy identity

$$\frac{1}{E \pm i\eta} = \mathcal{P}\left(\frac{1}{E}\right) \mp i\pi\delta(E)$$

where $\mathcal{P}$ is the Cauchy principal value. This allows us to calculate the density of states ρ from the imaginary part of the Green's function, here for example in the space-basis:

$$\rho(r, E) = \mp \frac{1}{\pi} \mathrm{Im}\mathbf{G}^{\pm}(r, E) .$$

These densities of states serve an important purpose, since together with statistical occupations like the Fermi- or Bose-functions they can be used as a density matrix to describe the state of a quantum-mechanical system.

1.5.3 Dyson's equation

Dyson's equation is used for a perturbative treatment of a system. It shows a way to calculate the Green's function of the full system with perturbation $\mathbf{G}$ from the Green's function of an unperturbed system $\mathbf{g}$ and a description of the perturbation in that basis. Let us assume a Hamiltonian extended with a perturbation $\mathbf{V}$:

$$\mathbf{H} = \mathbf{H}_0 + \mathbf{V} .$$

Then the Green's function of that full Hamiltonian is

$$\mathbf{G}^{\pm}(E) = [(E \pm i\eta)\mathbf{1} - \mathbf{H}_0 - \mathbf{V}]^{-1}$$

and the Green's function of the unperturbed Hamiltonian $\mathbf{H}_0$ is

$$\mathbf{g}^{\pm}(E) = [(E \pm i\eta)\mathbf{1} - \mathbf{H}_0]^{-1} .$$

Dyson's equation then states the full Hamiltonian as

$$\mathbf{G}^{\pm}(E) = \mathbf{g}^{\pm}(E) + \mathbf{g}^{\pm}(E)\mathbf{V}\mathbf{G}^{\pm}(E)$$

which can be easily checked by multiplying with

$$(E \pm i\eta)\mathbf{1} - \mathbf{H}_0 - \mathbf{V}$$

from the right. Dyson's equation can be turned into an iterative equation for $\mathbf{G}_n^{\pm}$ allowing one to calculate the Green's function for the complete system.
In a generalization the perturbation $\mathbf{V}$ is replaced by the energy-dependent self-energy $\mathbf{\Sigma}(E)$, whose determination is often more involved.

1.5.4 Nonequilibrium Green's function

The nonequilibrium Green's function (NEGF) method is a perturbative method to calculate transport properties. The basic idea of the nonequilibrium Green's function method is to analyze a system coupled to one or several reservoirs of particles by treating the coupling as a perturbation to the system under investigation.
In a sense it is a scattering approach, defining what happens when a particle (electron, phonon, photon) of a certain energy encounters a system and interacts with it. Elastic scattering leaves the particle energy unchanged, but may result in momentum transfer, which is then typically neglected. In contrast to that inelastic scattering has a possible energy transfer.

In practice the calculation of the NEGF consists of three parts: The scattering in a system, the ingoing/outgoing bath and the coupling between bath and system under investigation.
The calculation of the transport properties through a contact is equivalent to a scattering matrix approach [29, 30]. The scattering matrix of a system connects the ingoing and outgoing states. Its entries give the probabilities that this in-going state ends up in that outgoing state. To fulfill energy conservation the sum of the energy of the final states has to be equal to the one of the ingoing states.
The calculation of a bath of particles or quasi-particles that are sent into the contact region will be as a bath density of states together with an occupation function.
The coupling between the bath and the scattering region is calculated in an extended central cluster, where the Green's function of the fixed lead atoms is replaced by the bath Green's function.

Let us assume a system coupled to two reservoirs through an interaction $\mathbf{t}$

$$\mathbf{H} = \begin{pmatrix} \mathbf{H}_{LL} & \mathbf{t}_{CL} & 0 \\ \mathbf{t}_{LC} & \mathbf{H}_{CC} & \mathbf{t}_{CR} \\ 0 & \mathbf{t}_{RC} & \mathbf{H}_{RR} \end{pmatrix} .$$

We view the coupling as a perturbation and first calculate the unperturbed Hamiltonian and the Green's function of the central part and the reservoirs $g_{RR,LL,CC}$.
The self energies are calculated as

$$\mathbf{\Sigma}_L^{\pm} = \mathbf{t}_{CL}\mathbf{g}_{LL}^{\pm}\mathbf{t}_{LC}$$

from which the coupling density of states can be calculated

$$\mathbf{\Gamma}_{L,R} = \mathrm{Im}\mathbf{\Sigma}_{L,R}^{a}$$

to finally get the transmission as

$$T = 4\mathrm{Tr}[\mathbf{\Gamma}_L\mathbf{G}_{CC}^{+}\mathbf{\Gamma}_R\mathbf{G}_{CC}^{-}] .$$

Here the lead DOS is already included, but its occupation is still missing. For the overall current one needs to use that occupation to integrate over the energy scales in question

$$I(V) = \int T(E,V)(f_L(E) - f_R(E))dE .$$

1.5.5 Ballistic transport

The description of the contact can be extended to be arbitrarily complex by including the interactions to ever higher order. Here the role of the Green's function as a perturbative approach is evident. The typical first assumption is ballistic transport - the particles are either reflected or go through the contact unchanged. They do not change their energy or their direction - momentum and energy are conserved. Adding just the possibility of direction changes gives elastic transport. Inelastic transport allows for changes in energy and direction, although the calculations get so complicated that most of the time only changes in energy are added perturbatively.

The elastic transport is the first order in the perturbative expansion of the Green's functions, encompassing the coupling of different electronic states. As a single-particle method it can not describe interactions of the moving electrons itself. For example the Coulomb blockade, the reduction of charge transport when the contact is already charged through an additional electron, is not described through the simple, first order Green's function model.

1.6 Simulations

To use these methods for anything more than simple model systems, simulations are necessary to fill those matrices with values describing real systems. The simulations of atomic contacts provide a special challenge. For the description of the electrons in a fixed atomic structure decades worth of scientific work and research has been invested with little fundamental advances due to the long-range interactions. The atomic structure are another system with many years of research invested in it. Here the problem is not so much the description of the system, but the description of the dynamics, especially when it concerns so called rare events or other time scale separations.
The combination of both atoms and electrons together with their interaction combines both problems. From the electrons come the long-range interactions and the assorted scaling problems and from the atomic description come the problems of dynamics and time scale separation.

In this thesis Density Functional theory is used to simulate the electronic system and its interaction with the atoms. The atomic system is relaxed into a configuration of minimal energy and the interaction between those two systems is dealt with perturbatively within DFT [4].

1.6.1 Simulating metallic contacts

The study of stable contacts allows us to focus on the atomic ground states. Which is very welcome since calculating dynamic electronic effects is already difficult and expensive, but extending this further to atomic dynamics is beyond the current state of the art, especially if one considers that switching events can be rare events.

Metallic contacts provide a larger possible structural configuration space than molecule contacts - more shallow minima in the configuration space are possible than there are for the covalently bonded molecules. The advantage of molecules is their stable structural arrangement. This makes them a reproducable system to investigate in molecular electronics and allows the experiments

to focus on other interesting transport phenomena like inelastic scattering, redox reactions, optical switching, current-supported chemical reaction, phononic transport and many others.

Regarding investigation of exactly those structural rearrangements this stability makes molecules unlikely to exhibit those properties - the chances are very high that one will instead see rearrangements in either the metallic leads or the contacts to the metal than in the molecule itself. Furthermore the low conductance of molecules reduces the electron-phonon scattering events needed to pump the atomic system. Together with the increased phononic conductance, this makes it very likely that the atomic system is thermalized considerably better in molecular conductors.

Simulating metallic contacts has its own challenges. The electronic wave functions can be quite extended and it can be difficult to approximate these well with local bases. Periodic bases on the other hand do not deal well with the surface structures, requiring large basis sets to approximate those well.

1.7 Summary

In this chapter electromigration in metallic atomic contacts was introduced with a particular focus on the theoretical descriptions of those systems consisting of atoms and electrons. This proceeded to describe the simulations methods and modellings used on such systems and finally perturbative approaches to calculate the transport through those structures.

The second chapter 2 will extend the models used for the interaction of electrons and atoms and the simulation methods used. Specifically, the current-induced forces acting on the atoms will be derived, their implementation shown, and the resulting Langevin equation for the atoms of the contact will be discussed.

Chapter 2

Basics

This chapter consists of two parts explaining how electromigration in atomic contacts was approached. The basic idea is simplifying the full equation describing electrons and atoms coupled with each other and the nonequilibrium bath by integrating the electronic degrees of freedom into the terms of a Langevin equation describing the atoms.

The first section presents how the inelastic scattering of non-equilibrium electrons can be integrated into forces acting on the atoms and how these forces were calculated in the simulations.
The second section discusses the Langevin equation describing the atomic motion. Special focus is on the non-conservative effects of the current-induced forces and their random nature and what that means for electromigration.

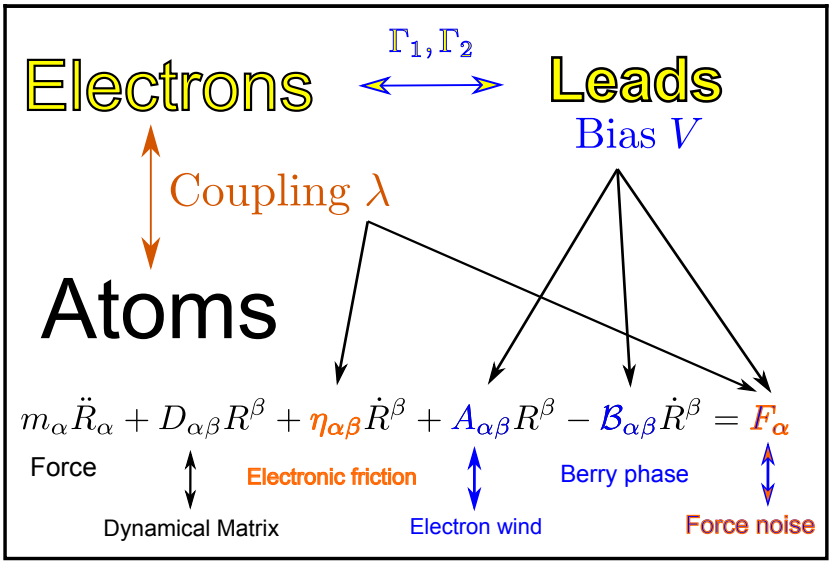

Figure 2.1: An overview sketch of the derivations in this chapter. The Langevin equation at the bottom describes the atomic system. The matrices of the force terms are calculated through DFT and NEGF methods.

2.1 Current-induced forces

In this section the current-induced forces are derived, following the works of Todorov et al. [6] as well as Lü et al. [5]. These are lowest order expansions in the atomic degrees of freedom (both perturbation in space as well as velocity) as well as first order expansions in the electron-vibration coupling. The electronic system is coupled to reservoirs not in equilibrium as in the nonequilibriums Green's function formalism.
In this derivation subsection, I will use Todorov et al. [6] for a derivation of current-induced forces using a density matrix formulation and electron-vibration scattering density of states. Lü et al. [5, 7] themselves use an influence functional formulation for the derivation, over which I will not go in this work. Bode et al. [29, 30] use a scattering matrix formulation, which also provides a nice picture on the problem. For an overview of the field, see the review by Dou and Subotnik [31].
The calculation section uses Lü et al. [5] together with the IETS calculation paper of Bürkle et al. [4], because that is the one I used for the implementation in the numerical simulation.

2.1.1 Contact model

The goal is to describe the atomic structure and its dynamics when electrons flow. For this we "integrate" the electronic system in non-equilibrium and its interaction with the atoms into forces acting on the atoms.

The basic model is a system of atoms and electrons described quantum-mechanically through a Hamiltonian with their interactions. For the atomic system we assume harmonic potentials - for a displacement from the resting position there is a force acting against that displacement proportional to the displacement distance. The proportionality constant of that restoring force is the force constant of the harmonic potential.

Both coupling the system to baths and integrating the nonequilibrium electronic system may change those force constants and there will also be friction-terms and a random force noise acting on the atoms due to the electron-atom interaction.

Adding just the electron-atom interaction already gives rise to electronic friction on the atomic movement. The electronic system is assumed to be at a temperature of $T = 0\,\mathrm{K}$ in the DFT calculations, so any excitation of the atomic system above quantum fluctuations is transferred to the electronic system.

The Born-Oppenheimer approximation assumes a time-scale separation of the electron and the atomic system. In this approximation the electrons follow the atomic motion instantaneously. Under this assumption the electron wave-function can be calculated or at least approximated in a suitable basis set. The wave-function is a complete description of the system in question - in this case the wave-function is approximate in the electron density functional describing the electrons in a fixed potential given by the ionic atoms.
This electronic system of the contact is then coupled to the electronic systems of the leads. Those are large enough to have thermodynamic properties, specifically a bulk density of states and an occupation according to the Fermi distribution. These properties of the leads do not change with the few electrons moving out, in this sense they are serving as thermodynamic baths. The

baths do not need to be in equilibrium with each other - they can have different temperatures or potential energies. Since the temperature is not so important for electrons, the primary way to introduce a nonequilibrium is a difference in electrical potential. This difference is the bias voltage V.

2.1.2 Derivation of the forces

The paper by Todorov et al. [6] presents an approach to derive the current-induced forces. For this they use a shared Hamiltonian for electrons and atoms of a form:

$$\hat{H} = \left[\hat{H}_e + \sum_\beta \left(\frac{\hat{P}_\beta^2}{2M_\beta} + \frac{1}{2}M_\beta\omega_\beta^2\hat{X}_\beta^2\right)\right] - \sum_\beta \hat{F}_\beta\hat{X}_\beta \ .$$

The atomic system consists of the atom coordinates X with index β, a combination of atom number and direction. The atomic system is assumed to be harmonic, with the known quantum harmonic oscillator solutions to its system. The electron-vibration coupling $\sum_\beta \hat{F}_\beta\hat{X}_\beta$ is treated as a perturbation to the system. $\hat{F}_\beta$ is a tricky parameter by itself, in the derivation here we assume it is a scalar strength of the coupling multiplied with a 1-electron operator.

The idea is to use time-dependent perturbation theory to a low order to develop the density matrix $\hat{\rho}$ of the combined system

$$i\hbar\dot{\hat{\rho}}\left(t\right) = \left[\hat{H}\left(t\right), \hat{\rho}\left(t\right)\right] \ ,$$

with the goal to calculate an effective force F_α on the atoms α through a trace over the perturbed density matrix

$$F_\alpha\left(t\right) = \mathrm{Tr}\left\{\hat{F}_\alpha\hat{\rho}\left(t\right)\right\}$$

up to second order in the electron-vibration coupling $\left\{\hat{F}_\beta\right\}$ through the commutator of the coupling term with the mometum of the atomic system $\hat{P}_\alpha$ through

$$\hat{F}_\alpha = \frac{1}{i\hbar}\left[\hat{P}_\alpha, \left(-\sum_\beta \hat{F}_\beta\hat{X}_\beta\right)\right] \ .$$

The unperturbed density matrix of the whole system is $\hat{\rho}_0\left(t\right) = \hat{\rho}_{0,1e}\left(t\right) \otimes \hat{\rho}_{0,\mathrm{osc}}\left(t\right)$, with the time-dependent electronic density matrices of the electrons $\hat{\rho}_{0,1e}$ and the atomic vibrations $\hat{\rho}_{0,\mathrm{osc}}$.

The electronic density matrix is expanded to first order in time-dependent perturbation theory through:

$$\hat{\rho}_{1e}\left(t\right) = \hat{\rho}_{0,1e} - \frac{1}{i\hbar}\sum_\beta \int_0^t \left[\hat{f}_\beta\left(\tau - t\right), \hat{\rho}_{0,1e}\left(t\right)\right] X_\beta\left(\tau\right) d\tau$$

where $\hat{f}_\beta\left(\tau - t\right)$ is the 1-electron operator of the electron-vibration coupling

$$\hat{f}_\beta\left(s\right) = \exp\left(i\hat{h}_e s/\hbar\right)\hat{f}_\beta \exp\left(-i\hat{h}_e s/\hbar\right) \ .$$

For the unperturbed electron density matrix $\hat{\rho}_{0,1e}(t)$ we use the Landauer picture for steady state transport

$$\hat{\rho}_{LP} = \int_{-\infty}^{\infty} \hat{\rho}_{LP}(\epsilon)\, d\epsilon,$$

$$\hat{\rho}_{LP}(\epsilon) = n_F(\epsilon - \mu_1)\, \hat{d}_1(\epsilon) + n_F(\epsilon - \mu_2)\, \hat{d}_2(\epsilon) \ ,$$

with the partial density of states operators of the scattering wavefunctions coming from reservoirs 1 and 2

$$\hat{d}_1(\epsilon) = \sum_{i_1} |\psi_{i1}\rangle\, \delta(\epsilon - \epsilon_{i_1})\, \langle\psi_{i1}|$$

$$\hat{d}_2(\epsilon) = \sum_{i_2} |\psi_{i2}\rangle\, \delta(\epsilon - \epsilon_{i_2})\, \langle\psi_{i2}| \ .$$

Now one can substitute the Landauer picture density matrix for the electrons and use the explicit time-development for the oscillator position

$$X_\beta(t) = a_\alpha \cos(\omega_\beta t - \phi_\beta)$$

and velocity

$$V_\beta(t) = -a_\beta \omega_\beta \sin(\omega_\beta t - \phi_\beta)$$

to calculate the forces F_α to second order, since the first order forces vanish in a steady state minimum. Comparison of terms of the linearized forces

$$F_\alpha(t) = -\sum_\beta K_{\alpha\beta} X_\beta(t) + \sum_\beta L_{\alpha\beta} V_\beta(t)$$

allows one to identify the dynamical matrix

$$K_{\alpha\beta} = \frac{1}{i\hbar} \int_0^t \mathrm{Tr}\left\{ \hat{f}_\alpha \left[\hat{f}_\beta(\tau - t), \hat{\rho}_{LP} \right] \right\} \cos(\omega_\beta(\tau - t))\, d\tau$$

connected to the atomic coordinates and the friction matrix

$$L_{\alpha\beta} = \frac{1}{i\hbar\omega_\beta} \int_0^t \mathrm{Tr}\left\{ \hat{f}_\alpha \left[\hat{f}_\beta(\tau - t), \hat{\rho}_{LP} \right] \right\} \sin(\omega_\beta(\tau - t))\, d\tau$$

connected to the atomic velocities. These matrices can be taken apart into their symmetric and antisymmetric parts, which can be connected to different physical effects

$$K_{\alpha\beta} = \mathrm{Re} \int_{-\infty}^{\infty} \mathrm{Tr}\left\{ \hat{f}_\alpha [\hat{g}^+(\epsilon + \hbar\omega_\beta) + \hat{g}^+(\epsilon - \hbar\omega_\beta)] \hat{f}_\beta \hat{\rho}_{LP}(\epsilon) \right\} d\epsilon$$

$$L_{\alpha\beta} = \frac{1}{\omega_\beta} \mathrm{Im} \int_{-\infty}^{\infty} \mathrm{Tr}\left\{ \hat{f}_\alpha [\hat{g}^+(\epsilon + \hbar\omega_\beta) - \hat{g}^+(\epsilon - \hbar\omega_\beta)] \hat{f}_\beta \hat{\rho}_{LP}(\epsilon) \right\} d\epsilon$$

with $\hat{g}^+(\epsilon)$ being the retarded 1-electron Green's function.

How this is connected to the matrices calculated in the program will be explained in the next section.

2.2 Calculating the forces

To combine the current-induced forces derived with the matrices calculated in simulations, I follow the derivation of Lü et al. [5] given in their Supplementary Information. I combine that with the formulation of IETS calculation from the paper of Bürkle et al. [4], which adapted the IETS calculation from an earlier paper of Frederiksen et al. [16] to TURBOMOLE - the same code that I adapted and changed for the simulations presented later.

The central property here is the "equal-time coupling weighted effective electron-hole pair density of states" or friction kernel $\Lambda_{ij}^{\alpha\beta}(\omega)$ [32], giving the strength of scattering into the phonon-mode of energy ω. They use this density of states to derive all the forces codified in $L_{\alpha\beta}$, $K_{\alpha\beta}$ divided into symmetric and anti-symmetric parts and their force noise term.

2.2.1 Scattering density of states

The $\Lambda_{ij}^{\alpha\beta}(\omega)$ gives the scattering probability and strength of an electron transmitted between lead i and j into modes α and β. It is given as

$$\Lambda_{ij}^{\alpha\beta}(\omega) = \int \mathrm{Tr}\left[\mathbf{A}_i(E+\omega)\mathbf{M}^\alpha \mathbf{A}_j(E)\mathbf{M}^\beta\right]\left(n_F(E+\omega-\mu_i) - n_F(E-\mu_j)\right)\frac{dE}{(2\pi)^2}$$

where $\mathbf{M}^\alpha$ are the electron-vibration coupling matrices and $\mathbf{A}_i$ the spectral density of the scattering states of lead i. Both of these will be explained in the following paragraphs. Furthermore $\hbar$ is set to 1 and the ω are the frequencies of the phonons.

$$(\mathbf{M}^\alpha)_{ab}(R) = \langle\psi_a|\,\nabla_\alpha \mathcal{H}_e(R)\,|\psi_b\rangle$$

is the coupling matrix, the derivative of the electronic-energy with respect to the movement of the atoms. The indices α can be either a combined atom-dimension index or a phonon mode - if it is a phonon mode, this $\mathbf{M}^\alpha$ is the electron-phonon coupling λ described in Ref. [4]. The indices a and b denote the electron basis functions used to describe the system.

This density of states Λ is formulated with the spectral density of scattering states connected to the lead with index i

$$\mathbf{A}_i(R;E) = \mathbf{G}(R;E)\mathbf{\Gamma}_i(E)\mathbf{G}^\dagger(R;E)\ .$$

Here, $\mathbf{G}$ are the coupled Green's functions of the contact region and $\mathbf{\Gamma}_i$ is the coupling term to lead i.

The coupling matrix $(\mathbf{M}^\alpha)_{ab}(R)$ is similar to the Electron-Vibration coupling constants $\lambda_{\mu\nu}^\alpha$ in Ref. [4], although that λ is defined in the phonon modes and normalized to the energy of the phonon mode. The λ is normalized to have units of energy in order to fit the second quantization formulation in the paper [4].

The basic formula for $\Lambda_{ij}^{\alpha\beta}(\omega)$ as written above is an integral in the energy space with shift depending on the phonon frequency ω. The $\mathbf{A}_i$ matrix is the electron-scattering matrix of one side. To get this matrix the surface Green's function at a specific energy has to be calculated.
In the paper [5] they present an approximation to this integral by making a $T = 0\,\mathrm{K}$ extension, only looking at the lowest order in ω. They are replacing the broadened Fermi functions n_F with step functions and assume a constant

spectral density of scattering states $\mathbf{A}_i(E)$ in a small region ω around the Fermi energy μ_i.
This is similar to but not yet the full wide-band approximation, where one assumes that the behavior around the Fermi energy is similar to that at the Fermi energy itself - constant electronic density of states $\mathbf{A}_i$ and electron-vibration scattering.
The only energy dependent term is the electron-scattering matrix $\mathbf{A}_i$. If that term is constant around the Fermi-energy, it just integrates up the appropriate values of the electron-vibration coupling $\mathbf{M}$ over the range of the bias. In other words: The $\mathbf{A}_i$ describe the densities of states of the electron orbitals of the contact coupled to the leads, the $\mathbf{M}$ determine how strongly those electron states couple to the atomic motion and the Fermi functions n_F state if those electronic states are occupied.

This approximation results in the lowest order intra-electrode friction term

$$\Lambda_{ii}^{\alpha\beta}(\omega) \approx -\frac{\omega}{(2\pi)^2}\mathrm{Tr}\left[\mathbf{A}_i(\mu_i)\mathbf{M}^\alpha\mathbf{A}_i(\mu_i)\mathbf{M}^\beta\right] ,$$

and the inter-electrode friction term for a bias larger than the phonon-energies $eV \gg \omega$

$$\begin{aligned}\Lambda_{ij}^{\alpha\beta}(\omega) \approx &\int_{\mu_j}^{\mu_i} \mathrm{Tr}\left[\mathbf{A}_i(E)\mathbf{M}^\alpha\mathbf{A}_j(E)\mathbf{M}^\beta\right]\frac{dE}{(2\pi)^2} \\ &- \frac{\omega}{8\pi^2}\left(\mathrm{Tr}\left[\mathbf{A}_i(\mu_i)\mathbf{M}^\alpha\mathbf{A}_j(\mu_i)\mathbf{M}^\beta\right] + \mathrm{Tr}\left[\mathbf{A}_i(\mu_j)\mathbf{M}^\alpha\mathbf{A}_j(\mu_j)\mathbf{M}^\beta\right]\right) .\end{aligned}$$

For this inter-electrode friction term the wide-band approximation can be used again for the first integral through setting the scattering density of states constant $\mathbf{A}_i(E) = \mathbf{A}_i(\mu_i)$, $\mathbf{A}_j(E) = \mathbf{A}_j(\mu_j)$ and defining $\mu_i = \mu_j + eV$. This results in

$$\begin{aligned}\Lambda_{ij}^{\alpha\beta}(\omega) \approx &\frac{eV}{(2\pi)^2}\mathrm{Tr}\left[\mathbf{A}_i(\mu_j)\mathbf{M}^\alpha\mathbf{A}_j(\mu_j)\mathbf{M}^\beta\right] \\ &- \frac{\omega}{8\pi^2}\left(\mathrm{Tr}\left[\mathbf{A}_i(\mu_j)\mathbf{M}^\alpha\mathbf{A}_j(\mu_j)\mathbf{M}^\beta\right] + \mathrm{Tr}\left[\mathbf{A}_i(\mu_j)\mathbf{M}^\alpha\mathbf{A}_j(\mu_j)\mathbf{M}^\beta\right]\right) .\end{aligned}$$

Now we use those approximations to calculate the different force and friction terms.

2.2.2 Direct force and dynamical matrix

The dynamical matrix $D_{\alpha\beta}$ is the matrix of the force constants

$$D_{\alpha\beta} = \frac{\partial^2 H}{\partial x_\alpha \partial x_\beta} ,$$

the derivative of the overall energy H of the system to small perturbation x from the resting positions. This describes the forces acting on atom-direction α when another atom is moved in direction β.

This is already a linear approximation to the overall conservative force

$$f_\alpha = -\frac{\partial H}{\partial x_\alpha}$$

that emerges from the Born-Oppenheimer approximation. This conservative force would also include the static parts of the bias electrical field. For the treatment in the current-induced forces approach all these influences are ignored and the unperturbed, steady-state dynamical matrix is used.

Since the contacts are assumed and measured to be stable in their atomic configurations without changes due to small applied bias, at least the dynamical matrix approximation itself seems valid. In regard to possible changes in the force-constants due to a coupling to the leads and an applied bias there is literature claiming a small influence. Bai et al. [33] uses the SMEAGOL package on top of SIESTA to calculate current-induced forces from the expectation value of the ionic momentum operator following the derivation of DiVentra [34]. Their framework is a Au-H_2-Au junctions, where they use these forces to reevaluate the force constants in the phonon picture, finding changes around 5%. This change is not enough to produce a configuration change. An interesting aside is their comparison of the influence of the electrical field and the current scattering on the atoms, which gives negligible effects of the field, also validating the steady state approximation to conservative force.

2.2.3 Electronic friction

The electronic friction matrix $\eta^{\alpha\beta}$ is calculated from the friction force f_{fr} defined as[5]

$$f^{\alpha}_{fr} = \sum_{ij\beta} \int_t^{\infty} dt' \int_{-\infty}^{\infty} \frac{d\omega}{\omega} Re \left[\Lambda^{\alpha\beta}_{ij}(R(t), R(t'); \omega) e^{i\omega(t-t')} \right] \dot{R}_{\beta}(t') \,.$$

This is expanded around $\omega = 0$ to get

$$f^{\alpha}_{fr}(t) = -\sum_{\beta} \eta^{\alpha\beta} \dot{R}_{\beta}$$

with the electronic friction matrix

$$\eta^{\alpha\beta} = -\pi \sum_{ij} \frac{\partial}{\partial\omega} \mathrm{Re} \left[\Lambda^{\alpha\beta}_{ij}(R(t), R(t); \omega)) \right] |_{\omega=0} \,.$$

Together with the approximation for Λ

$$\begin{aligned}
\frac{\partial}{\partial\omega}\Lambda^{\alpha\beta}_{ii}(\omega) &\approx -\frac{1}{(2\pi)^2}\mathrm{Tr}\left[\mathbf{A}_i(\mu_i)\mathbf{M}^{\alpha}\mathbf{A}_i(\mu_i)\mathbf{M}^{\beta}\right] \\
\frac{\partial}{\partial\omega}\Lambda^{\alpha\beta}_{ij}(\omega) &\approx -\frac{1}{8\pi^2}\left(\mathrm{Tr}\left[\mathbf{A}_i(\mu_i)\mathbf{M}^{\alpha}\mathbf{A}_j(\mu_i)\mathbf{M}^{\beta}\right] + \mathrm{Tr}\left[\mathbf{A}_i(\mu_j)\mathbf{M}^{\alpha}\mathbf{A}_j(\mu_j)\mathbf{M}^{\beta}\right]\right)
\end{aligned}$$

this yields in sum over all lead combinations

$$\begin{aligned}
\eta^{\alpha\beta} = \frac{1}{8\pi}(&\mathrm{Tr}\left[\mathbf{A}_R(\mu_R)\mathbf{M}^{\alpha}\mathbf{A}_L(\mu_R)\mathbf{M}^{\beta}\right] + \mathrm{Tr}\left[\mathbf{A}_R(\mu_L)\mathbf{M}^{\alpha}\mathbf{A}_L(\mu_L)\mathbf{M}^{\beta}\right] \\
&+\mathrm{Tr}\left[\mathbf{A}_L(\mu_R)\mathbf{M}^{\alpha}\mathbf{A}_R(\mu_R)\mathbf{M}^{\beta}\right] + \mathrm{Tr}\left[\mathbf{A}_L(\mu_L)\mathbf{M}^{\alpha}\mathbf{A}_R(\mu_L)\mathbf{M}^{\beta}\right] \\
&+2\mathrm{Tr}\left[\mathbf{A}_R(\mu_R)\mathbf{M}^{\alpha}\mathbf{A}_R(\mu_R)\mathbf{M}^{\beta}\right] + 2\mathrm{Tr}\left[\mathbf{A}_L(\mu_L)\mathbf{M}^{\alpha}\mathbf{A}_L(\mu_L)\mathbf{M}^{\beta}\right]) \,.
\end{aligned}$$

This electronic friction is in the wide-band approximation independent of bias through the coupling to the leads. Its effect is a coupling of the atomic motion to the electrons and an equilibration of those systems. Since density functional theory and the approximations here assume a temperature $T = 0\,\mathrm{K}$ for the electronic system, any energy of the atomic system is removed.

2.2.4 Electron wind

The electronic wind force matrix $A^{\alpha\beta}$ is calculated from the electron wind force [5]

$$f_{ew}^{\alpha}(t) = -\pi \sum_{ij\beta} \mathrm{Im}\left[\Lambda_{ij}^{\alpha\beta}(R(t), R(t); 0)\right] (R_\beta(t) - \langle R_\beta \rangle) .$$

This is the typical determination of the harmonic terms - the force proportional to a small perturbation to a resting position $R_\beta(t) - \langle R_\beta \rangle$. The relevant term is the imaginary part of Λ, the scattering density of states - Λ is its own complex conjugate, so its diagonal terms are real.

The curl of this force is interesting, because it states if such a force can be integrated to a potential. The calculation of the curl gives

$$\frac{\partial f_{ew}^{\alpha}}{\partial R_\beta} - \frac{\partial f_{ew}^{\beta}}{\partial R_\alpha} = 2\pi \sum_{ij} \mathrm{Im}\left[\Lambda_{ij}^{\alpha\beta}(R(t), R(t); 0)\right] .$$

The curl is therefore non-zero if the imaginary part of the electron-phonon scattering matrix Λ is itself anti-symmetric in α and β, which will happen with high enough applied bias. Accordingly

$$A^{\alpha\beta} = -\pi \sum_{ij} \mathrm{Im}\Lambda^{\alpha\beta}$$

is the matrix encoding the forces due to electron-phonon scattering in the Langevin equation and will also turn anti-symmetric[5].

Non-conservative forces

The electron wind matrix $A_{\alpha\beta}$ is anti-symmetric. This means the electron-wind force is a non-conservative force - there are closed curves in phase space, where the atomic system gains energy through the electron wind.

The curl of the force $\partial_\alpha f^\beta - \partial_\beta f^\alpha$ has to vanish in order for this force to be integrated as a potential - from this the energy conservation also fixes the potential energy of the system. In a non-conservative system the energy is only overall conserved. A non-conservative force acts as a coupling to a heat bath and is an indicator that the system underlying the calculations is coupled to a heat bath.

Accordingly the non-conservative force is accompanied by a dissipation together with a fluctuating or random force (that may be colored instead of white) according to the fluctuation-dissipation theorem. This changes the system under investigation from one with constant energy (NVE) to one with energy fluctuation around a temperature (NVT). This changes classical trajectories from closed ones to exploring ones. Quantum-mechanically it is more difficult. As the occupation of the harmonic wave-function increases, it is also exploring more space, but interacting with the rest of the system and reducing tunnel barriers. Leaving the harmonic approximation and including anharmonic terms in the approach has been tried for a long time without significant advances.

[5] Here the wide-band limit is already included in the calculation of Λ, so the bias dependency is in there already.

The harmonic approximation itself is the second order term in a development around a minimum. Anharmonic (higher order) terms are less relevant than those.

Normally one could construct at least the Born-Oppenheimer potential energy surface, consisting of stable and metastable minima. All minima are metastable with enough temperature. If one couples the system moving on that surface to a heatbath, the system is only in minima long enough to integrate enough of the electronic motion and scattering for that to be a relevant effect.

Example To illustrate the non-conservative aspects we take a look at the electron wind term and show that this non-conservative term does not lead to additional minima or shifts of the position of minima in the potential energy landscape. To do that we show that with the addition of the electron wind the search for the a system at rest (without force acting on it) turns into an eigenvalue problem for the voltage, which has not a single point as solution but a whole eigenvector along which the system could move without restrictions.
We start with the force equation in the displacement $\vec{u} = \vec{x} - \vec{x_0}$

$$\vec{F} = (\mathbf{D} + V\mathbf{EW}) \cdot \vec{u} \,,$$

with the dynamical matrix $\mathbf{D}$ and the linear version of the electron-wind force matrix $\mathbf{EW}$ as defined in section 2.2.4.
Since the dynamical matrix $\mathbf{D}$ is non-singular, the only configuration without a force acting at $V = 0$ is the resting position $\vec{u} = \vec{0}$. There may be other $\vec{F} = \vec{0}$ possibilities if we apply a voltage V and therefore have a relevant second term, so we search for them by setting the overall force to zero:

$$\begin{aligned} \vec{0} &= (\mathbf{D} + V\mathbf{EW}) \cdot \vec{u} \\ \Leftrightarrow \vec{0} &= (\mathbf{EW}^{-1}\mathbf{D} + V \cdot \mathbf{1}) \cdot \vec{u} \,. \end{aligned}$$

Under the assumption that the electron wind matrix is invertible, this presents an eigenvalue problem with the voltages as eigenvalues. If one reaches a high enough voltage, there will be no force acting on the system if it moves along the eigenvector belonging to that voltage.
One can not find a specific position along this vector that one can use as a new resting position. The whole process is not a driven process but a change in the prefactor of the harmonic potential. This prefactor of the harmonic potential should be 0 for the voltage eigenvalues, corresponding to a equipotential line along the eigenvector. Change of sign from positive to negative in this prefactor is a change from a stable harmonic potential to an unstable one.
This change in sign is what is searched for through the methods illustrated in the next section.

2.2.5 Berry phase

The Berry-phase friction matrix $\mathcal{B}^{\alpha\beta}$ is derived with the definition of the Berry-phase

$$\mathcal{A}^{\alpha}(x) = -i \sum_{n} n_F(\epsilon_n) \, \langle \phi_n(x) | \nabla_\alpha \phi_n(x) \rangle \,.$$

The Lorentz-like force corresponding to the Berry-phase is found to be [5]

$$f_B^\beta = \sum_\alpha \left(\frac{\partial \mathcal{A}^\alpha}{\partial R_\beta} - \frac{\partial \mathcal{A}^\beta}{\partial R_\alpha} \right) \dot{R}_\alpha \,.$$

The term in the parenthesis corresponds to a magnetic field,

$$\mathcal{B}_{\alpha\beta} = \frac{\partial \mathcal{A}^\alpha}{\partial R_\beta} - \frac{\partial \mathcal{A}^\beta}{\partial R_\alpha} \,,$$

which can be related back to the effective electron hole density of states Λ by

$$\mathcal{B}_{\alpha\beta} = \mathrm{Im} \sum_{ij} \int \frac{d\omega}{\omega^2} \Lambda_{ij}^{\alpha\beta}(R, R; \omega) \,.$$

Here we expand Λ in ω again and take the zeroth order. Assuming the integral in Λ is best approximated by the mid point between the Fermi-energies of the leads, this results in

$$\mathcal{B}_{\alpha\beta} = eV \cdot \sum_{ij} \mathrm{Tr} \left[\mathbf{A}_i((\mu_j - \mu_i)/2) \mathbf{M}^\alpha \mathbf{A}_j((\mu_j - \mu_i)/2) \mathbf{M}^\beta \right] \int_0^\infty \frac{d\omega}{\omega^2} .$$

We correct the infrared divergence at $\omega = 0$ in the integral with a cut-off frequency corresponding to the smallest frequency in the atomic motion Ω, to get

$$\mathcal{B}_{\alpha\beta} = eV \mathrm{Tr} \left[\mathbf{A}_i((\mu_j - \mu_i)/2) \mathbf{M}^\alpha \mathbf{A}_j((\mu_j - \mu_i)/2) \mathbf{M}^\beta \right] \frac{1}{\Omega} \,.$$

2.2.6 Fluctuating forces - force noise

The fluctuating forces or the force noise are connected to the heat-bath or effective temperature through a fluctuation-dissipation theorem or, in the more general case, a Green-Kubo relation [35]. The force noise vanishes in the short time-scales and they have no effect in ground state approaches, which is why they will play no role in the next section and the following chapter. Nevertheless their strength described by their power-spectrum is important for any argument going beyond these limits, as will be done for the consideration of switching in chapter 4.
So, according to Lü et al. [5] the power spectrum of the fluctuating forces is given approximately by

$$\langle F_\alpha(\omega) F_\beta(\omega)^* \rangle = \sum_{ij} \Lambda_{ij}^{\alpha\beta}(R, R; \omega) \coth \left(\frac{\omega + \mu_i - \mu_j}{2 k_B T} \right)$$

or more or less the electron-phonon scattering density of states in dependence of space coordinate R and phonon frequency ω as well as the Fermi energies of the respective leads μ_i, μ_j and the thermal energy scale $k_B T$.

In the equilibrium limit ($\mu_i = \mu_j$) this reduces to

$$\langle F_\alpha(\omega) F_\beta(\omega)^* \rangle = \sum_{ij} \Lambda_{ij}^{\alpha\beta}(R, R; \omega) \coth \left(\frac{\omega}{2 k_B T} \right) = \frac{1}{\pi} \eta_{\alpha\beta}^{eq} \omega \coth \left(\frac{\omega}{2 k_B T} \right)$$

with $\eta^{eq}_{\alpha\beta}$ the appropriately defined friction coefficients in equilibrium. In the classical limit of high temperatures ($k_BT \gg \omega$) this reduces to a classical fluctuation-dissipation relation

$$\langle F_\alpha(\omega)F_\beta(\omega)^*\rangle^{eq} = \frac{\eta^{eq}_{\alpha\beta}}{2\pi}k_BT\,. \tag{2.1}$$

In the nonequilibrium case $\mu_i - \mu_j = eV$ the force-power spectrum of different leads can be developed in the limit $eV \gg \omega, k_BT$ to

$$\langle F_\alpha(\omega)F_\beta(\omega)^*\rangle\,(eV) \approx \left(\Lambda^{\alpha\beta}_{12}(R,R;\omega) - \Lambda^{\alpha\beta}_{21}(R,R;\omega)\right) \propto eV\,.$$

Comparison with the fluctutation-dissipation theorem in eq.2.1 gives an effective temperature of the current-carrying enviroment proportional to the energy of the bias eV with a proportionality factor largely given by the electron-phonon scattering.

2.3 Semi-classical generalized Langevin equation

In the last section all the matrices for this Langevin equation were derived and calculated:

$$m_\alpha\ddot{R}_\alpha + D_{\alpha\beta}R^\beta + \eta_{\alpha\beta}\dot{R}^\beta + A_{\alpha\beta}R^\beta - \mathcal{B}_{\alpha\beta}\dot{R}^\beta = F_\alpha \tag{2.2}$$

This section discusses the equation and the system it describes in two subsections. The first one deals with the analytical form of the Langevin equation and how the specific form we have here can be approached as a quadratic eigenvalue problem. The most central concept here is the runaway voltage - the voltage where an eigenmode turns unstable.
The second subsection deals with Langevin dynamics and investigates how the system described by the Langevin equation develops over time and can lead to switching. Here the important difference between runaway voltages and switching-voltages - the voltages at which a contact changes its configuration - will be discussed.

This system description is different from the quantum-mechanical ones in the introduction and the last section. For one it has an explicit time-dependency and the energy is only conserved on average. The equation describes a system in the canonical ensemble coupled to a bath of a temperature T instead of the microcanonical description with a fixed temperature E.
Nevertheless the equation can be solved in some sense. Analytically it poses a quadratic eigenvalue problem, which will be discussed in the next subsection. There we will find eigenmodes of the system that are not constant but damped. The forces acting on these eigenmodes are different for every eigenmode and voltage, which gives an anisotropy in the kinetic energy or effective temperature of the system. The most important concept of this subsection is the one of the runaway voltage - the voltage where an eigenmode turns unstable.

2.3.1 Solving the equation

Expanding to the lowest order around the Born-Oppenheimer configuration results in a Langevin-like equation 2.2. Here $D^{\alpha\beta}$ is the standard dynamical

matrix and $A^{\alpha\beta}$ is the anti- symmetric matrix describing the electron wind force. Fourier-transforming this equation results in

$$R_\alpha(\omega) = G^{\alpha\beta}(\omega)F^\beta(\omega)$$

with a Green's function (with setting all masses $m_\alpha = m$)

$$G^{\alpha\beta} = \left(-m\delta^{\alpha\beta}\omega^2 + D^{\alpha\beta} + i\omega\eta^{\alpha\beta} + A^{\alpha\beta} - i\omega\mathcal{B}^{\alpha\beta}\right)^{-1} .$$

The poles of this Green's function determine the frequencies of the eigenmodes and their lifetime. The easiest way to access these is seeing this as a quadratic eigenvalue problem in ω and solving that in a linearized version, which will be done over the course of this section.

This current subsection deals with solving the quadratic eigenvalue problem of the matrix

$$-m\delta^{\alpha\beta}\omega^2 + D^{\alpha\beta} + i\omega\eta^{\alpha\beta} + A^{\alpha\beta}(V) - i\omega\mathcal{B}^{\alpha\beta}(V)$$

in dependence of the bias voltage V. This equation is reached by Fourier-transforming the Langevin equation 2.2 from the time into the frequency domain, which changes the second order differential equation into an algebraic, quadratic eigenvalue problem for the frequencies ω.

At zero bias the antisymmetric terms to the restoring force $A^{\alpha\beta}(V)$ and the friction $\mathcal{B}^{\alpha\beta}$ vanish, leaving only

$$\left(-m_\alpha\delta^{\alpha\beta}\omega^2 + D^{\alpha\beta} + i\omega\eta^{\alpha\beta}\right) ,$$

as a simple eigenvalue problem. This eigenvalue problem describes the eigenmodes of the atomic system through the eigenvectors and connected frequencies of the dynamical matrix $D^{\alpha\beta}$ together with an additional damping term through electronic friction $\eta^{\alpha\beta}$ that adds an imaginary term to frequency.

Quadratic eigenvalue problem

Solving the quadratic eigenvalue problem in the general case is still an open problem. The mathematical overview paper of Tisseur and Meerbergen[36] is the primary source for this application. The linearization scheme used to tackle the problem in the code was also adopted from that paper.

The solutions to eigenvalue problems are the roots of the characteristic polynomial. For the linear eigenvalue problems the characteristic polynomial has the rank n of the matrix and accordingly n zeros in the complex plane. For the quadratic eigenvalue problem, the characteristic polynomial has a rank of $2n$ and accordingly many zeros.

To tackle the quadratic eigenvalue problem, one can create a matrix of double size, whose linear eigenvalue problem has the same characteristic polynomial.

The matrix problem

$$\left(-m\omega^2\mathbf{1} + \omega(i\eta - \mathbf{B}) + (\mathbf{D} + \mathbf{A})\right)\vec{x} = 0 \tag{2.3}$$

is transformed into the linear eigenvalue problem

$$\begin{bmatrix} 0 & \mathbf{1} \\ -(\mathbf{D}+\mathbf{A}) & -(i\eta-\mathbf{B}) \end{bmatrix} \begin{bmatrix} \vec{x} \\ \vec{u} \end{bmatrix} - \omega \begin{bmatrix} \mathbf{1} & 0 \\ 0 & -m\mathbf{1} \end{bmatrix} \begin{bmatrix} \vec{x} \\ \vec{u} \end{bmatrix} = 0$$

with the same characteristic polynomial. Here the vector $\vec{u}$ is defined as $\vec{u} = \omega\vec{x}$. In practice we will see that $\vec{u} \approx -\vec{x}$ since the imaginary part is much smaller than the real part for nearly all eigenvalues encountered.

This linear eigenvalue problem can be solved with standard tools for the general eigenvalue problem, although care has to be taken since the eigenvalues and -vectors are complex.

Eigenfrequencies and damping

In general the eigenfrequencies as well as the modes will turn out to be complex. Since the solution to a wave-equation with frequency ω is $\propto \exp(\pm i\omega t)$, the real part of a complex frequency corresponds to the known frequency in the time domain, while the imaginary part states a growth or decay rate (depending on sign) for that frequency.

As there is no unlimited exponential growth in stable physical systems, only eigenmodes with negative damping can be assumed to exist in reality. The contact investigated is only stable if all modes occupied have negative damping without bias. The eigenfrequencies of those modes are investigated while increasing the voltage. Typically, the real part of the frequencies changes only slightly compared to the damping. If the damping has a zero crossing, the mode associated to this frequency will be pumped beyond the description of the system. The voltage connected to such a zero crossing of a previously stable eigenmode of the system is called a runaway voltage V_{thr}.

These runaway voltages are the main result of the current-induced forces calculation. They are an indication how stable the contact is against bias-voltages and allows to compare different structures, metals and approximations done in the simulation.

Simple example

To illustrate the calculations done, we take a look at a simplified system, consisting of only two modes $\vec{x} = (x_1, x_2)^T$

$$m\ddot{\vec{x}} = \begin{pmatrix} \omega_1 & W(V) \\ -W(V) & \omega_2 \end{pmatrix} \vec{x} - \begin{pmatrix} \eta & B(V) \\ -B(V) & \eta \end{pmatrix} \dot{\vec{x}} \,.$$

Here, ω are the eigenfrequencies of the unperturbed phonon mode and η is the electronic friction, connected to the electron-vibration coupling and the damping of the phonon mode. The voltage dependent forces are W, the direct wind force, similar to the electron-phonon scattering rate, and B is the Berry phase of the system, also connected to the scattering of the electrons at the phonons. The voltage dependent forces are calculated linear to first order in the voltage applied to the system. One can view them as the shared effect of transmitted electrons scattering at the vibrations, which transfers energy into the phononic system.

Applying a Fourier transform in the time domain to this equation turns it into a quadratic matrix equation:

$$-m\omega^2\hat{\vec{x}} = \begin{pmatrix} \omega_1 & W(V) \\ -W(V) & \omega_2 \end{pmatrix} \hat{\vec{x}} - \begin{pmatrix} \eta & B(V) \\ -B(V) & \eta \end{pmatrix} i\omega\hat{\vec{x}} \,.$$

Lü et al. [5] calculated the damping $\operatorname{Im}\Omega$ of the complex frequency Ω for a simple two mode system to

$$\operatorname{Im}\Omega \approx -\frac{\eta}{2} + \frac{WB}{2\omega\Delta} \,,$$

where ω is one of the unperturbed frequencies involved and $\Delta = \omega_1 - \omega_2$ is the detuning of the two frequencies involved in the simple two mode system.

Setting this to zero and putting in the linear values from the simulations for $W(V) = W_0 V$ and $B(V) = B_0 V$ gives the threshold voltage V_{thr}:

$$\eta = \frac{W_0 B_0 V_{thr}^2}{\omega\Delta}$$

Or sorted by the threshold voltage:

$$V_{thr} = \sqrt{\frac{\Gamma\omega\Delta}{W_0 B_0}} \,.$$

The threshold voltage behaves as a square root of the electron-vibration-coupling $V_{thr} \propto \sqrt{\eta}$, proportional to the frequency $V_{thr} \propto \sqrt{\omega\Delta} \approx \omega$ and inversely proportional to the combined electron-vibration-scattering $V_{thr} \propto \frac{1}{\sqrt{W_0 B_0}}$.

Simulation example

In order to illustrate what the analysis of the Langevin equation means in practice Fig. 2.2 shows the real (a) and imaginary (b) part of the eigenvalues for a matrix encoding the Langevin equation as in eq. 2.3.1 in dependence on bias voltage applied to the system. The real part, shown in Fig. 2.2(a), of an eigenvalue corresponds to the frequency of an eigenmode and the imaginary part to a damping of that mode. The frequencies (a) of the eigenmodes stay constant with respect to the bias voltage and are in the typical range for the phonon modes of lead (Pb), from which this example is taken. The damping (b) on the other hand is strongly voltage dependent, although only for specific modes.

The voltage at which the damping of a mode changes sign (dashed line in Fig. 2.2(b)) is called a runaway voltage. If there are several runaway voltages, as is often the case, these are sorted by the absolute value and called first, second, third, etc. runaway voltage. This denomination is also transferred to the associated runaway mode, which is the eigenvector to the eigenvalue, and generally a collective motion of the atoms in the contact.

The first runaway voltage is considered the most important one, since the associated mode has the strongest coupling to the nonequilibrium electronic system and is very likely to be involved in any changes in the configuration. Nevertheless, the higher runaway voltages and modes can also have an important influence on the dynamics of the system, since they are coupled to the electronic system and receive energy proportional to the bias voltage. This is especially important if the runaway voltages are close to each other.

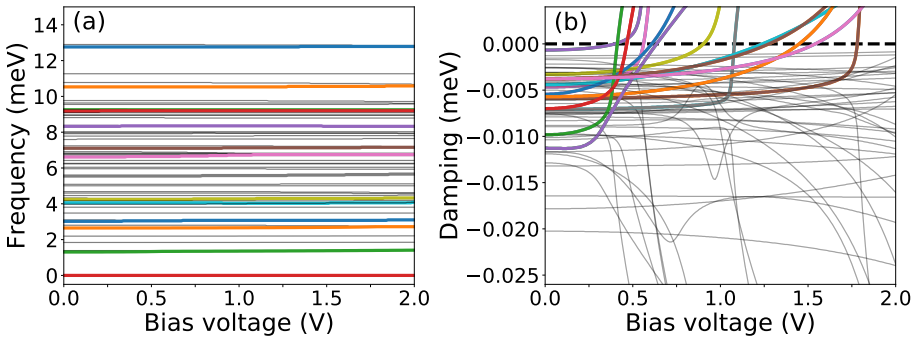

Figure 2.2: Shown are the real (a) and imaginary (b) part of the eigenvalues of the voltage dependent matrix of the Langevin equation for one of the investigated contacts. The real part (a) corresponds to the frequency of an eigenmode and the imaginary part to a damping of that mode. The voltage at which the damping of a mode changes sign (crosses the dashed line in (b)) is called a runaway voltage. The modes exhibiting a runaway voltage are colored.

2.3.2 Langevin dynamics

To understand how systems following equation 2.2 exhibit switching behavior and which influence different parameters like mass and damping have, some test simulations will be presented and discussed in this subsection. Here the important difference between runaway voltages and switching-voltages will be discussed.
Since the integration of the electronic degrees of freedom start at individual scattering events, this process spans the crossover of ballistic to diffusive motion. The time-scale of this crossover is $\propto m$, which makes the role of mass for the dynamics at and before that crossover important.
The effective friction term as a combination of non-conservative forces and equilibrium friction serves as a heat-bath with an effective temperature.

Ballistic and Brownian motion

The processes investigated in current-induced forces span the scales between ballistic movement, whose trajectory extent is proportional to the mass m, and Brownian motion, which governs the long time exploration of the phase space and would be independent of m. The scattering events themselves do not reach the large number required for Gaussian modelling. Crossing the barrier creates a electronic response that should be fast enough to dissipate the energy of the system and dampen the motion of the system into the new minimum.

According to Ref. [5] the force-force correlation function is

$$\langle f_\alpha(t) f_\beta(t') \rangle = \frac{\eta_{eq}^{\alpha\beta}}{2\pi} k_B T \ .$$

When the energy scale of the bias is much greater than the phonon and thermal energy scales $eV \gg \hbar\omega, k_B T$, the force-force correlation behaves proportional

to the bias eV [5], which then serves an effective temperature scale. Integrating the Langevin equation in the 1D case ($\eta^{\alpha\beta} \to \eta$) gives a space-autocorrelation function of

$$\langle \Delta x^2(t) \rangle = \frac{2k_B T}{\eta} \left(t - \frac{m}{\eta} + \frac{m}{\eta} e^{-\eta t/m} \right) .$$

In the long-time limit, this results in the Einstein-Relation for the Diffusion-"constant"

$$\frac{2k_B T}{\eta} t = 2Dt .$$

In the ballistic limit one gets

$$\langle \Delta x^2(t) \rangle = \frac{k_B T}{m} t^2 = D_{eff} t^2 ,$$

where the relevant time scale to divide these two regimes is $\tau \approx m/\eta$. In the crossover regime around $t \approx m/\eta$ one can assume similar temperature scales.

As an example, aluminum has an eight times smaller mass and an about two times stronger electron-phonon coupling η compared to lead. This reduces the time scales on which the ballistic motion used for the runaway voltage is relevant by a factor of at least 8. For aluminum has a four times higher "effective" diffusion coefficient $D_{eff} = \frac{k_b T}{m}$. This diffusion coefficient is the relevant parameter to describe the dynamics of the structure. Its effect is similar to a four-fold reduction of the barrier heights.

Switching

For the switching process itself there is not just the anisotropy of the generalized Langevin equation, but also the anisotropy of the structure given in the Born-Oppenheimer potential surface that has been linearized for the runaway voltage approach. To illustrate this, we assume an atom whose vibration along an axis is pumped. It now matters a lot how the potential along that vibration mode is formed: If the potential is flat and the atom is free to move, it will most likely move away from its position very quickly and all approximations and calculations done there are invalid. In that case one can not know in which of the two possible directions of the runaway mode the atom will move.
However, if there is another atom at rest in one direction of the runaway mode the trajectory of the mode will be changed by higher order terms in the interaction and the phase space will be explored differently. Being hemmed in on both sides typically means a dissipation of the excited mode, either in another mode of the atom or as a propagating excitation into the atomic system.

Switching model

To illustrate the properties of the Langevin equation relevant to switching - anisotropy of the trajectories and effective heat bath - we construct a simple 2D model system consisting of a particle with coordinates $\vec{x} = (x, y)^T$, where both coordinates obey a Langevin equation[5, 7] of the form:

$$m\ddot{x} = -k(x - x_0) - \gamma\dot{x} + \sqrt{2k_bT\gamma}W(t) \tag{2.4}$$

The system propagates in a potential consisting of two harmonic minima at $\vec{x}_1 = (1, 1)$ and $\vec{x}_{-1} = (-1, -1)$. The relevant potential is switched at at the line of same distance from both minima.

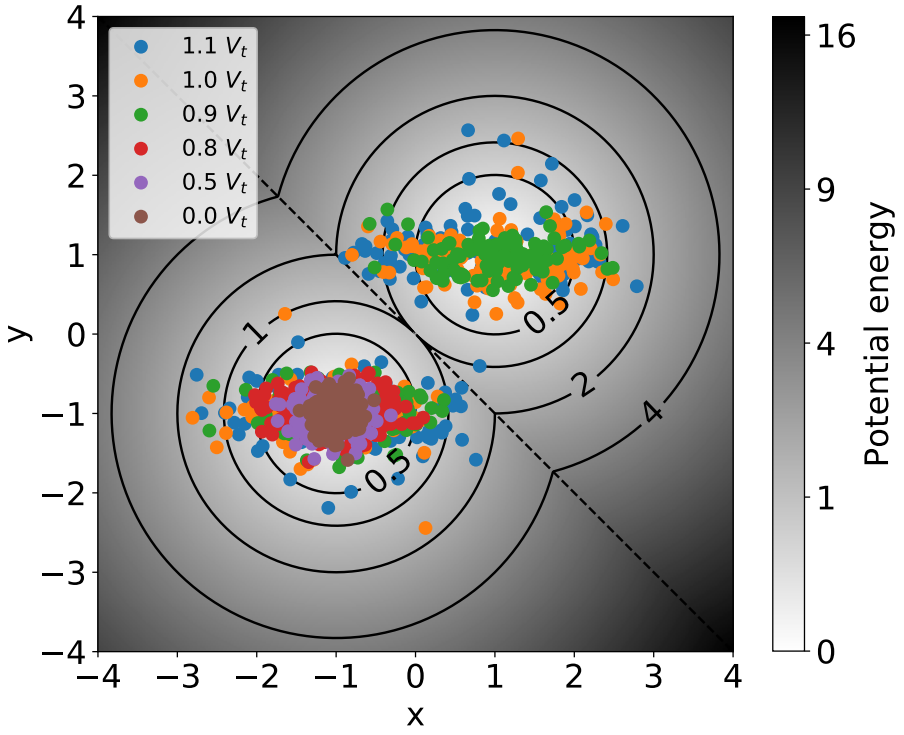

Figure 2.3: Sample trajectories of a Langevin model simulation. The model system consists of two harmonic minima at $(1, 1)$ and $(-1, -1)$ whose sphere of influence is their half-space delimited by the diagonal drawn as a dashed line. The trajectories under different voltages are started at the minima at $(-1, -1)$. With increasing voltage the trajectories become anisotropic and start leaving their starting minima at $0.9V_{thr}$. The simulation model parameters are $m = 2$, $k = 1$, $\eta = 0.1$, $k_BT = 0.01$, $c = 0.1$.

For this model simulation we neglect the generalized part of the Langevin equation and do not resolve time-scales below delta-correlated force-noise. Therefore, the force noise term $\sqrt{2k_BT\gamma}W(t)$ fulfills the classical fluctuation-dissipation theorem. The friction couples the system to a heat bath with energy k_BT simulated through a normally distributed Wigner process $W(t)$. Additionally the

system is coupled through the friction and force noise terms to a non-equilibrium electronic system with energy scale V.

What is really added to the model simulation are non-conservative forces. That means the dynamical matrix k and the friction matrix γ contain voltage-dependent anti-symmetric terms, which can turn the system non-conservative, allowing energy to be pumped into the system in excess of its ability to dissipate it. To model this the friction term in x-direction is set to be voltage dependent in a form $\gamma(V) = \gamma_0 - c \cdot V$ with $V_{thr} = \frac{\gamma}{c}$ as the defined voltage at which the sign of the friction term changes from damping to pumping. The fluctuating term increases with voltage according to $\sqrt{2k_bT\gamma_0 + c_D \cdot c \cdot eV}$.
In Fig. 2.3 simulated trajectories of this system are shown. With increasing voltage these trajectories grow more extended especially in the direction of decreasing friction. When the trajectory crosses the diagonal there is a high likelihood for relaxation into the other minimum.

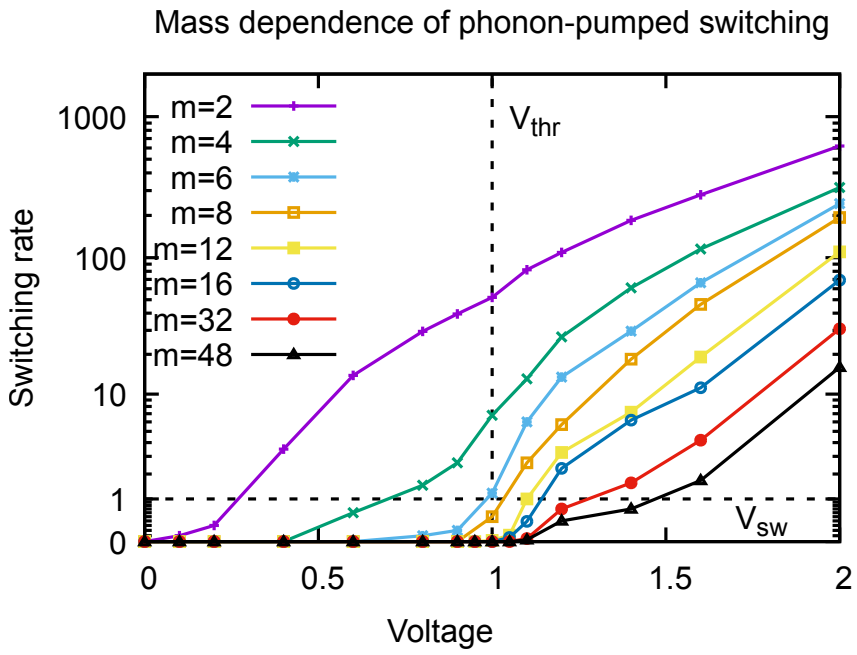

Figure 2.4: Switching rates for model simulations with different masses drawn over voltage applied to the system. The voltage at which the switching rate exceeds 1 per million time steps is defined as a switching voltage V_{sw}. The overall switching rates decrease with increasing mass, and for higher masses a voltage exceeding the runaway voltage is necessary to switch the system.

In equation (2.4) the whole right side scales with the inverse of the mass. This changes the phonon frequencies $\sqrt{k/m}$ and momentum relaxation times m/γ but leaves the overall extent of the trajectories independent of mass. The time scales are nonetheless changed by a factor $\propto m$, heavier particles move slower through those trajectories. This is a property of the over-damped classical system - in the ballistic limit the trajectory extent in a harmonic oscillator is

proportional to the inverse square root of the mass $\sigma_r \propto m^{-1/2}$, same as for the quantum-mechanical harmonic oscillator.

If one assumes a $m^{-1/2}$ dependence of the fluctuating forces, one gets a mass dependence of the switching rates that is not just a time scaling. This is shown in Fig. 2.4. There are two different exponential growth regimes - before crossing the threshold voltage, additional voltage acts as an effective temperature making switching more likely. After crossing the threshold voltage the mode leading to switching is effectively pumped, boosting the switching rate considerably.

2.4 Summary

In this chapter the derivation and calculation of current-induced force matrices as previously presented in the literature [5, 6] was followed to derive a Langevin equation. Especially notable here was the wide-band approximation stating that transport properties can be developed for the bias from the behavior at the Fermi energy. The wide-band approximation is most likely valid in metals for the electrons and would need quite strong electron-vibration coupling to be valid for electron-vibration scattering, which is true for certain metals.
A temperature of zero was also assumed, which is tricky because the Langevin equation has a noise term dependent on temperature. This noise term can also come from quantum-fluctuations or scattering events, which would turn it non-gaussian. This means that the large number of independent random events needed to get the fully gaussian behavior has not been reached - instead of a random force with continuous, gaussian behavior one would need a treatment of individual scattering events transferring energy quanta between the systems. For most of the discussion of the noise terms of the Langevin equation this term was therefore neglected and the focus lay specifically on the effect of bias voltage on the Langevin equation describing the atomic system.
The most important result of this chapter are the runaway voltages. They are an indication of the contact's stability against bias-voltages and allows one to compare different structures, metals and approximations done in the simulation, which bases to take, and how to calculate different parameters. Those runaway voltages were calculated for break junctions of different metals, results of which are presented in the next chapter.

Chapter 3

Runaway voltages in metallic contacts

This chapter presents simulation results for a set of metallic contacts with a focus on creating a reasonable sample of contact geometries and investigating how the runaway voltage behaves as an indicator for the contact stability for the different metals and structures. The investigated metals are gold (Au), aluminum (Al) and lead (Pb).

The first section presents the simulation setup, how the individual contacts were created, and what the important results are using an example contact series of lead. The important results for a single contact are the electric transmission and the runaway voltages. The transmission can be resolved back into the individual transmission channels, whose distribution is a signature of the contact [37–40]. The runaway voltages as presented in the last chapter are the fundamentally new result of this work. A contact typically has several runaway voltages of which the smallest one is considered the most important for the behavior of the contact. To get an overview the five lowest runaway voltages are presented for most contacts.

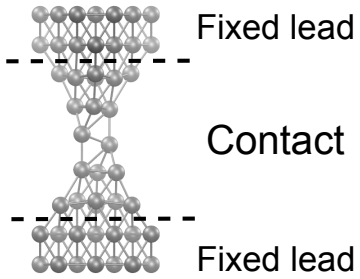

Figure 3.1: Example Pb contact.

The second section presents the results of all metals and discusses their differences and similarities. The transmission for the contacts simulated is mostly between 0 and 6 G_0 with some configurations reaching 10 and above. The runaway voltages calculated are in the range of slightly below 100 mV up to significantly above 1 V, which is also the range observed for experimental switching voltages [8, 13].

3.1 Simulation setup

As an example to investigate the current-induced forces formalism and the relevance of runaway voltages for real systems, metallic atomic contacts were chosen. This example system allows us to compare with experiments and use prior work done in creating sufficient samples [15, 18]. A discussion of other possible example systems for electromigration is given in the appendix A.

The metallic contacts simulated consist of a central region, contacting leads, and a description of the bulk electron density. The central region is the contact investigated in depth and the positions of its atoms are flexible. This is different for the leads, whose atomic positions are fixed in an ideal crystalline configuration. The leads are necessary to calculate a coupling of their electronic states to those in the contact. The electronic states of the lead are then replaced with those of the bulk description [41].

The central region consists of only around twenty atoms between crystalline layers fixed at a certain distance between 5 and 20 Å. This construction allows for a wide range of possible structural configurations, several of which can be stable against atomic displacements.

To investigate the switching process in simulations several distance series of break contacts of Al, Au and Pb needed to be set up. The form and the distance of the lead layers is the primary control parameter of this setup. Any method applied produces a contact structure contingent on these boundary conditions - in Molecular Dynamics (MD) by creating a trajectory of a certain temperature and in Density Functional Theory (DFT) by minimizing the potential energy of the contact structure.

This can be started by setting up the contact in LAMMPS [42] with embedded atom method (EAM) inter-atomic potentials [43, 44], having 7 layers in the z direction, of which the outer two on both sides are fixed in the crystal structure. The outer layers are then moved away from each other. This leads to a thinning of the contact until breaking. The contacts simulated consist of around $60 - 80$ atoms, of which around 20 are mobile.

All structures created are fed into the DFT program package TURBOMOLE [45] to first relax the structure under the constraints of DFT. The functional used for all calculations is the one defined by Perdew, Ernzerhof and Burke (PBE) [46]. The basis sets chosen are a split valence polarization (def-SVP [47]) for gold, and triple zeta valence polarization (def-TZVP [48]) for lead and aluminum[1]. This structure relaxation is necessary in order to get the ground state electronic and phononic structure as well as the electron-vibration coupling [4][2].

All of these are needed for the calculation of the electronic transport and the current-induced forces as described in ch. 2. This is done in our nonequilibriums Greens function (NEGF) code to calculate all of the parameters of the Langevin equation in dependence of an applied voltage in the wide-band limit.

As an important parameter, threshold voltages V_{thr} were identified by a change of sign in their damping - at voltages higher than this threshold, modes which were previously damped are instead pumped by the scattering of the nonequilibrium electrons. This leads to a runaway excitation of that vibrational

[1] See appendix B for computational details.

[2] See appendix C for details regarding phononic spectra and electron-vibration coupling.

mode. The central investigation of this chapter is the determination, whether that threshold or runaway voltage is a relevant parameter for real systems. That means, if this calculated runaway voltage is in ranges comparable to experimental switching voltages and behaves similarly between metals and contact geometries. Similarity here indicates that the runaway voltage and therefore active pumping of phonon modes is a relevant mechanism for nano-scale switching and electromigration.

3.1.1 Contact setup

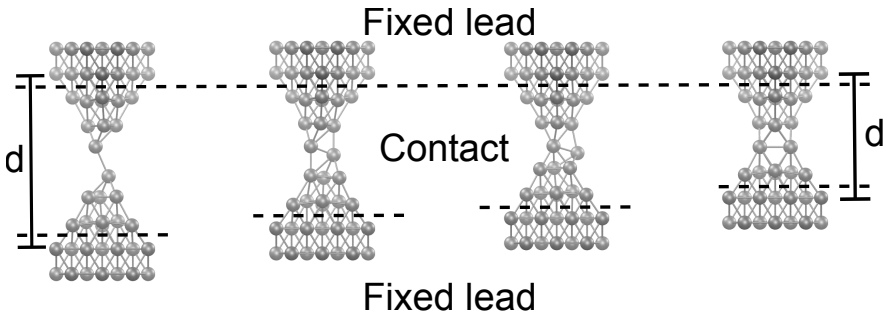

Figure 3.2: Some relaxed structures of a lead push contact (Pb DFT 111) with distances between the fixed leads of $d = 19.7$, 17.8, 16.5 and 14.5 Å from left to right.

The basic process of creating a contact is setting a distance between the leads and then relaxing the central part of the contact structure. Example structures resulting from that are shown in Fig. 3.2. Small changes of this distance should lead to quasi-adiabatic processes moving along the current local minima in the energy landscape. The forces acting on the boundary conditions are ignored in the setup used here, although some approximation of those forces can be extracted from the derivative of the total energy with respect to distance.

Structural changes happen beyond a linear response and change the structure significantly in a mechanical switching process. Especially around those mechanical switching distances hysteretic behavior can be found, where the configuration assumed at that distance is dependent on the direction from which it was approached. These distances are interesting for other switching investigations because at least two metastable configurations in the phase space exist for the same boundary conditions.

Overall there are two broad classes of switching methods: Mechanical switching, e.g. by changing the distance [15, 18], and electronic switching e.g. through current-induced forces. In this chapter the stability of mechanically created contacts is investigated with respect to current-induced forces.

There are several ways to create a sample of contacts to simulate. The two start configurations used here are a perfectly crystalline slab that will be pulled apart, and pyramid structures, which are then pushed against each other. The pushing and pulling process is done by reducing or increasing the distance between the crystalline layers in small steps and letting the structure in between relax. There are other control parameters like orientation and lattice offset, but

for the studies in this thesis the distance of the crystalline layers is the primary control parameter.

3.1.2 Example contact

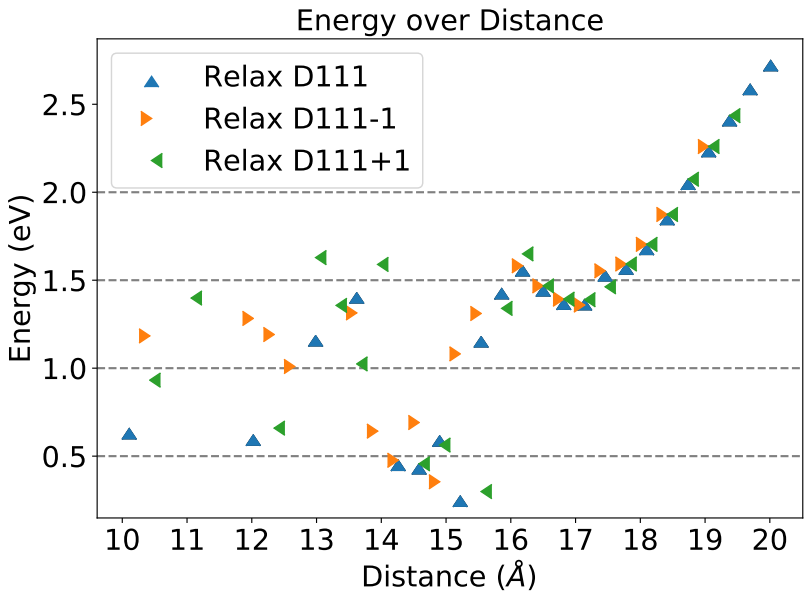

Figure 3.3: This figure shows the change in total energy of a relaxed lead contact structure (Pb DFT 111) over distance. The different colors indicate different initial configurations. D111 is the initial relaxation and for ± 1 the relaxed structures of D111 of one distance step less or more were used. The energy scale used here is relative to the minimal value of all contacts +150 mV.

The Pb structures discussed here were created from a DFT-relaxed gold push contact, by first changing the atom types and rescaling the atom distances according to their respective lattice constants. The structures were then relaxed again in TURBOMOLE.

For some contacts and distances there is only a single optimal structure at a certain distance. However, there are quite often several metastable states, and finding the optimal configuration would require changes extending into the lattice.

Energy

To get an understanding of the changes that such a process entails, Fig. 3.3 shows the overall energy of lead contacts at different distances.

Overall, the energy is lower with smaller distances between the layers, since the crystal structure is energetically preferred. One can imagine this as a minimization of surface tension, although this continuum picture is prone to errors in these atomic structures.

For the larger distances, the energy of the contacts describe a nearly parabolic behavior with a local minimum around 17 Å. Here the contact gains potential energy by closing the distance between tip lead atoms until it starts to apply pressure to the system, which increases the energy again and finally leads to a restructuring of the contact.

This minimum seems very stable against the pull process and a harmonic approximation could be done around that minimum to get an effective spring constant of the contact. At distances between 18 and 20 Å the energy behaves nearly linear with distance, which gives a constant force of around $0.5\,\mathrm{eV\,Å^{-1}} \approx 0.8\,\mathrm{nN}$. This force is in similar ranges as the experimental force values from a comparable experiment for gold of $2 - 10\,\mathrm{nN}$ [49], where they also found a constant force on the last conductance plateau before rupture.

For the area between 16 and 17 Å one can assume a quadratic dependency of the energy on the distance and calculate a force constant with

$$k = \frac{2\Delta E}{\Delta x^2} \approx \frac{2 \cdot 0.18\,\mathrm{eV}}{(1\,\text{Å})^2} \approx 0.29\,\mathrm{nN\,Å^{-1}}\ .$$

This fits to an energy scale of $E = \hbar\omega = \hbar\sqrt{\frac{k}{m}} \approx 2.7\,\mathrm{meV}$ with the mass of lead of 207 u. This energy scale fits very well to the lower vibration energies of lead in such contacts.

At distances smaller than 16 Å the energies do not behave continuously with the distance. This is visible in a broad scatter in energy of overall 1.5 eV and up to 1 eV at the same distance. It is important to state at this point that all of the structures found are local minima of the energy of the electron density functional.

Transmission and conductance

Figure 3.4 shows the transmission of electrons transmitted at the Fermi energy over the distance of the crystalline boundary layers. This overall transmission T is equivalent to a conductance of the same number in conductance quanta

$$G = \mathrm{G_0}T = \mathrm{G_0}\sum_i \tau_i$$

and can be broken down into conductance channels i of transmissions $0 \leq \tau_i \leq 1$. What is shown in the figure corresponds to what is called a conductance trace in Mechanically Controlled Break Junction (MCBJ) experiments [21]. In experiments it is only possible to determine relative distance by how much the piezo elements move the sample, so a direct comparison of distance curves is not possible, although the ranges would be interesting.

The conductance goes down with larger distance, from around 7 to a plateau between 16 and 18.5 Å at $2.5\,\mathrm{G_0}$, which then breaks down fast. Lead has four valence electrons of which only few contribute significantly to the conductance. Overall the $2.5\,\mathrm{G_0}$ conductance value lies well within experimental ranges [50].

Even on the observed plateau, where the conductance is stably reproduced, the conductance can still vary quite a bit for certain contacts. At a distance of 17 Å, in the middle of the plateau, states of different conductances can be observed. Especially at the contacts with a distance slightly above 17 Å a minuscule energy difference leads to a transmission difference of nearly $1\,\mathrm{G_0}$ in the

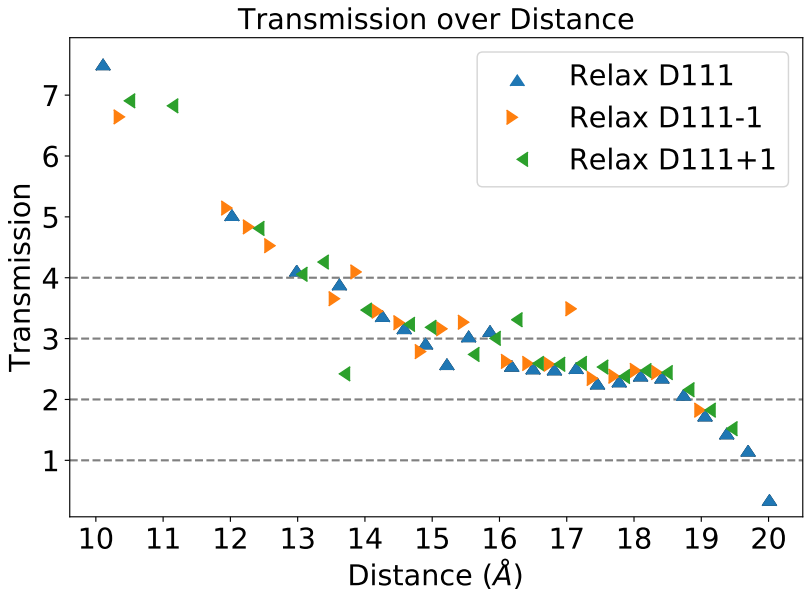

Figure 3.4: This figure shows the electronic transmission of a relaxed lead contact structure (Pb DFT 111) over distance. The different colors indicate different initial configurations before the relaxation. D111 is the initial relaxation and for ±1 the relaxed structures of D111 of one distance distance step less or more were used. Transmission larger than 1 are due the addition of different transmission channels.

D111-1 contact. At distances smaller than 16 Å nearly every distance shows states of different energy and conductance. The conductances stay within reasonable deviations, so these values are useful in statistics. At distances smaller than 12 Å the relaxation routine of TURBOMOLE has problems finding a suitable structure, most likely due to the closeness of the fixed boundary conditions and the complicated crystal structures possible there.

Runaway voltage

Fig. 3.5 shows the lowest runaway voltage for the contact. The runaway voltages are in the range between 50 and 250 mV for most distances. The left picture shows the exception to that rule, the nearly broken contact at ≈ 20 Å has a runaway voltage at over 1 V, considerably above all contacts of higher conductance.

The runaway voltage typically increases a lot shortly before rupture. This happens for all metals investigated, as will be seen later. The transmitting channels are coupling less strongly to the vibration of the atoms. One can imagine the electrons tunneling through the contact largely without interacting with the atoms of the contact.

The scatter in the runaway voltages is significant, as it is for all investigated contacts. The runaway voltage is not just very sensitive to the distance, but also to different energies at the same distance. On the conductance plateau between

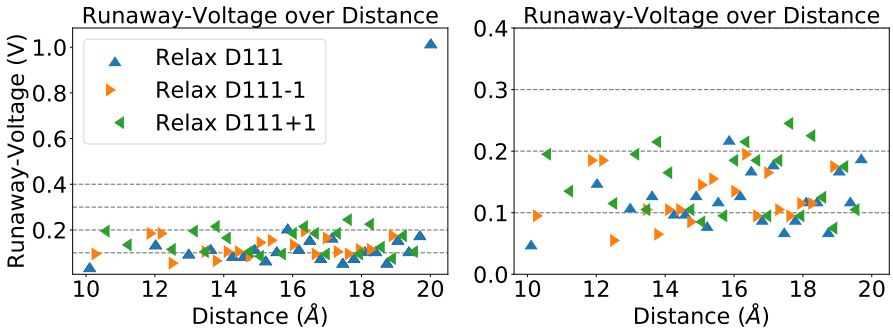

Figure 3.5: This figure shows the lowest runaway voltage of a relaxed lead contact structure (Pb DFT 111) over distance. The right picture is a zoom of the left. D111 is the initial relaxation and for ±1 the relaxed structures of D111 of one distance step less or more were used. The scatter of the data points is quite strong, but there are several distances where at least two of three contacts' runaway voltages coincide (shown by the touching tips of the triangular markers).

16 and 19 Å (see Fig. 3.4), where the transmissions are nearly the same, the range of the scatter is smaller, with most runaway voltages being within 25% of each other.

There are nevertheless special cases like the point where the runaway voltages are very different for almost identical transmissions and energies. For example slightly above 17.5 Å, where the runaway voltages are 80, 110 and 245 mV for transmissions at 2.342, 2.346 and 2.533 and energies of +23 µeV, ±0 and −90.84 meV. When changes in the µeV-range can create changes of such magnitude in a derived parameter the modeling limits of density functional theory are reached and results of single simulations are no longer enough to draw conclusions. Only by sampling the phase space of the calculations and drawing statistics over those sample sizes larger than one single pull-curve one is able to investigate this value more in depth.

3.2 Contacts of different metals

In this section the results for the simulations for gold, lead and aluminum contacts are presented and discussed. The main focus is again on the conductance and the runaway voltages. The transmission is additionally split up into the transmission channels to allow a more in-depth analysis. For the runaway voltage the five lowest voltages per contact are presented with decreasing color intensity from lowest to highest.
The contacts are largely divided into push contacts (DFT) and pull contacts (MD). In the push contacts perfect, DFT-relaxed pyramids were pushed into each other. In the pull contacts the structures were pulled apart from the perfect crystal in MD and then relaxed in DFT.

3.2.1 Lead contacts

Figures 3.6 and 3.7 show transmissions and the first five runaway voltages for different distances of several simulated lead push 3.6 and pull 3.7 contacts.

Figure 3.6 shows the channel transmissions, overall transmission, and the five lowest runaway voltages for a lead push contact. The contact consists of two pyramids in [111] crystal direction being pushed into each other. For the geometries see fig. 3.2. The first column shows the result of the relaxation of those configurations.

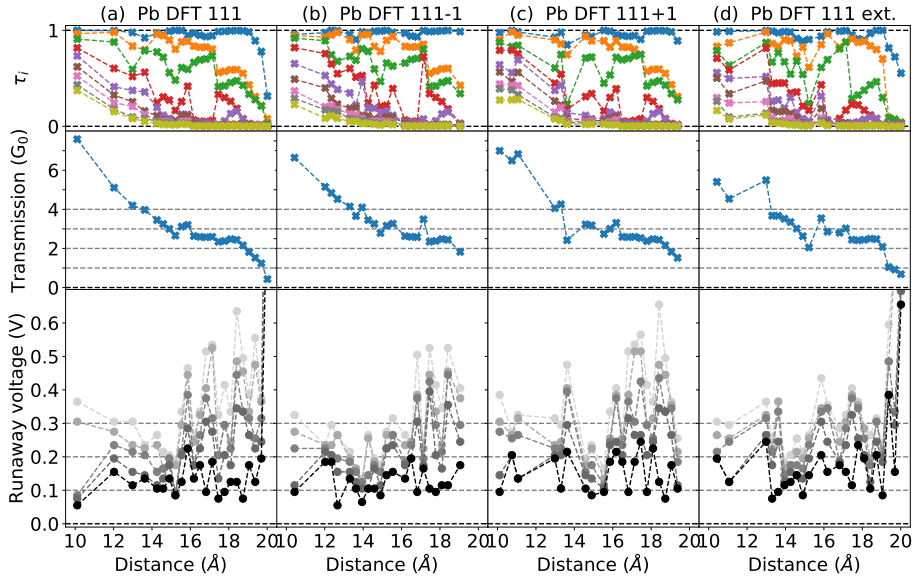

Figure 3.6: Transmission channels (top), transmission (middle), and the 5 lowest runaway voltages (bottom) for a simulated lead push contact. This contact is created by pushing two pyramids in [111] direction into each other. The first column (a) shows the initial relaxation, the second and third column (b+c) show results of subsequent relaxations after changing the boundary layers, and the fourth column (d) shows the results after extending the boundary layers by 20 atoms each.

The conductance values are in ranges that would be expected from experiment [8]. Conductance plateaus around $3G_0$ can be found, especially for the leads in [111] crystal direction, Fig. 3.6 and 3.7(a). The runaway voltages (bottom panels) have significant scatter with the lowest one being around $100 - 200\,\mathrm{mV}$ consistently for all contacts.

In the central panel of Fig. 3.6 an extended conductance plateau at around $2 - 3\,G_0$ is visible. On this plateau runaway voltages scatter a lot until they increase shortly before rupture. Less transmission means less overall scattering into the phonons and due to that a higher runaway voltage.

Although the distances are chosen to be equidistant, there are several holes in the plots. These are related to distances where the relaxations did not converge. This non-convergence is quite common for these small metallic contacts and even starting from converged configurations and exchanging the boundary conditions, as depicted in the second and third column, does not guarantee convergence. Distance changes can lead to other stable configurations by introducing small changes in the boundary conditions. Around these switching events hysteresis is likely to appear.

The fourth column of Fig. 3.6 shows simulations where the boundary layers were extended to check the influence of boundary sizes. This extension was done in width as well as depth of the boundary layers, nearly doubling the number of atoms simulated with an associated factor of $4 - 8$ in the required calculation time. The conductance values in the central panels stay quite similar. For the shorter distances there are less relaxed structures. The first runaway voltage in the lower panels stays in the same range of around $100 - 200\,\mathrm{mV}$, though the second and higher runaway voltages are visibly decreased on the conductance plateau between 16 and 19 Å.

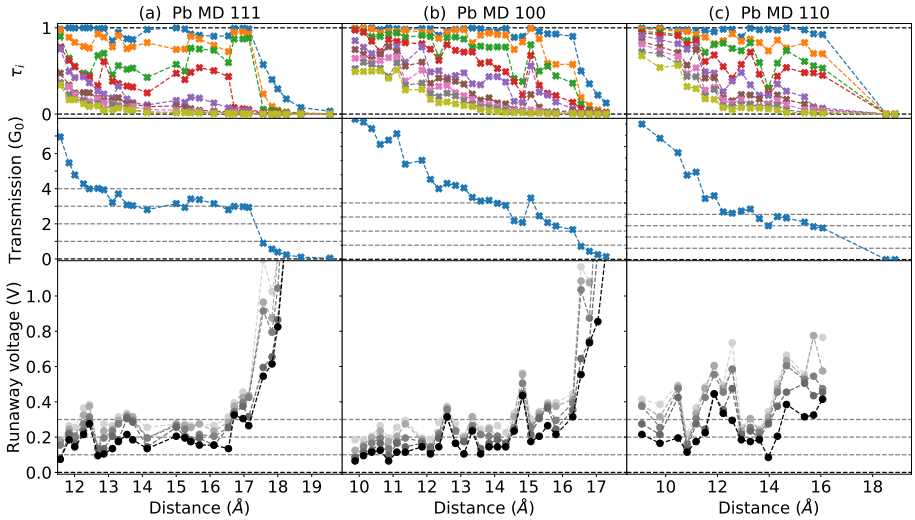

Figure 3.7: Channel transmission (top), transmission (middle), and runaway voltages (bottom) of simulated lead pull contacts. The contacts are pulled from a perfect crystal in [111] (a), [100] (b) and [110] (c) direction.

Fig. 3.7 shows the transmission and runaway voltages for another set of contacts. These contacts are pull contacts from a perfect crystal in [111] (a), [100] (b), and [110] (c) direction respectively. The contacts were created and pulled with LAMMPS using EAM potentials and these structures were then relaxed into local energetic minima using TURBOMOLE.

The scatter of the runaway voltages is lower for the MD pre-created pull contacts. The different orders of runaway voltages are also closer to each other. This conforms to earlier experiences with MD pull contacts [15], indicating that MD pull contacts tend to produce smoother, more continuous changes in the structures. That means that the plateaus seen in experiment appear less often in simulated pull contacts. The most likely reason for that is an additional relaxation and smoothing in the MD in excess of that happening in experiment. Nevertheless these are structures relaxed in DFT, so they are candidate contacts.

As with the push contact, the [111] direction exhibits a conductance plateau at $3\,G_0$ with the first runaway voltages in a similar range of $100 - 200\,\mathrm{mV}$ and an increase for for distances shortly before the contact breaks. No relaxed structures were found for the distances on the plateau between 14 and 15 Å. At the end of the plateau one sees a nearly perfect transmission of the first three transmission channels with a fourth only appearing below 17 Å. The appearance of that fourth channel coincides with a reduction of the transmission of the first three transmission channels, leaving the overall transmission at $3\,G_0$.

The [100] and [110] directions are largely unremarkable, yielding only more statistics. The [100] direction exhibits a plateau at $4\,G_0$ between 13 and 14 Å. The contacts between 14 and 16 Å show similar transmission signatures, although several distances did not relax there. In the [110] direction the interesting area for single atom contacts between 16 and 18 Å is bereft of stable structures.

Summary Pb Overall Pb gives a good overview of most properties of the simulated contacts. It additionally serves as a testbed for some other variations, like relaxing the same distance for different intial configurations and extending the leads. The calculated conductances are quite stable, but - due to their larger scatter - runaway voltages absolutely require statistics using different contact configurations.

3.2.2 Gold contacts

Gold contacts are the typical testbed for conductance calculations, since their very simple electronic structure as an s-conductor has several properties making them very suitable for theoretical and simulational approaches. Gold is not chemically reactive, its atomic structure is very stable at low temperatures, and it exhibits well separated conductance plateaus with nearly constant, quantized conductance [39].

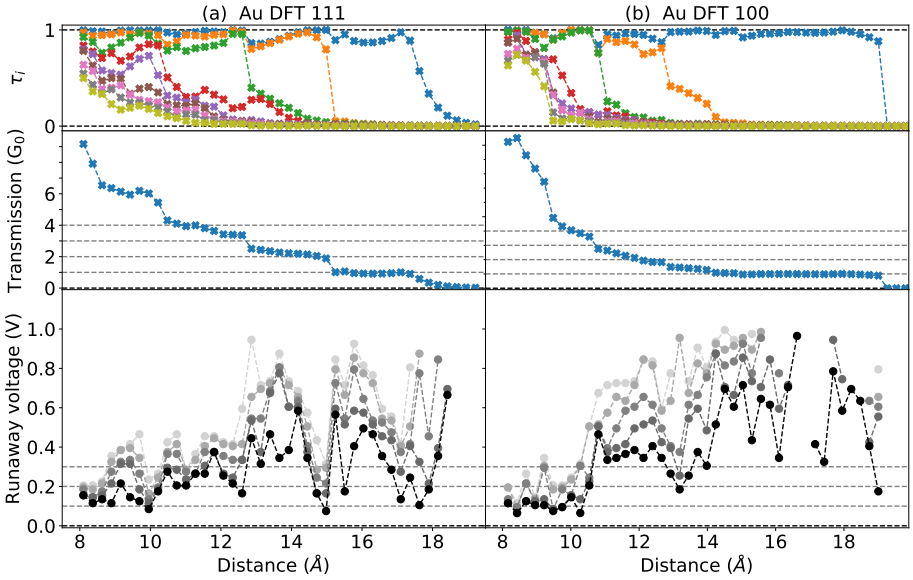

Figure 3.8: This figure shows channel transmission (top), transmission (middle) and the 5 lowest runaway voltages (bottom) of simulated gold push contacts. These are DFT-created structures with the leads in [111] (a) and [100] (b) crystal directions.

These conductance plateaus can be seen for the simulated gold push contacts shown in Fig. 3.8. Especially in [111] direction the simulations exhibit nearly perfect conductance steps jumping from nearly zero transmission to one at 13, 15 and 17 Å. The runaway voltage shows no clear correlation with the plateaus. Mean and variance of the runaway voltage decrease overall with increasing conductance and decreasing distance. This is different for the distances close to a switch of plateaus, where the runaway voltage tends to scatter more than on the plateaus on both sides. This may be due to the comparatively stable electronic structure, with similar electronic occupation and scatter on the plateau. The stretching phonon mode of the contact does not seem to be strongly involved in the current-induced forces, since there are no changes over fundamental variance in the runaway voltages on the plateau.

For the [100] direction the long $1\,G_0$ plateau exhibits overall higher runaway voltages, again with significant scatter. For some configurations around 17 Å the electron-phonon scattering gets so low that no runaway voltage could be found in the investigated voltage ranges.

Both of the DFT push contacts exhibit a low runaway voltage of slightly

above 100 mV for distances less than 10 Å and conductances above 4 G_0. For smaller distances the runaway voltage tends to increase.

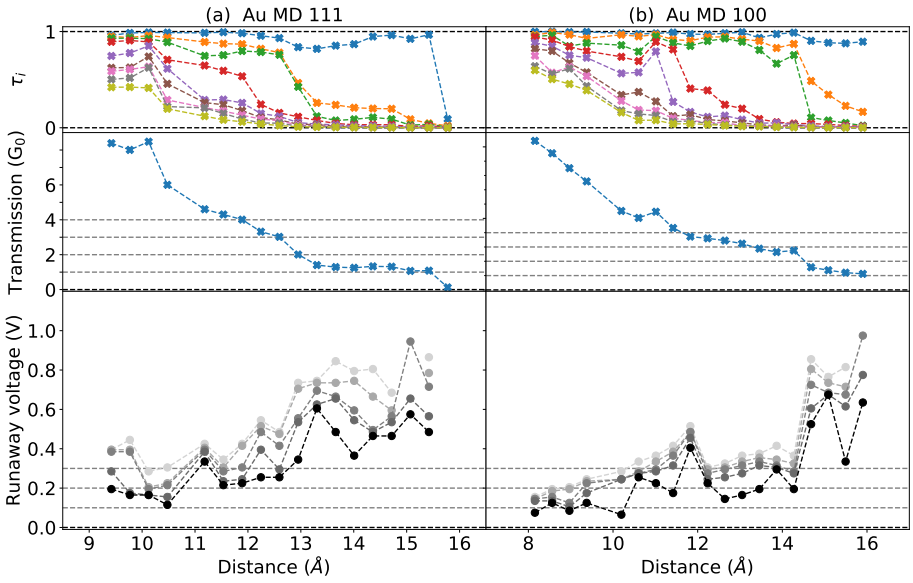

Figure 3.9: Shown are channel transmission (top), transmission (middle) and the 5 lowest runaway voltages (bottom) of simulated gold pull contacts. These are MD-created structures with the leads in [111] (a) and [100] (b) crystal directions.

This increase of the runaway voltage with distance is very visible in the pull contacts (MD) in Fig. 3.9. The scatter of the runaway voltages is broad, but the overall tendency is an increase for contacts with smaller conductance. The conductances for the pull contacts exhibit less clear plateaus than the push contacts. Nevertheless plateaus are still visible, e.g. a 1 G_0 plateau in 3.9 (a) from 13 to 15.5 Å and in 3.9 (b) a 1 G_0 plateau from 15 to 16 Å as well as a 3 G_0 plateau from 12 to 14 Å. On most of these plateaus additional channels appear at the midway point and open further with shorter distances, even though these channels do not open fully until the contacts switches to the next plateau.

Summary Au The gold contacts provide an avenue of a more specific comparison through their comparatively stable configurations and well developed plateaus, as well as a broader base to compare against through their ubiquity in experiments and other simulations. The runaway voltages are in the ranges of experiment and continue to vary strongly from contact to contact. Specifically for gold the runaway voltages decrease with increasing conductance, something that was not seen in lead.

3.2.3 Aluminum contacts

Figures 3.10 and 3.12 show transmissions and the first five runaway voltages for different lead distances of several simulated aluminum contacts. The conductance values are in the ranges expected from experiment [37]. Overall the runaway voltages of aluminum are higher than those of the other materials investigated, which is why the plots of the runaway voltages go up to 1.7 V instead of the lower values of the other metals.

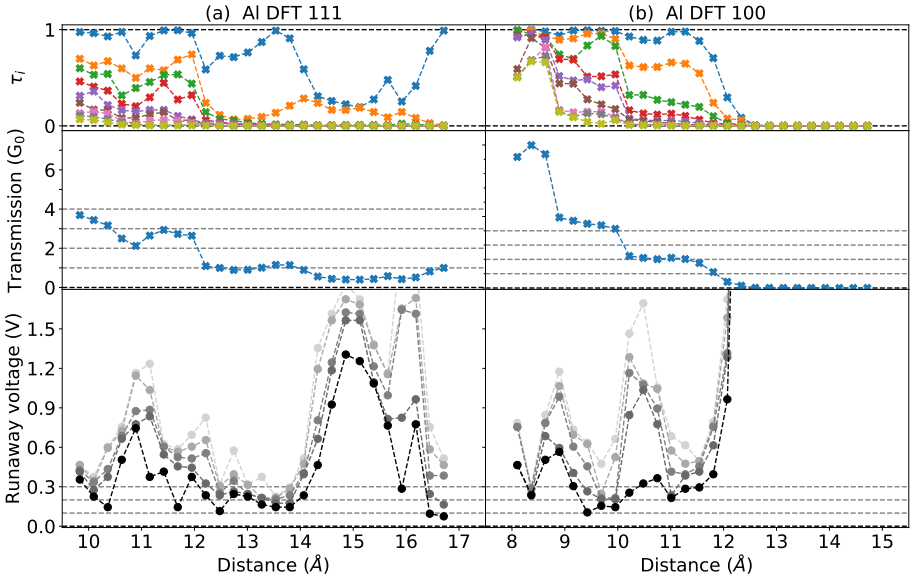

Figure 3.10: Shown are channel transmission (top), transmission (middle) and the 5 lowest runaway voltages (bottom) of simulated aluminum push contacts. These are DFT-created structures with the leads in [111] (a) and [100] (b) crystal directions.

Fig. 3.10 shows two DFT created push distance curves with leads in [111] (a) and [100] (b) direction. The conductances are in the same range as experimental data and exhibit clean steps. The runaway voltages of these push contacts are mostly between 100 and 300 mV, but there are peaks up to 700 mV and even 1.7 V. This may be due to a lower electron-vibration scattering at the Fermi energy due to the higher phonon frequencies of aluminum.

The conductance plateaus are very pronounced, especially the [111] direction in Fig. 3.10 (a) shows an extended 1 G_0 plateau between 12 and 17 Å. On this plateau the conductance of the highest transmission channel dips below 0.5 around 15 Å before it increases again to 1 shortly before rupture. There is also a 3 G_0 plateau between $11 - 12$ Å where the channel distribution indicates the addition of a second atom to the contact region. This contact is the focus of Fig. 3.11.

Figure 3.11 shows the aluminum push contact in [111] direction together with a selection of configurations (b-f). The configurations at the top (b+c) show the switch from the single atom contact to a two atom contact. The configurations at the bottom (d-f) focus on the dip in the transmission and the extraordinarily

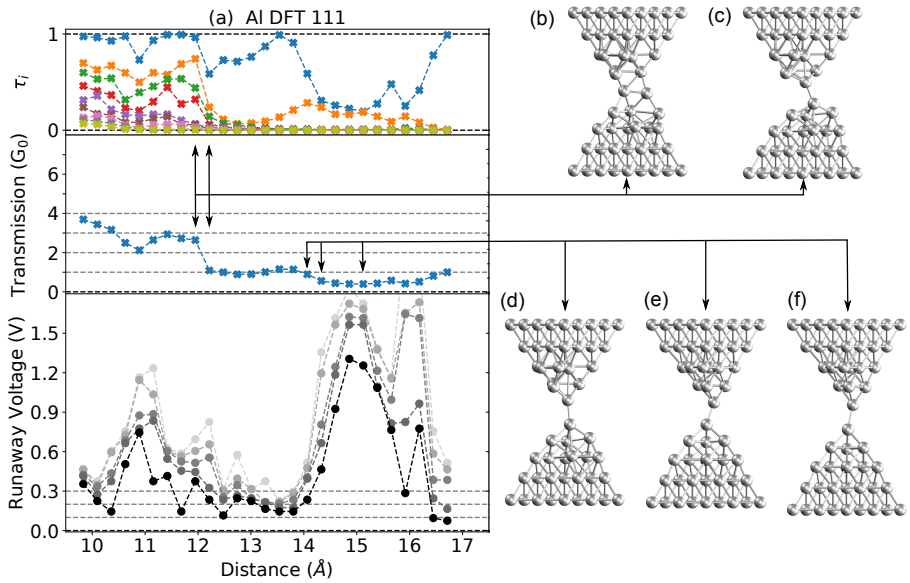

Figure 3.11: Shown on the left are channel transmission (top), transmission (middle) and the 5 lowest runaway voltages (bottom) of the simulated aluminum push contact in [111] direction from fig 3.10(a)). The right side shows a selection of configurations.

high runaway voltage. The perfect pyramids at higher distances (f) seem to have a very low electron-vibration scattering leading to a high runaway voltage. The electron-vibration scattering and the runaway voltage increases, when the pyramids are pushed together enough such that they apply pressure on each other (e) and finally relax into a slightly distorted configuration (d).

On the $1\,G_0$ plateau in the DFT [111] contact (pyramids (f) and the rightmost arrow in Fig. 3.11) the first runaway voltage exhibits a peak reaching over $1.2\,V$ around $15\,Å$. This is consistent with experimental work, in which it was found that aluminum contacts around $1\,G_0$ are sometimes stable to higher voltages and currents than contacts of higher conductance [13]. The third to fifth runaway voltages also all exhibit a peak around $16\,Å$ with a large separation between the second and third runaway voltage.

An even stronger separation of the first and the higher runaway voltages is found in the DFT [100] contact (Fig. 3.10(b)) at $11 - 12\,Å$. Such separations seem to be quite common with aluminum, also appearing in 3.12 (a) around $13\,Å$ and 3.12 (b) around $12\,Å$. This indicates that in those simulations this single mode is significantly more involved in processes due to electron-phonon coupling.

Figure 3.12 shows aluminum pull contacts with layers in [111] (a), [100] (b) and [110] crystallographic direction (c). The [111] and [100] directions show a plateau structure typical for atomic contacts, while the [110] contact reaches much higher conductances and smaller distances. The [110] contact also does not exhibit many geometries with conductances below $7\,G_0$, which would be the niveau expected of atomic contacts.

The runaway voltages for the [100] and [111] pull contacts are for the most

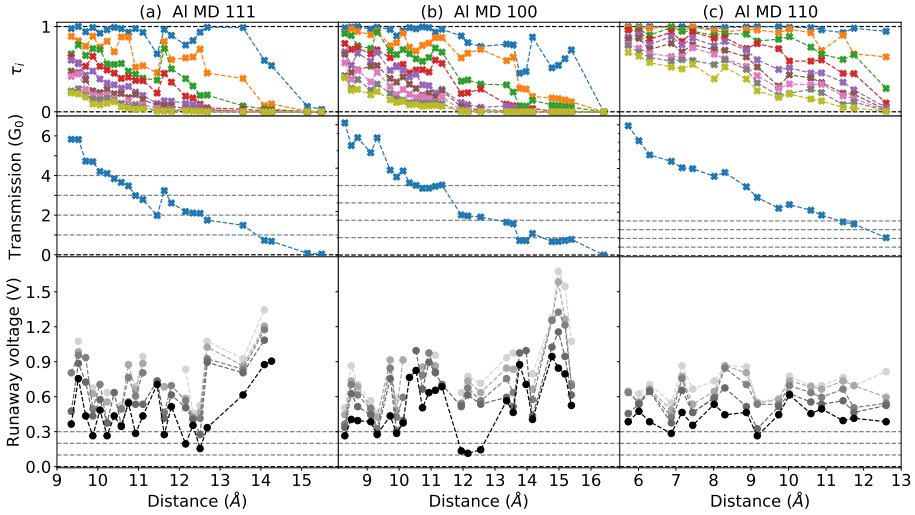

Figure 3.12: Shown are channel transmission (top), transmission (middle) and the 5 lowest runaway voltages (bottom) of simulated aluminum pull contacts. These are MD-created structures with the leads in [111] (a), [100] (b) and [110] (c) crystal directions.

part between 0.1 and 0.9 V with quite high variance. This variance is reduced in the [110] direction, where the first runaway voltage is in the range of 0.25 to 0.5 V. This seems likely to be connected to the high conductance above $6\,G_0$, where for all metals the runaway voltage does not scatter as much as for the more atomic contacts. The more bulk-like contacts behave more like macroscopic contacts and are not as strongly determined by single scattering modes.

Summary Al Of all investigated metals aluminum has the highest absolute value and variance in runaway voltages and also exhibits some interesting features in the runaway voltage peaks and difference in the first and higher runaway voltages. Overall this wide range of features makes aluminum the metal most difficult to describe and also one where the simple description falls short of describing all features of the contact.

3.2.4 Summary

The push and pull contacts of the different metals provide a sample of atomic contacts whose derived properties like transmission and channel distribution fit to values expected from experiment [39] and other simulations [15]. The significant scatter of the calculated runaway voltages and the fundamentally stochastic nature of the electromigration process prevents results derived from individual contacts from being representative. Only statistical analysis and comparison, between different metals and with experimental results, allows one to determine if the runaway voltage is a relevant parameter for the analysis of electromigration in those contacts. This statistical view will be the topic of the next section.

3.3 Statistical analysis

After looking at the individual contacts in the last section this one focuses on the statistics of those contacts. Following a discussion of the statistical methods, the main results presented are aggregated distance curves and conductance histograms, as well as histograms of the runaway voltage binned for different conductances.

3.3.1 Sampling

The experimental investigation of atomic contacts shows a wide variety of phenomena and properties [3]. For metallic contacts of only one sort of atom this variety is reduced to effects of the atomic structure together with the extended electron-wavefunction of a Fermi sea. Even this reduced variety is huge, with experimentalists using statistical measures to classify the atomic contacts, for instance through histograms as a representation of the probability distribution [37, 51–53].

For a theoretical treatment this provides a different challenge. Purely theoretical treatment aims for systems, where all random and stochastic effects are either gone or a result of the calculation - this allows clear predictions and easily understandable conclusions. In the case of atomic contacts the typical reasoning is that the conductance properties follow from the atomic structure. Only in very few cases the structure is simple enough and the derivation clear enough to follow directly, e.g. the monatomic gold chains with their nearly perfect conductance quantization [54, 55]. In experiments different atomic geometries are sampled, which is difficult to include in purely theoretical treatments.

This poses two questions for simulations. First, whether the structures are similar to those encountered in experiment and whether the structures' probability distributions are representative. And second, whether the individual calculations are correct under all the assumptions explicitly and implicitly taken in the simulation. Those questions will be discussed in the following subsections.

Variations in simulations

In the simulations the primary variance for a given metal is in the structures the contacts exhibit. Through the relaxation schemes in TURBOMOLE those are fixed to a local minimum contingent on the boundary conditions. The boundary conditions consist of the structure of the fixed leads, its distance in z direction and the offset in xy direction.

The easiest of those conditions to vary continuously is the distance, which is also the parameter most suitable for comparison with experiments. For this reason the distance was chosen as the primary control parameter for the contacts.

If the distance is varied in small enough steps, there is the assumption that the contact and its properties will evolve continuously. This is the quasi-adiabatic behavior expected of the effective zero temperature relaxation of DFT. This assumption of continuously evolving properties has its limits for example in the conductance steps and the associated structure changes, which are not continuous in simulations and experiment.

For electromigration studies this $T = 0\,\mathrm{K}$ assumption is only justifiable for practical reasons, since the coupling to a non-equilibrium bath will introduce an effective temperature to the electronic system. The addition of the atomic vibrations coupled to the heat bath also transfers this temperature scale to the structure - even using the Born-Oppenheimer approximation singular atomic geometries and electronic densities can only be examples and statistical methods over the derived properties are necessary to investigate the system.

In the following paragraphs possible sources of differences between experimental results and those of the simulation will be presented. These sources of differences are important to keep in mind, but their relevance has to be considered with respect to the inherent variance of the problem.

Validity of theory

Initially, the suitability of the theoretical models should be considered as a possible source of deviations between the calculations performed and experimental observations. Modelling assumptions may not be valid for the system in question, e.g. that the system is described only by the harmonic potential. This is representative of the typical question in perturbative calculations of where to curtail the expansion to actually calculate something. Relevant examples for transport are the linear limit in response to differences in the baths and the restriction of the higher order Feynman-diagrams in the scattering formulation and the Keldysh-formalism.

In the case of atomic contacts, the Langevin equation used to calculate the runaway voltages could not be suited for the system in question, e.g. if the quantum mechanical effects are too strong. Furthermore, the harmonic approximation for the potential in the Langevin equation could be invalid, because the anharmonic parts of the potential energy surface become relevant at lower voltages than the occurrence of the switching process.

In the calculation itself, the wide-band limit could be unsuitable - there are at least two potential errors sources in this: The surface Green's function is not as flat as assumed and the scattering into the phononic system changes significantly with the difference in Fermi energy of the surface electrons. The wide-band limit assumes that the surface Green's function, as well as the transmission, are constant in the energy range investigated.

And finally, there are sources of differences in the numerics underlying the simulations, like convergence problems through unsuitable or too small basis sets, unsuitability of the exchange correlation functional for the description of relevant correlations in the system, and problems in deriving perturbative quantities out of simulations not optimized to that perturbation.

Some of these are explicitly not errors of theory or the calculations themselves, but inherent trade-offs in the numerical realization of the theory on computers. In theory these errors are are often controllable, e.g. through increasing numerical precision, decreasing time steps, increasing the size of the sample, extending the basis set or decreasing convergence limits, but practically these corrections are connected with significant increases in computational costs.

Since not all of these errors can be arbitrarily reduced, discerning them from variations in the system may be impossible. Even worse, natural variations of the system may be seen as errors. Those natural variations can not be removed from the system without describing something else. While the error of the

mean falls as $\sqrt{N}$ with the sample size N, the variance is an actual property of the system, which can also be measured and compared in most experimental systems [56].

Overall there will be a trade-off between the precision of a single simulation and the amount of data points available for statistical evaluation, due to the large computational costs of getting just one data point. Since the inherent variance of the system is so large, precision is considered of lesser importance to the contacts investigated here.

3.3.2 Simulated conductance histograms

The obvious first step for comparison are aggregated distances curves and conductance histograms, as they are also produced in experiments. The amount of data points gathered here from DFT calculations reach 100-200, which is at the low end of those gathered from tight-binding contact simulations of several hundreds to nearly a thousand data points [15] and significantly below experimental data sets of several thousand data points.

Fig. 3.13 presents pull curves and conductance histograms for the three metals simulated. In general, the distance curves (a-c) exhibit the plateau structure expected from the metals with notable differences in the plateaus lengths. Here gold (b) has the cleanest step structure with plateaus up to $6\,G_0$. These plateaus grow more skewed with higher conductance, which is also visible in aluminum (c), e.g. in the plateau around $4\,G_0$ and 10 Å. The lead simulations exhibit more or less one long plateau around $3\,G_0$.

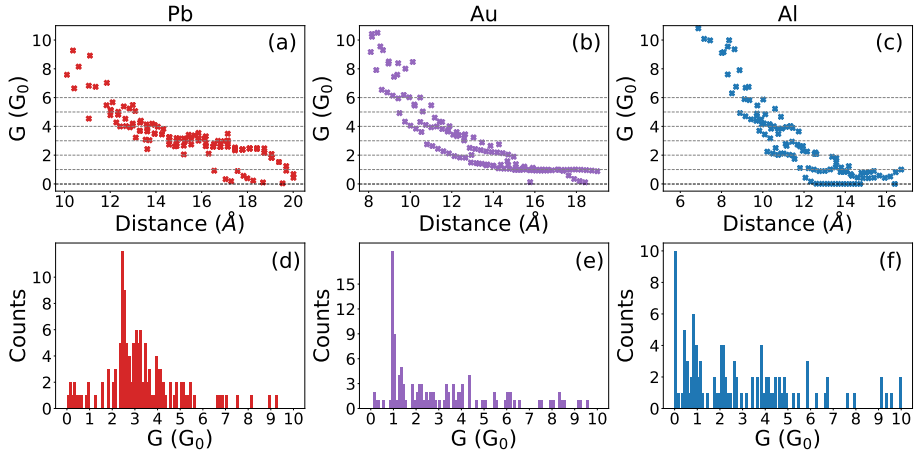

Figure 3.13: Aggregated pull curves (top row) and conductance histograms (bottom row) of the three simulated metals (from left to right: lead, gold, aluminum) exhibiting the quantized conductance steps in the single-atom regime.

These large tendencies in conductance can also be seen in the conductance histograms Fig. 3.13 (d-f). There lead (d) exhibits many contacts around $3\,G_0$ with a strong peak at $2.5\,G_0$ - this is quite different than the behavior in the experiment, where there is a wide peak in between 1 and $2\,G_0$ [8]. For lead stable structures with conductances around $1\,G_0$ were rarely found in simulations, leading to a lack of data points between 1 and $2\,G_0$.

The simulations of gold (e) show a picture more similar to experimental results in the histogram with a high and narrow peak around $1\,G_0$ and wide structures between 2 and $3\,G_0$ and around $4\,G_0$.

Aluminum (f) shows wide structures around $1\,G_0$, around $2\,G_0$, and again at $4\,G_0$. The distribution below $1\,G_0$ is similar to experimental ones, as is the one around $2\,G_0$. The contact structures around $4\,G_0$ are not due to one plateau alone and may be due to a sampling difference in experiment and simulation. These structures will be discussed again, since those values also exhibit surprisingly large runaway voltages in the push contacts as seen in Fig. 3.10.

3.3.3 Runaway histograms

The central results of the simulations are the calculated runaway voltages. The question is if those runaway voltages are a reasonable parameter for the description of electromigration processes - whether the runaway voltages give a reasonable approximation for the stability of contacts. This would imply that contacts with a lower runaway voltage switch at a lower voltage in experiment and vice versa. To investigate this the simulated contacts have been compared with experimental atomic switches of the metals in Ref. [8].

In order to analyse the runaway voltage, all the simulated contacts have been put into histograms binned to the integer conductance, presented in figures 3.14 and 3.15. Binned for conductance means that all contacts exhibiting a conductance between e.g. 0.5 and $1.5\,G_0$ have been sorted into a $1\,G_0$ bin. From those conductance bins the histograms were created.

The histograms in figures 3.14 and 3.15 show that the runaway voltages are for the most part between 0.1 and 1 V, a range which fits to experimental data of switching voltages shown in the lower rows. The variance of the samples is quite high, as expected from the multitude of possible configurations.

For Pb in Fig. 3.14(a) the variance is comparatively low in most conductance bins. Most data points come from contacts having a conductance between $2-3\,G_0$, as also seen in the conductance trace in 3.13(a+d) and fitting well to the experimental data in (c). Overall the mean stays around 200 mV with no large changes for both simulations and experiment. The three simulation data points at $6\,G_0$ are too few to make a clear statement. In experiments the $6\,G_0$ conductance bin has more counts than the ones for 4 and $5\,G_0$, something which could not be reproduced in simulations, where such high conductance contacts are limited by the comparatively small sizes of the simulated contacts. The $1\,G_0$ data is also dominated by low conductance contacts that have a high runaway voltage in simulations, which are not found in experiment.

For Au in Fig. 3.14(b) the variance in simulations is higher than for lead but confined to similar ranges. In simulations the most common conductance range is around $1\,G_0$. This is also the conductance bin with the highest variance and runaway voltages reaching up to 800 mV, which can be attributed to the low conductance together with high variance in the electron-vibration coupling itself. This $1\,G_0$ behavior is the same in experiment (d), although there the most common switches have conductances between $2-4\,G_0$. In simulations the variance decreases with higher conductance, which is also found in experiment. There is a difference in the behavior of the mean voltage between experiments and simulations. While in experiment the mean switching voltage stays roughly constant around 400 mV, it decreases significantly with higher conductance in

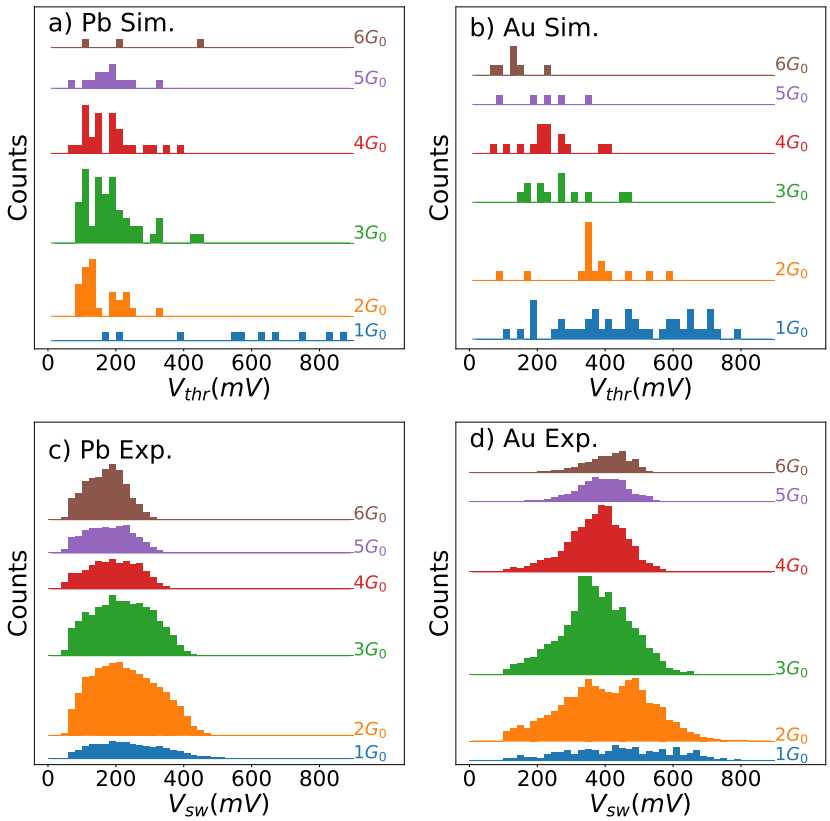

Figure 3.14: Histograms of the calculated runaway voltages in simulations for lead (a) and gold (b). Additionally histograms of measured switching voltages for lead (c) and gold (d). The runaway voltages were binned for conductance ranges of $\pm 0.5\,\mathrm{G_0}$ around the conductances values of $1-6$ as written to the right of the histograms. Experimental data from [8].

simulations, going from over 400 mV down to below 200 mV. This may again be due to the small contacts in simulation, but this higher stability with higher conductance is also specific for gold in experiments, where the other metals tend to have lower switching voltages with higher conductances. Gold is the only metal investigated where the switching voltage not only stays constant but actually increases somewhat for 5 and $6\,\mathrm{G_0}$ (see Fig. 3.15(b)).

For aluminum in Fig. 3.15(a) the behavior in simulation is very different compared to the other metals. First, the variance in simulations is huge for all conductances, especially for $4\,\mathrm{G_0}$. This is very different from the behavior in experiment (c), where the switching voltage is always below 500 mV and decreases in mean and variance with higher conductance. The switching voltage histograms for experimental aluminum contacts become ever more askew with higher conductance, having their maximum at the left border of the measuring range around 70 mV.

The statistical values of the relevant voltages of all metals in Fig. 3.15(b+d) show a mixed picture. The data of the simulations often has large changes from

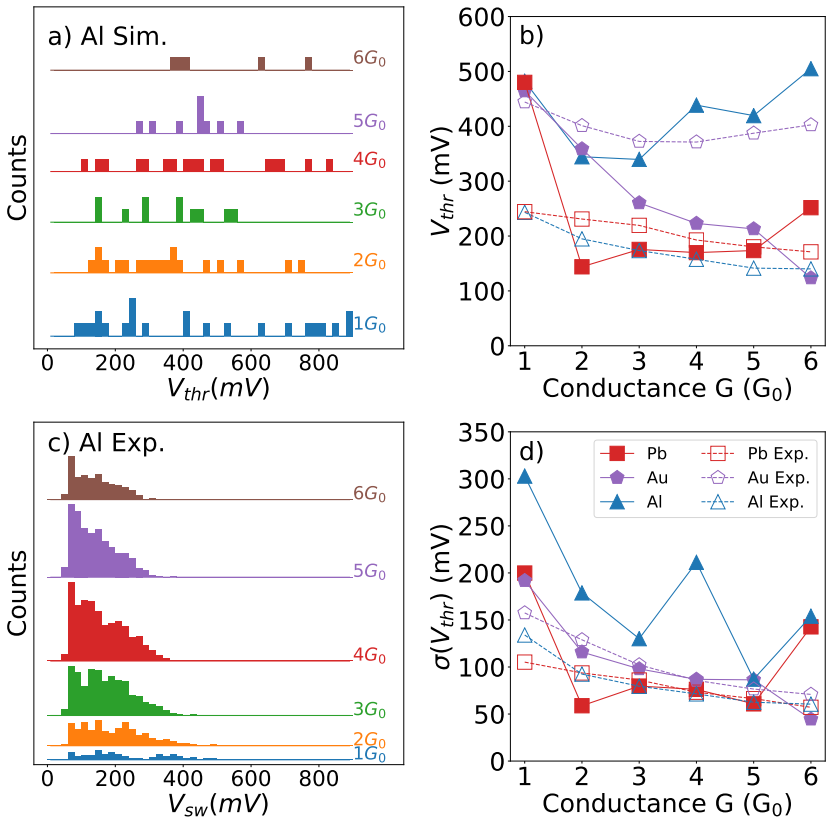

Figure 3.15: Histogram of the calculated runaway voltages in simulations for aluminum (a) and measured switching voltages (c). Additionally the statistical values of runaway and switching voltage for the different metals in (b) (means) and (d) (standard deviation). Experimental data from [8].

one conductance bin to the next, which is very likely due to the low sampling of those bins and correlations between contacts in one bin through the push and pull process. The mean switching voltage in experiment is largely constant for each metal with a slight decrease with increasing conductance. This is expected from a combination of the fundamentally similar switching and scattering events with ever more electrons flowing through the contact. A similar argument of a statistical combination of electrons can be brought forward for the decrease of variance with conductance which is also seen in every metal in experiment and, with much more noise, also in simulations.

Overall, lead has the highest similarity between experiment and simulation. Especially at $2-5\,\mathrm{G_0}$ the differences are below 30%. The 1 and $6\,\mathrm{G_0}$ case have considerably smaller samples with much larger differences.

For gold it starts quite well at small conductances - at 1 and $2\,\mathrm{G_0}$ the experimental and simulated means are within 1 standard deviation of each other. At higher conductance the experimental gold contacts grow more stable while the runaway voltage, and with that the predicted stability of the simulated contacts, decreases strongly. Although this difference in mean is larger, the difference in

standard deviation between experiment and simulation is smallest for gold. This stability reinforces the suitability of gold as a testbed for atomic contacts.

The discrepancy in the calculated behavior of aluminum and the experimental values is obvious in the comparison of the mean and the standard deviations in 3.15(b+d). The standard deviation of simulated aluminum is at least a factor of 2 above the other metals, while the mean runaway-voltage never gets close to the experimental switching voltage. The simulated runaway voltage of aluminum is closer in value and tendency to the experimental behavior of gold, being around 400 mV and showing tendencies to be more stable with higher conductances. While aluminum is still in the right ranges, its switching does not appear to be well described by the runaway voltage. Since aluminum is generally well described in DFT, this is more likely due to other effects than the runaway being important for switching. One candidate explanation for that would be the thermal excitation combined with the lower mass as investigated in the simplified switching model in section 2.3.2.

Summary statistics The comparison with experimental data [8] gives the best overlap of histograms and values for Pb, which is one of the reason why Pb contacts are used in the next chapter for simulations in the direction of current-induced structure changes. The other reasons are comparatively lower calculation costs and the low melting temperature of the metal, which makes its surface structure more likely to change with applied current or temperature. For Au the 1 and 2 G_0 cases show a very good compatibility between experiment and simulations, reinforcing their role as test bed for comparison of experiment and simulations. The stability of its atomic structure is the reason why gold was not used for the switching simulations in the next chapter. In experiments the mean switching voltage tends to decrease slightly for the other metals to which gold is an exception, with the mean switching voltage increasing again after 4 G_0.
For aluminum the experimental switching voltages are a factor of 2 below the simulated ones and the behavior is quite different with experimental aluminum decreasing in mean switching voltage for higher conductance, even developing a peak at 70 mV. The large differences in histograms and derived values make aluminum the metal least suitable to be described with the runaway scheme used to describe the current-induced forces in the simulations.

3.4 Summary

This chapter presented simulation results for push and pull contacts of the metals Al, Pb and Au.

Their sample creation proved to be difficult and expensive, especially the interesting distances costing a lot of calculation time. Nevertheless, reasonable sample sizes could be produced, allowing a comparison of the different metals.

The transmission data for the contacts simulated fit well to experimental results, exhibiting the right range of conductances and conductance steps at the values also seen in experiments for those metals.

The runaway voltages are in the ranges (100 mV to 1 V) comparable to experiment and exhibit a wide scatter around the metal-specific values. This is similar to result of experimental switching voltages [57], although the values align only for lead and low conductance gold contacts.

The great overlap between experimental and simulated voltages relevant for switching, together with variability of structure in atomic contacts is the reason why Pb contacts will be used in the next chapter to simulate switching.

Chapter 4

Current-induced structure changes

This chapter presents some current-induced switches found with the formalism introduced in chapter 2 and applied to several Pb contacts as described in chapter 3.

The fundamental idea is that the Langevin equation formalism adds a direction to the current-induced processes. Along this direction the atoms of the contact can be moved by the scattered electrons, possibly leading to new configurations. This opens up the way to use a current-induced process to simulate switching. It additionally allows one to investigate the contacts formed by this approach - to explore the structural phase-space accessible through current-induced activation.

4.1 Setup

In the previous chapter a sample of metallic contacts was presented, along with their relaxed structures and the current-induced forces in dependence of their voltage. The relaxed structures are stable in the sense that they are in a local minimum of the motion of the atoms. This makes them candidates for contact structures realized in experimental setups.

Exploring the phase space around these stable minima is a search in an $3N$-dimensional space with N being the number of atoms. The phase space of possible atomic configurations and the associated electron density is given by the connected Born-Oppenheimer potential energy surface. An exhaustive search is plainly not feasible, but the runaway-voltages presented in ch. 2 and investigated with regard to stability in ch. 3 are associated to runaway-modes. These runaway-modes are collective motions of the N atoms, one-dimensional lines in that $3N$-dimensional phase space, considerably reducing the dimensionality of the search space.

Perturbing the contact in the direction of a runaway-mode will, in the general case, produce unstable configurations. But if the perturbation moves the configuration over a barrier, structural relaxation may find another stable state.

4.1.1 Reaction paths

A reaction path connects two different reaction states, i.e. local minima in the potential energy surface over the full configuration space. A parametrization of the distance along the reaction path is called a reaction coordinate. The highest potential energy along the reaction path is called the reaction barrier.

The reaction barriers used in chemical kinetic theory are based on simple thermal Markov processes as introduced in section 1.4. This is of course a simple one-dimensional picture - most systems under investigation have a high-dimensional phase space and it is at least equally important how many similarly likely reaction paths are open as the properties of the most likely one.

To be precise, it should not just be the barrier height but also the width. Even more precisely, one should probably use a path-integral formulation similar to the tunneling effect in quantum mechanics. There the energy of the particle is connected to its velocity and therefore to the time it needs to move over the barrier as well as the knocking frequency[1].

In this chapter two reaction paths are used, a linear shift in phase space between two stable minima to get an impression of the reaction barrier, and the reaction path consisting of the shift along the runaway-mode and the relaxation path afterwards.

4.1.2 Effect of bias

For these stable reaction states the current-induced forces program calculates the effect of a voltage applied to the system. The current-induced forces are calculated from the properties of the system in and around the minima. The electronic structure alone determines the elastic transmission of the electrons. The dynamical matrix and the electron-phonon coupling allow one to calculate the inelastic scattering of the non-equilibrium electrons. The effects of this is a transfer of some energy into the atomic system.

This energy is at first in specific vibration modes and can thermalize or dissipate with the phonon-phonon and electron-phonon coupling. If the voltage, the associated current, and therefore the number of scattering events increases, this dissipation is not enough. Above a certain threshold voltage some phonon modes are excited far above their equilibrium temperature. Of course this energy cannot grow without bounds. Non-linear effects and higher order scattering processes may dissipate this energy. One such process could be a change of the structure, a switch to another configuration, where that specific mode is not pumped anymore.

The heating part of the current-induced forces is investigated in the paper of Lü et al. [20] as part of asymmetric heating in symmetric structures. The approach there is basically a coupling of the phonon modes to a heat bath in the contacts itself. This means the pumped phonon mode is strongly coupled to the non-equilibrium electrodes and the energy flowing into that mode is transported off more slowly, leading to a pumping of that mode above the bath temperature. The associated effective excess kinetic energy will be somewhere between the effective electron temperature and the bath temperature. Part of the excess energy of the electrons from the higher voltage reservoir is indeed dissipated into the contact. A number of electrons with energy up to $e\Delta V$ can

[1] The frequency at which the particle attempts to overcome the barrier.

be dissipated, and one question is how much of that energy goes in the phonon modes of the contact itself. In the paper they find excess kinetic energy in the ranges of up to 40 meV for 1 V bias in metallic contacts.

The difference in the approach in this thesis is that a specific mode or set of modes are giving a direction to a switching process. This is explicitly not excess heat in the sense of directionless or random movement. This specific movement does not so much reduce the energy barrier for a switching process, but instead increases the effective temperature, which has a similarly exponential dependence on the switching rates. Increasing the effective temperature also increases the knocking frequency at which the switching process is tried. Calculating the time-scales explicitly requires not just the potential energy surface of the correct reaction path, but also dynamical effects on this path, i.e. the current-induced forces.

4.1.3 Simulating switching

The contact phase-space investigated is bounded by at least two layers of atoms frozen in the ideal lattice. The primary control parameter is the distance between the leads. Only the atoms in the contact region are allowed to move in the structure relaxation and for calculation including electron-vibration scattering. The variation of the distance parameter is done in steps with relaxations in between, leading to an evolution through local minima. It is not guaranteed that these are global minima. This is closer to experimental realizations of such contacts, where it is very unlikely that one has the sample in the absolute ground state, even at low temperatures, since the stretching/compression process itself heats the sample. Indeed, the experimental data shows a wide variety of possible configurations and conductance states, which have been explored through statistical approaches, for example through histograms [52, 53].

Previous simulations managed a switching only by varying the distance between the fixed leads [15, 18], which is also used here for the initial contacts. To approach current-induced switching it is necessary to have different conductances for configurations with the same distance between leads. To this end, a distance curve is simulated, where the contact is either pressed together or pulled apart. This creates a selection of distances and configurations with different conductances. These curves exhibit many features of experimental pull curves like conductance plateaus and switching processes. At the distance-dependent switching processes, a hysteresis with respect to the distance should be possible and that could be simulated by reversing the change in distance leading to the switch. With this scheme, different configurations with different conductances for the same lead distance have been found.

4.1.4 Switching candidates

A pair of different configurations for the same boundary conditions are switching candidates. To get a current-induced switch one needs to show that a mode excited by the current can induce that switch. If a switching mode is found for both directions, it is a bistable phonon-pumped switch.

To get a valid switch one has to check several additional conditions: The first question is if the configurations have different transmission values. Only configurations with different transmissions would be called switches in experiment.

Next, there is the question if those configurations are separated by an energy barrier. This is necessary to prevent random switching due to thermal noise, something that would be observed as a telegraph oscillation of the conductance in experiment.

Monostable switches and field effects are other things one can consider here, but for a metal with a delocalized electron wave function there should be no internal field and charge effects - the charge of the atoms should be shielded by the electrons.

If two switching candidates are found, a reaction path between the configurations is created by linear interpolation. A single DFT calculation on these configurations then shows if there is a reaction barrier between these configurations, indicating that those meta-stable structures are locally stable and inhibited from simple switching. If that is the case, one has a switching candidate consisting of two well-separated configurations with a difference in conductance.

Following this, the runaway modes of the configurations are checked. At and above the runaway voltage, movement along those modes requires no energy cost and accordingly we vary the contacts by a multiple of those modes. The configurations gained thusly are relaxed again to find the local minimum. If a configuration different from the starting one is found, this candidate switch now has a mechanism - phonon pumping - through which it can be switched.

4.2 Results

The actual contact investigated is the push contact in the [111] crystallographic direction. One important difference to the one presented in Chapter 2 is that the contacts for the switching dynamics are calculated in the smaller def-SVP basis. This basis calculates significantly faster than the def-TZVP. The def-SVP basis exhibited better visible switching distances than the def-TZVP contacts. The electronic transmission behaves linearly on the plateaus for lead in the def-SVP basis and its runaway-voltages are considerably above experimental values, which is why the def-TZVP basis was used for the analysis and comparison with experiment in chapter 2. Despite many of those properties speaking for def-TZVP, the large amount of calculations necessary for phase space investigations in switching setup makes speed the primary driver to get result.
The distance of the first layer of crystalline Pb is set to values between $15-20\,\text{Å}$ in 15 steps of about $0.3\,\text{Å}$ each.

Figure 4.1 shows the transmission, energy and runaway-voltage of the Pb push contact. The transmission overall decreases linearly with distance from around 3 down to $1 - 1.5\text{G}_0$. This transmission curve also exhibits 3 jumps to different conductances, which are candidates for switching behavior. The energy curve shows a local minimum at $17\,\text{Å}$ that turns into a linear slope for higher distances and more complicated behavior for shorter distances. It is interesting that the second switch happens close to that minimum. The runaway-voltages show a stronger scatter than all the other values - which is expected since they derived values based on density functional perturbation theory. On average the runaway voltage decreases with higher distance - a property that is not found in the def-TZVP basis. Another notable point is is that the configurations close to the local energetic minimum exhibit considerably higher runaway-voltages of more than $1\,\text{V}$ - this indicates that the scattering

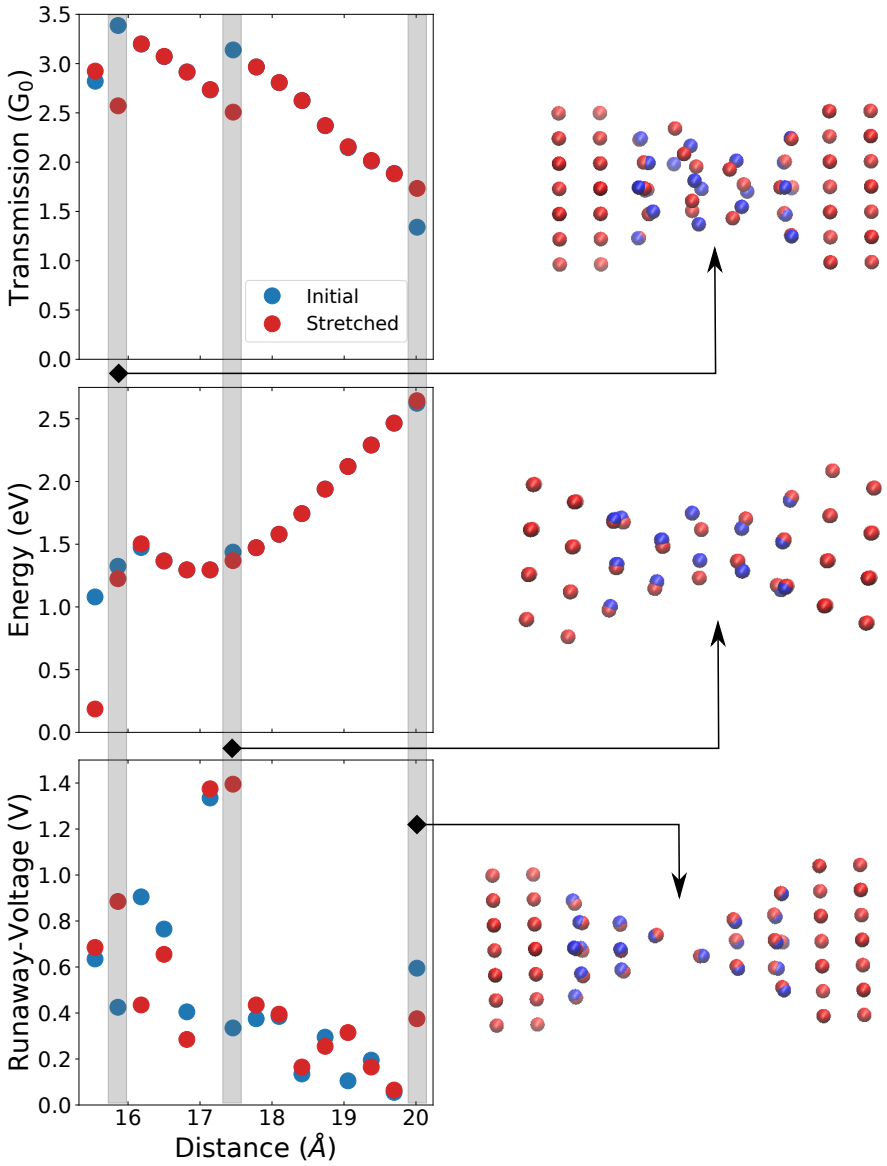

Figure 4.1: The transmission (top), total energy (middle) and run-away voltage (bottom) for a break contact of Pb atoms. Blue is the initial relaxation, red is another relaxation after stretching. The grey bars indicate candidates for switches.

into the phonons is considerably reduced in the structural minimum.

Candidate switch 1

Figure 4.2 shows the specific configurations at 15.8 Å. While the number per "layer" is about the same, the structure between the fixed leads is very different for the two conductance states. A linear interpolation between these structures

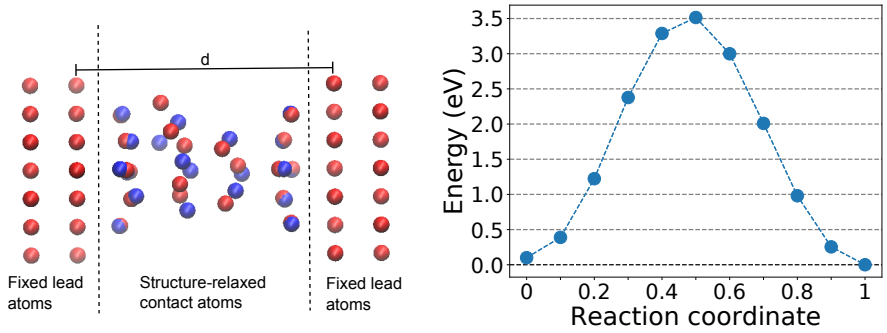

Figure 4.2: The left picture shows the configurations for the contact distance $d = 16\,\text{Å}$. Blue is the initial relaxation, red is another relaxation after stretching. The right picture shows the total energy of the linearly interpolated configurations.

with 10 steps has been constructed to analyze this. The total energy of these unrelaxed, intermediate structures is shown in the right panel. The difference in energy of the relaxed structures is in the low 100 meV range. This is far below the reaction barrier of around $3 - 4\,\text{eV}$.

To change these two configurations into each other, a rotation of a large part of the structure is necessary. No pumped phonon mode enabling that switch has been found. The most likely explanation for this is that this rotation does not couple well to the electronic current. The charge carriers would need to be scattered nearly orthogonally to their direction of motion. This is very unlikely in a two-particle process which respects momentum conservation. A three-particle process pumping such a mode is not included in our calculations, but would be at least similarly unlikely.

Candidate switch 2

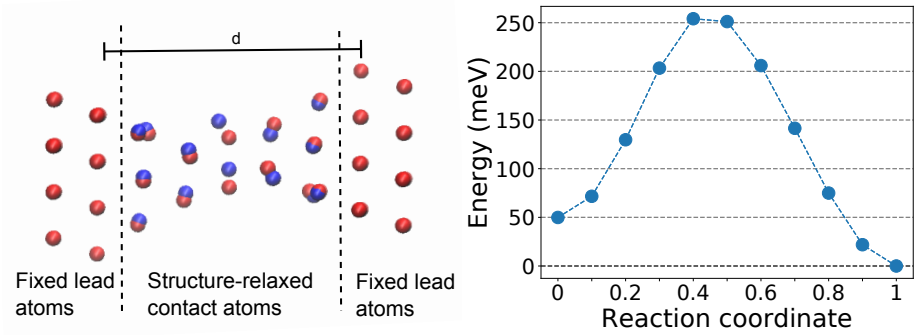

Figure 4.3: The left picture shows the configurations for the contact distance $d = 17.4\,\text{Å}$. Blue is the initial relaxation, red is another relaxation after stretching. The right picture shows the total energy of the linearly interpolated configurations.

In comparison the candidate switch 1 the two conductance configurations

shown on the left of Fig. 4.3 are divided by a much smaller energy barrier of only about 200 meV. The configuration in blue has a conductance of $G = 2.7\,\mathrm{G}_0$ and shows a misalignment of the atoms in the middle with the direction of the electric current. The configuration in red has both atoms in the middle shifted into a straight two-atom contact with an increased conductance of $G = 3.6\,\mathrm{G}_0$.

The threshold voltage for pumping a phonon mode in the second configuration (red) is at 1.4 V, indicating the significantly increased stability of that configuration. This massive change in the stability is not directly visible from the potential energy difference of around 25 meV. This change is most likely due to a difference in the scattering into the phonon modes - the second structure gives less structural resistance to the flowing electrons. This could be guessed from the structure of the (red) contact, which looks cut out from the perfect crystal, but such guesses are often misleading and depend on the view angle.

The first configuration (blue) exhibits a slightly higher total energy and a considerably reduced threshold voltage of 0.4 V for pumping phonon modes. For this a mode enabling the switch to the second configuration was found by moving the configuration some distance along the pumped phonon modes and then relaxing again. A scheme of this process is shown in Fig. 4.4.

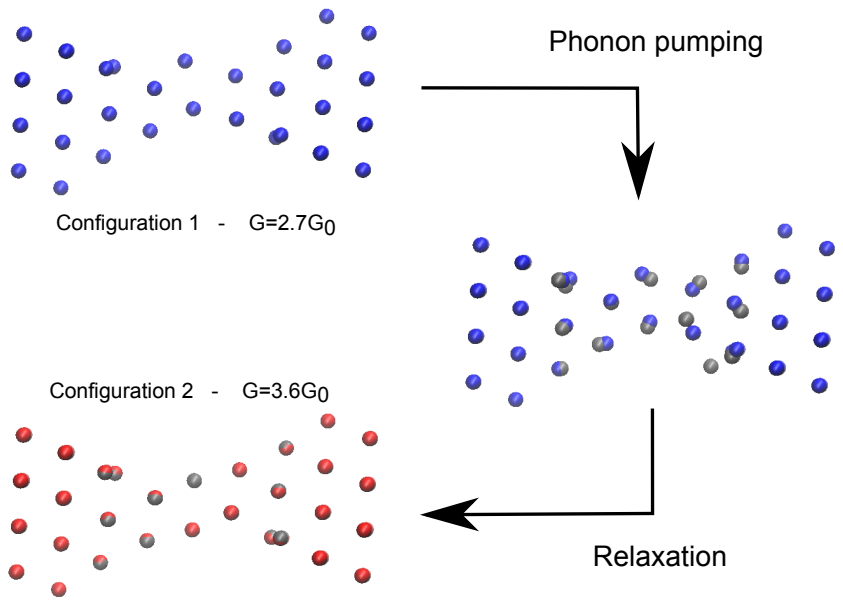

Figure 4.4: This initial structure for lead distance $d = 17.4\,\text{Å}$ (blue) with a conductance of $G = 2.7\,\mathrm{G}_0$ is displaced along the runaway phonon mode (metallic). The displaced structure is then relaxed into the second configuration (red) with a conductance of $G = 3.6\,\mathrm{G}_0$.

This process of perturbing the contact along a mode requires between 4 and 8 additional relaxation runs per excited mode for different displacements along

the pumped mode. Since not all modes necessarily lead to switching, i.e. they can be stabilized through higher-order terms, several of the modes with the lowest threshold voltage are checked this way. In general, this leads to several dozens relaxation runs for the first runaway-modes. Overall, the number of relaxation runs is quite similar to the number required to simulate the different distances of the break contact. This is computationally quite expensive, but any relaxations not leading to a new stable configuration can be dropped. In this case all other phonon modes and distances tried resulted in relaxation back to the original configuration.

Candidate switch 3

The atomic configurations of the two states of the final switch shown in Fig. 4.5 look very similar. The change in the configuration is a collective motion of all of the mobile atoms in the contact. The largest changes are in the two atoms of the tips of the contacts. Nevertheless, the barrier between these configurations has a height of 8 meV starting from configuration 1 (blue), and 13 meV starting from configuration 2 (red). Compared with temperatures below 50 K in experiment, this barrier is quite unlikely to be crossed by thermal excitation alone.

The heating due to conservative forces calculated in Ref. [20] in the range of < 10 meV could be enough to cross this barrier by itself. The non-conservative heating is of course significantly above this value, but lacks the directionless aspect of a system in thermal equilibrium.

For both configurations a phonon mode could be found whose excitation enabled relaxation into the other configuration. In configuration 1 (blue), the runaway voltage of this mode is more than 0.8 V, in configuration 2 (red) it is more than 0.4 V. This difference of 0.4 V in he respective runaway voltages is counter to the difference in the reaction barrier height of 6 meV.

The combination of the small barrier and high runaway voltages and associated heating makes it quite likely that the configurations are not stable under current. This could mean that in reality one would see either telegraph oscillations or an averaged conductance over the possible states, if the configurations are not that well separated under current.

Summary switching candidates

The runaway-modes of the first switching candidate did not manage to cross a reaction barrier towards a different configuration. The two configurations found by stretching were not connected by a bias voltage -dependent reaction coordinate.

The second switching candidate has a runaway-mode moving the contact from one configuration into the configuration exhibiting lower total energy, higher conductance, and no runaway-mode changing the contact back. This is a one-way switch into a configuration with lower resistance.

The third switching candidate has runaway-modes for both configurations connecting them. This would be a candidate for a bistable switch. The small difference in atomic position, low reaction barrier, and comparatively high runaway voltage makes it more likely that this switch exhibits a telegraph oscillation, rather than it being a truly bistable switch.

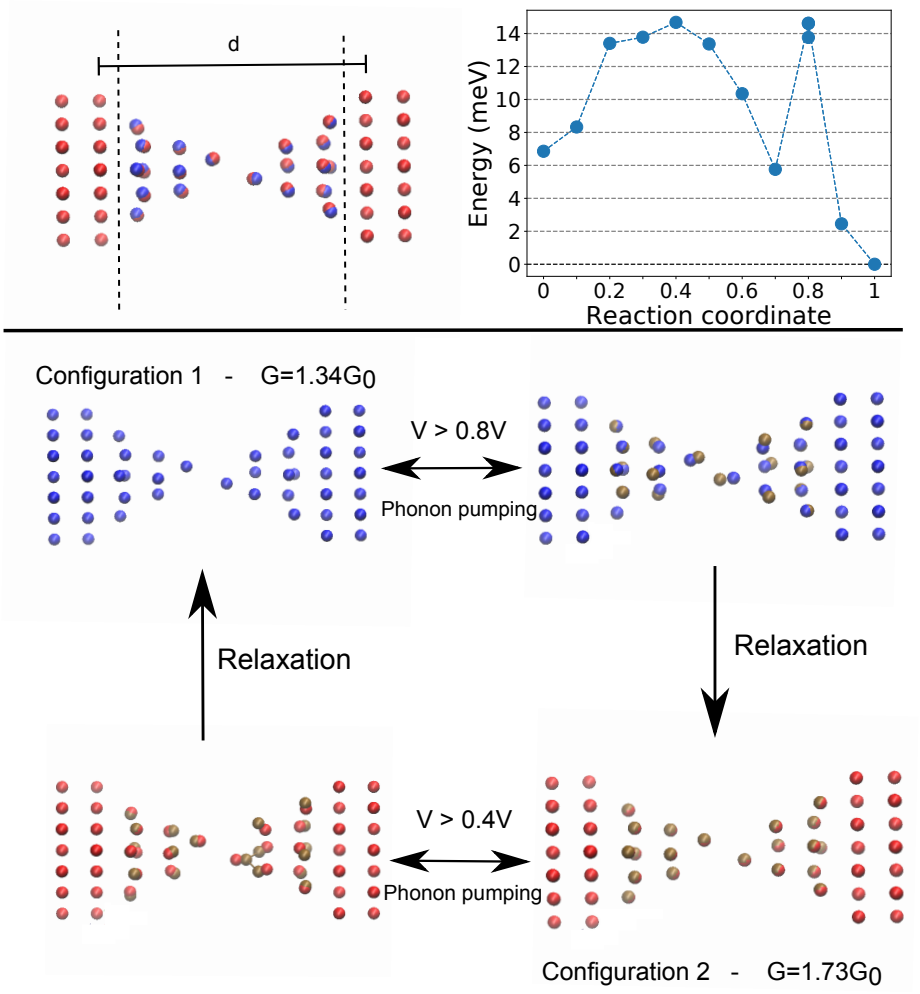

Figure 4.5: The configuration for $d = 20\,\text{Å}$ exhibits a bistable switch between configuration 1 (blue) with a conductance of $G = 1.34\,G_0$ and configuration 2 (red) with a $G = 1.73\,G_0$. The configurations are separated by a reaction barrier of $8 - 13\,\text{meV}$. Example displacements along the pumped phonon mode are shown in gold.

4.3 Discussion

Moving the atoms of the contact along the runaway modes can lead to switching the contact configuration to another stable contact. This simulates a current-induced switching between atomic configurations with different conductance. The cause of that switch are current-induced forces pumping a phonon mode.

The Langevin equation describing the current-induced forces also provides a dissipation mechanism for the excess energy needed for the switch. If the new state does not couple as well to the non-equilibrium electron bath, electronic friction will dissipate the additional energy. To investigate if that can lead to different configurations and switching processes depending on the bias direction, it would be necessary to leave the wide band approximation and calculate the integral over the bias voltage explicitly.

Reaction path analysis

The reaction path analysis presented here is quite simple with only linear interpolations between the stable states. A more in-depth approach to the theory of current-induced reactions is given in refs. [58–62].
The view they present on current-supported switching is a chemical reaction - the example they use is a proton-transfer. For this approach they define the system in relation to a reaction coordinate x and develop the system from the two end-points. The coupling between the electronic system and the movement of the atomic system is formulated in terms of that reaction coordinate.

This definition starting from the reaction coordinate makes it quite difficult to apply this in simulations of general systems. The assumption of a simple continuous transition between the two states is a good first step but definitely needs to be checked. The question if the properties in the transient states can be described correctly by current methods is especially difficult. If that reaction coordinate could be found, the projection of general electron-atom coupling onto that reaction coordinate is possible. It is very likely that this projection would need higher order terms in all perturbations, since some of the approximations used may not be valid, e.g. the harmonic potential.

Finally, the quantum-mechanical treatment they use for the reaction coordinate lacks the dissipation or decoherence necessary to prevent switching back. The Langevin equation used in this thesis automatically provides a dissipation mechanism through the electronic friction.

In conclusion, finding the reaction path for a switching process in simulations is a difficult problem and subject to current research. The eigenmodes as switching direction presented in this thesis are an approach to finding a reaction path - they managed to find the end-points and starting from those some direction for the process.

Contact evolution

The use of runaway-modes reduces the search space for additional stable configurations from $3N$ dimensional to one-dimensional. This is an exponential speed-up allowing much faster sampling of the configuration space of a contact between fixed layers. The cost in relaxations is around $10 - 50$ relaxations per switching candidate. This number of relaxations is similar to those needed for a

distance curve, although the individual relaxations tend to go faster, since one perturbs a relaxed state. Some of the advantages of that speed-up are lost, since not all of those relaxations produce new configurations. This means that the resulting sample size of different contacts is significantly below the one gained from distance curves.

It nevertheless opens the way to investigate electromigrated contact evolution instead of just mechanical contact evolution. One would typically assume, that the lower energy configuration, are preferred but in connection with the effective temperature from the electron bath this may be quite different.

4.4 Summary

In this chapter the atomic vibration modes excited by current-induced forces were used to investigate switching behavior. Three distances with two configurations each constituting a switch candidate were identified. These configurations were perturbed along their runaway-modes and then relaxed again to find stable configurations.

Of these three switching candidates, one does not switch through the investigated runaway modes and one is a one-way switch to a configuration with lower resistance. The last switching candidate has runaway modes connecting the configurations in both directions. This connection makes it a candidate for a bistable switch, although the separation of the configurations in space and energy is so small that transient stability is more likely.

The high number of structure relaxations necessary, together with low yield of new configurations, makes the simulation of a full evolution of an electromigrated contact very expensive. Nevertheless, the proprosed scheme is a first approach to simulating current-induced switching from first principles.

Chapter 5

Conclusion

In this thesis the topic of electromigration in atomic contacts was investigated through theory and simulation. Programs were written to calculate the current-induced forces derived in literature [5, 6] and to analyse the dynamics of the Langevin equation for the atoms. The Langevin equation is gained through linearizing the atomic motion and averaging the electric current and its scattering over timescales relevant for the atoms and long enough for an averaging of the electrons.

Investigating the Langevin equation for the atoms produced runaway voltages as criteria at which a vibration mode of the contact becomes unstable. Although we found similarities, this is still a model system and the real switching process is not guaranteed to work in the proposed way. Obvious points of failure would be the effect of anharmonic terms or some mechanism other than electron-vibration coupling dominating the switching process. The runaway voltage nevertheless provides not just a measure for the stability of a contact but also a measure of the scattering strength of electrons in that contact. The change in the electronic friction terms serves as a nonequilibrium heat bath for the atomic system. This heat bath couples in different strengths to different atoms and movement directions in the contact, leading to different effective temperatures and anisotropy in the direction of motion of the individual atoms.

The used current-induced forces approach theoretically includes all first order electron-vibration scattering terms. The non-conservative nature of these forces, which comes from them coupling to a nonequilibrium and the stochastic nature of the scattering events, prevents a complete treatment of them in ground state methods like DFT.

Compounding these modeling differences are approximations in the numerics and simulations, like the wide band approximation for transport calculations and all the known limits of DFT, like the bases and the exchange functional as well as its interaction with derived parameters like electron-vibration coupling and structures.

Part of the dynamics of the process can be recovered in the Langevin equation on the Born-Oppenheimer potential energy surface, although the resulting runaway voltage and mode treatment leaves out both the effective temperature of the current-induced forces and the anharmonic surface structure.

To see if these terms are relevant, comparisons of simulations and experiments are necessary. This opens up the interesting question of how to sample

the contacts. Here, the limited size of the contacts feasible in computation enhances the effect of boundary conditions on most contacts, especially when there is not much distance between the layers.

The high calculation costs slow down the progress considerably - especially the relaxation of a contact can take up to several weeks without significant additional speed-up being possible through further parallelization. This limits the sample sizes as well as the in-depth testing of many of the other parameters.

The runaway-voltages and their modes were investigated for a wide variety of metallic contacts. In addition to different metals (Au, Al, Pb), the boundary structures and the distance between these boundaries were varied. Overall, the runaway-voltages for atomic metallic contacts are mainly in ranges of $100 - 500\,\mathrm{mV}$ and seem to be specific to the materials investigated. The runaway-voltages also exhibit a strong dependence on the atomic and electronic structure, with variance for the same boundary conditions being large enough to make generalization of individual results ill-advised. A direct comparison between metals and with experiments is possible through statistics.

Such a comparison with experimental values indicates that runaway-modes are the dominant mechanism of electromigration only in specific cases, primarily low conductance gold contacts and lead. Simulations of metallic atomic contacts of Au, Al and Pb, as well as calulation of the current-induced forces for these contacts reiterated the complicated interplay happening even in very small contacts. While the scatter in the calculated runaway-voltage is quite large, the runaway-voltages behaved in many cases as one would expect from experimental investigations of these metals. Gold and aluminum contacts were shown to be comparatively stable atomic contacts with runaway-voltages in the mean reaching $300 - 400\,\mathrm{mV}$. These metals are the primary experimental testbeds for atomic contacts in part due to their high stability, so this is the expected result. It also fits with those metals having small resistivity through low electron-vibration scattering. The simulated lead contacts have considerably lower runaway-voltages of $100 - 200\,\mathrm{mV}$, which are close to experimentally measured switching voltages over the whole investigated conductance range [57]. This behavior of lead fits to its comparatively high resistance and low force constants, which makes it a prime candidate for phonon-pumping induced switching.

Finally, the runaway-modes associated with the runaway voltages were used in simulations of current-induced switching. Moving the contact along these runaway modes lead to finding other stable conductance states. The direction associated with this vibrational mode allows a targeted search for stable configurations in the contact structure phase space. This drastically reduces the dimensionality of the phase space that needs to be explored. Overall this is an approach to bridging the time-scale gap between electronic and atomic motion, which allows the simulation of switching and electromigration in atomic contacts from first principles.

Appendix A

Electromigration models

This chapter asks and tries to answer some questions regarding the model systems investigated. An example system illustrates the relevant processes happening, while minimizing the processes not relevant to the study. Finding one such system is a fundamental problem of the theory side.

Example systems in literature

Gold is the go-to example for the NEGF formulation of transport. Its atomistic structure is very stable and the electronic structure is easy to get right. Gold clusters well and results in nice stable surface structures/pyramids. Especially the gold chains were optimal study objects with nearly perfect electronic transmission - which is at the same time a problem for the electromigration approach through very low inelastic scattering.

For the more complicated setup of the paper introducing the runaway voltages [5], they presented mono-atomic gold chains and a benzene molecule as sample systems without calculating any dynamics from that. Experimentally a runaway voltage example in an atomic chain would be destructive, leaving no second state to confirm similarity to experimental measurements. A further problem here is that the mono-atomic chain is not the primary candidate for breakage/fusing - the electrons move very well through that chain and barely scatter at atoms. The chains themselves are quite stable against current-induced changes, it is more likely that the side of the contact with higher voltage heats up effectively [20].

Ad-atoms

Ad-atoms on surfaces or contacts have several properties making them very useful for the investigation of current-induced restructuring: They are comparatively unrestrained in their motion - this means that small electronic effects can have a measurable effect. They are easily accessible experimentally, for example by STM or simply on the surface of a conductor. Finally, their existence can be treated as a perturbation to the main-system making them accessible in theory.
But there are also some properties speaking against their suitability as candidates for the current-induced forces approach. The main reason is that the

electrons rarely move through an ad-atom, so in particular the scattering and the current-induced forces on the ad-atom itself are low. The same cannot be said for the thermal effects, which are more likely to have a strong influence on the behavior of ad-atoms since they are less constrained in their movement.
This does not mean that ad-atoms are uninteresting for studying electromigration. They are just difficult candidates to investigate current-induced forces in isolation rather than just general structural effects. In general ad-atoms will move stochastically and therefore away from areas of high effective temperature, and stay longer in areas of low effective temperature. For ad-atoms on metals this would mean that they move to the side with the lower potential - this is not the wind-force as created by momentum-conservation in scattering but a random/diffusive effect, which is difficult to separate from simple observations.

Gold monomer

The gold monomer - two gold pyramids sharing the tip atom - could be a good example system to present current-induced restructuring. Most electrons will flow past that tip atom, which has good chances to have a higher kinetic energy, which together with its prominent position could allow that atom to move. Sadly there most likely won't be a difference in conductance between the different atom positons, so no switching is measureable in experiment.

Tthe system was thought of when searching for the simplest two-state system - which would be a mexican hat potential or $x^4 - x^2$ potential. The x coordinate here could be the position of the tip atom depending on the distance of the pyramids behind it. This assumes that the structure of the pyramids is more stable than the position of the tip atom, which could be forced by fixing the atoms of the pyramids. The minima of the potential then move with the pyramids.

Hotspot analysis [20] indicates that the tip atom would have higher kinetic energy if on the side of higher electrical potential - the electrons can drop off energy there before skipping over the lower energy fermi sea faster than the excess energy can be scattered back into the crystal. The prediction from this would be that the tip atom moves to the side of lower electrical potential.

In experiments the overall structural effects and impacts of the hot electrons are most likely to be seen on the side with lower electrical potential, since their excess energy dissipates there. These large scale effects are however not accessible in DFT simulations.

Could there be an exchange of atoms?

An arbitrary mode can induce one atom to move to the position of another atom while that atom is moving somewhere else. This direct exchange has a few problems, which make it unlikely that it creates a stable configuration. First, the conductance would be the same, so there would be no switch, secondly the exchange would happen ever more often between those atoms with ever higher voltage. The exchange would serve as another motion/eigenmode of the same conductance state into which additional energy could flow in an exchange equilibrium with the atomic and electronic system.

What about molecular electronics?

The electronic transport properties for molecules have been and continue to be investigated a lot more than those of metallic atomic contacts for several very good reasons: a better controllable structure (both electronic and geometric), functional groups that may couple to interesting other properties like polarization, light-matter interaction, chemical reactions like the creation of covalent bonds within the molecule, and redox reactions. All of these can be investigated because the structure itself is very strongly fixed through the anisotropic covalent bonds.

In these covalent bonds the electrons are also well localized, with mainly tunneling serving as the transport mechanism and only molecules with a delocalized electron system having conductances in ranges coming close to those of the metallic contacts. This low conductance is a problem for the vibration-pumping scheme presented in this thesis - there are considerably less electrons moving through the molecules capable of pumping the atomic motion in there. Even if those motions are pumped they are quite likely to run into the anharmonic potentials of the covalent bonds very soon.

The weakest points against that motion are most likely the quasi-metallic contacts to the metal leads. So one has to consider at least three possibilities for switching: the molecule itself, its bonding to the leads, and the structure of the leads itself. For the phonon pumping scheme to work for switching in molecules, it would be necessary to have a molecule with high conductance and very good coupling of the reaction mode to the electron current. At the same time one would need very high damping after switching to not see telegraph oscillations or a quasithermal occupation of the switching states instead. For arbitrary molecules the current-induced forces are much more likely to break the bonding to the leads. The change of the leads can indeed be simulated in this scheme, although the effect here is more likely to be thermal, lacking any direction.

Appendix B

Computational aspects

This chapter discusses computational costs and some decisions made with respect to the choice of simulational frameworks.

What are the computational costs?

The calculations for typical contacts need around $1000 - 10000$ core-hours for structure relaxation and $400 - 1000$ core-hours for the dynamical matrix (the phonons) and the electron-vibration coupling. The most expensive part of the transport calculation is the calculation of the surface Green's function of the leads with around $2 - 4$ core-hours per energy step. Overall the NEGF calculations need about $15 - 30$ min on typical nodes.

Different samples and contacts can be parallelized. The limiting aspect is how long it takes to calculate a single contact. There the most expensive part is the structure relaxation with DFT with up to two node-weeks of calculation time - this is not efficient to parallelize further, the electronic system is too small for that. The DFT calculation costs scale with at least $O(N^2)$ [63] and more generally $O(N^3)$ with N being the number of electrons, the parallelization efficiency is more difficult to figure out - the easiest way is trying it out. The parallelization efficiency for doubling the number p of processing units (cores) with respect to the time T_p it takes to calculate is

$$\eta_{2p} = \frac{T_p}{T_{2p} \cdot 2} \,.$$

In the case of the contacts tested, this efficiency drops below 50% around 20 cores, meaning that it is more efficient to calculate another sample instead of using these processors to accelerate a single sample. The calculation of the force constants and the electron-vibration coupling is in comparison quite cheap at 1-2 node-days. The NEGF code I wrote takes about $15 - 30$ min without significant parallelization. The expensive part of that is the construction of the surface Green's function for a specific energy, taking around 10 min - this surface Green's function can be reused for all contacts with the same fixed lead structure, but has to be recalculated for each energy.

Could one accelerate the relaxation?

The problem is not the structure calculation by itself, but that in combination with the difficult electronic structure of metal contacts. Quite often the density functional itself will not converge or take quite a lot of time to do so. These convergence problems are most likely due to the complicated interaction of extended and local electron wave functions in metallic contacts.

To accelerate the structure relaxation, already relaxed structures were used as often as possible, but this reduces the quality of the sample - not just because the samples are correlated through reusage, but also because the samples created in this manner are conditional on "converges well in DFT" instead of truly independent samples.

Wouldn't plane waves be much better for metallic contacts?

Plane waves are the standard basis to use for metallic systems. They produce very accurate values for most bulk parameters (electronic band structure, phonons, electron-vibration coupling) and can deal very well with the extended wave functions of these systems. Setting the periodic boundary conditions far away from the structure in question also allows one to simulate the electronic structure of clusters very nicely. Such far away boundary conditions, however lead to huge basis sets to simulate local structures, which is one strike against them.

This periodicity of the underlying basis set is indeed the problem. The structures in the contact are not periodic - the experimental studies showed that the local atomic and electronic structures are the important contributor to the transport properties of an atomic contact - trying to reconstruct that with a basis set not suited to it is possible and may be interesting as a comparison, but did not seem like a good idea with the limited resources of time available.

Why not use tight-binding calculations?

Tight-binding calculations and parameters are fitted to bulk electronic band structures. This gives good results for the electronic transport through metallic contacts. This focus on bulk electronic properties leaves tight-binding calculations not suitable for the calculations of the atomic properties like structures and vibration frequencies, and even worse for the electron-vibration coupling. The bad approximation of the electron-phonon interaction leaves tight-binding unsuitable for the calculation of current-induced forces.

This is only exacerbated in structures dominated by surface effects instead of bulk effects, like the atomic contacts investigated in this thesis. The success of tight-binding calculations for the electronic transport through metal contacts may be due to proximity effects - the bulk electronic wave-function extends far enough into the contacts to dominated the transport properties.

Basis sets used

The basis sets used in the DFT calculation have shown quite some influence on the results of the calculations. This was especially strong in lead, where the runaway-voltage dropped by a factor of 2 when changing from def-SVP to

def-TZVP. Because of this the basis sets were re-checked for all metals.
The choice comes down to def-SVP [47], def-TZVP [48], def2-SVP and def2-TZVP [64, 65]. def-QZVP has been tried for a sample, but the calculation costs are even more prohibitive. In general the TZVP bases are better than the SVP bases, but also cost more to calculate. The def2 bases are updates, but also somewhat more expensive. The def2 basis often have the problem of also including f-shell orbitals, which had not yet been implemented into the transport calculations.
The guide for the ORCA-Input library recommends at least a TZVP basis for most calculations involving structures [66]. For gold, the best behaving and most tested material for atomic transport calculations, def-SVP is good enough. This may be due to the simple isotropic electronic structure of gold as an s-conductor. The transport properties like transmission and runaway-voltage are constant with the different bases of gold (def-SVP, def-TZVP, def2-SVP) that were tested.
For aluminum as a p-conductor with corresponding anisotropic wave-functions def-TZVP is the choice for production runs.
For lead, also a p-conductor, trials with def-SVP produced structures that looked good, and transmissions in the right ranges. But there appeared two problems in derived properties: The runaway-voltages were a factor of $2-3$ above experimental switching voltages and (worse) the conductance on the plateaus was not constant, but behaved in linear dependence on the distance - something not observed in experiment. Therefore def-TZVP, which does not exhibit such a behavior, was the basis set of choice for lead calculations.
For copper first test calculations ran with def-SVP and checks with def-TZVP are still ongoing.

Why are there no simulations of dynamics?

While time-dependent density functional theory packages exists, these methods do not feasibly span the time scale separation of around a factor 1000 between electrons and atoms, especially with the rare nature of switching events. Since most of the time the system is supposed to move in a stable minimum and the interaction of that motion with the non-equilibrium electrons is what is calculated as current-induced forces, approximating the stability of contacts and direction of switching from those calculations were deemed a reasonable first approach.

The phononic frequencies are in the range of $2-40\,\mathrm{meV}$, which conforms to ranges of $0.2-8\,\mathrm{THz}$, or time periods around single digit picoseconds. These picoseconds are also the time-scales of the switching process itself. With typical time-resolved electronic structure calculations the time-steps are in the range of atto- to femto-seconds, which allows one to simulate overall time-scales of pico- to, in extreme cases, nanoseconds.
In experimental investigations the switching voltages are resolved in hundreds of nanoseconds to microseconds, which can be assumed as the time the electronic system needs to pump the atomic system to induce a conformation change. Although this time could be shortened with appropriately high voltages, this still leaves unpleasantly large time-scales for explorative time-resolved electronic calculations.

Appendix C

Phonons and electron-vibration coupling

This appendix chapter deals with some of the more technical aspects of the simulation and modeling that do not help the basic argument. A large part is the electron-vibration coupling, which is assumed to provide reasonable values but could be checked further.

Density of states (DOS)

The wide range of different atomic structures and the properties derived from it, like electron structure, atomic vibration, and electron-vibration coupling, are difficult to present. Most of these properties are defined in complicated matrix elements in the basis used in the density-functional calculation. As an example the dynamical matrix of the force-constants is given by

$$M_{\alpha\beta}^{ij} = \left\langle i \left| \frac{\partial^2 H}{\partial x_\alpha \partial x_\beta} \right| j \right\rangle$$

where α and β are combined indices denoting a specific atom of $1..n$ and a direction of x, y, z; and i and j are indices running through the basis set $|i\rangle$ used to describe the electronic system. These matrices are difficult to represent. One simplification is summing over the electron basis and get a matrix only in the atomic coordinates. In the case presented above this is the dynamical matrix

$$M_{\alpha\beta} = \sum_{ij} M_{\alpha\beta}^{ij} \,.$$

For this matrix the spectrum of eigenvalues can be calculated. Since the dynamical matrix is symmetric, the eigenvalues will be real and can be plotted in a histogram. For general matrices with complex eigenvalues separate histograms for the real and complex part of the matrix are useful. This method is used to investigate the matrix in the Langevin equation 2.2 for $V = 0$. Its eigenvalues are complex with the real part corresponding to the frequency of the vibrations and the imaginary part to the electronic friction.

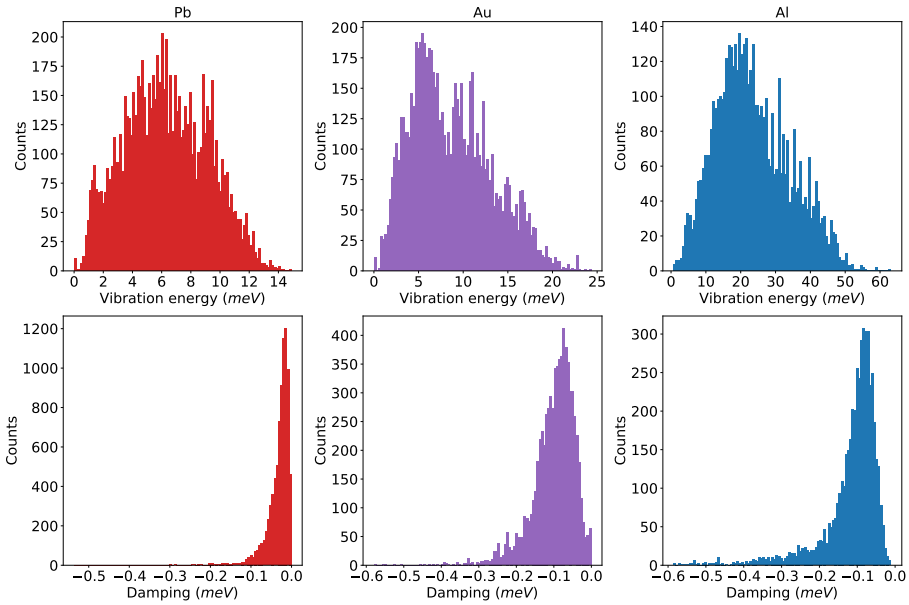

Figure C.1: The density of states of the vibrations (top) and the damping (bottom) of the three simulated metals.

Simulated vibration and damping density of states

Fig. C.1 presents the DOS of the real and imaginary part of the dynamical matrix, corresponding to the phonon energies and their damping. The phonon energies agree with experimental and bulk simulation data. The Debye energies of these metals are for Al $\approx 36\,\mathrm{meV}$, for Au $\approx 13.5\,\mathrm{meV}$ and for Pb $\approx 9\,\mathrm{meV}$ (experimental values from Ref. [67]). The damping - and connected with that the electron-vibration coupling - has not been measured directly. For all three metals there is a prominent peak and a long tail. The damping peak is around $40\,\mu\mathrm{eV}$ for lead and $80\,\mu\mathrm{eV}$ for gold and aluminum. The distribution is broader for gold and aluminum. Furthermore aluminum has a tail of highly dampened modes reaching up to $400\,\mu\mathrm{eV}$. From theoretical considerations and experimental measurements one would expect a electron-vibration coupling order of Au $<$ Al $<$ Pb. This is not reproduced in the calculated damping, where the strength of the maximal damping is in the reversed order Pb $<$ Al $<$ Au. If that is due to a problem in the calculation of the electron-vibration coupling or the current-induced forces calculation, one could investigate by plotting the spectrum for the uncoupled electron-vibration coupling matrix. The wide-band approximation itself has no influence on the spectrum shown, since that is without any bias voltage. What could be interesting to check is the effect of the position of the Fermi level on the damping.

Electron-vibration coupling

The electron-vibration coupling is the only fundamental calculated property that has not been checked for correctness in comparison to experimental values.

Even though it was assumed correct-as-is through its successful publication and integration into a commercial program suite [4], a discussion of its influence and possible checks of its validity are in order.

Are all the material-dependent effects due to errors in the electron-vibration coupling?

There are quite large differences in the calculated threshold voltage between different materials and different bases for the same material. Could that also explain the difference between the values of the simulated and experimental switching voltages for aluminum?

For all three materials the electronic structure as tested with conductivity agrees with experimental values, same for the phonons which agree with point-contact spectroscopy. The electron-vibration coupling is in that sense the only relevant parameter in the calulations that is difficult to verify experimentally. The variation in the structure itself has a significant influence, often larger than any other effect. Only statistics help to identify and differentiate the influences.

That the difference in runaway voltages for aluminum results alone from the difference of Gaussian and plane wave basis sets would mean a factor four alone through that, which is not reproduced in the other metals. The DFT simulation of aluminum works very well (all-electron possible) and the superconductivity calculations conform to experimental results.

One can check the electron-vibration coupling through the equivalence to some formalism within the Bardeen Cooper Schrieffer (BCS) theory of superconductivity [68], which also uses electron-vibration coupling directly. This has not yet been used to verify the electron-vibration coupling calculations of TURBOMOLE themselves, but an outline of it is given in the next subsection.

Checking the electron-vibration coupling

The electron-vibration coupling could be compared with inelastic electron transmission spectroscopy (IETS) measurements - at least in molecular conductors where the coupling between the electronic and the vibration system is weak enough for the vibration to appear as steps in the differential conductance or peaks in the second derivative of the conductance d^2I/dV^2. In metals the electron-density is higher and the electron-vibration coupling tends to be somewhat stronger, so the IETS results are often very broad and washed out. This supports the wide-band assumption used in the derivation of the current-induced forces, but also reduces its usefulness in checking the validity of the electron-vibration calculations.

There would be another way around these problems of verifying the electron-vibration coupling experimentally using the BCS theory of superconductivity. There the electron-vibration interaction is used to induce an attractive interaction between electrons, which allows those cooper pairs to condense into a Bose-Einstein condensate of macroscopic wave functions. In this formalism the electron-vibration coupling is defined very similarly to the way it is used in derivation of the current-induced forces.

This current section explains how that approach works following the manuscript of Heid [68]. It also explains the role of the electron-vibration coupling, how it is calculated, and for what it is used.

The electron-vibration coupling gives the scattering between electrons at the fermi energy and phonons. Typically it is formulated in the phonon basis - which is the natural basis for bulk vibrations.

In the BCS theory of superconductivity the electron-vibration coupling is introduced similarly to the version used here:

$$\begin{aligned} H = & \quad H_e + H_{ph} + H_{e-ph} \\ = & \quad \textstyle\sum_i \epsilon_i c_i^\dagger c_i + \sum_j \omega_j (b_j^\dagger b_j + \frac{1}{2}) + \sum_{ii'j} g_{ii'j} c_{i'}^\dagger c_i (b_j + b_{-j}^\dagger) \,, \end{aligned}$$

with c_i being the creation (annihilation) operators for electrons in a state denoted by i being an index over the states of the electrons, typically denoted by energy, spin and wave-vector (direction).
b_j is the same for the quanta of the atomic vibrations with frequency ω_j and the index j also containing the direction - not the spin, since vibration are bosons. The last sum describes the electron-vibration interaction of an electron going from state i' to state i while the energy and momentum for that change goes into the creation of a phonon in state j. The value $g_{ii'j}$ describes the probability amplitude of that specific scattering process (two-particle process) and is calculated by

$$g_{ii'j} = \sum_\alpha A_\alpha^j \left\langle i' \right| \frac{\partial V}{\partial r_\alpha} \left| i \right\rangle \ .$$

Here α denotes a specific atom and direction (or phonon mode) and A_α^j is the eigenvector in this direction. In the phonon basis A_α^j is often normalized by the mass and frequency through

$$A_\alpha^j = \frac{\vec{e}_\alpha(j)}{\sqrt{2M_\alpha \omega_j}} \ .$$

This can be used to derive an electron self-energy, whose imaginary part corresponds to a density of states

$$\begin{aligned} \mathrm{Im}\Sigma_{ep}(k,\epsilon) = -\pi \frac{1}{N_q} \sum_{k',q} |g_{k',k}^q|^2 [& \delta(\epsilon - \epsilon_{k'} + \omega_q)(b(\omega_q) + f(\epsilon'_k)) \\ & + \delta(\epsilon - \epsilon_{k'} - \omega_q)(b(\omega_q) + 1 - f(\epsilon'_k))] \,, \end{aligned}$$

which can be rewritten by introducing two spectral functions describing the probability of electron-phonon scattering events

$$\alpha^2 F_k^\pm(\epsilon,\omega) = \frac{1}{N_q} \sum_q \delta(\omega - \omega_q) \sum_{k'} |g_{k',k}^q|^2 \delta(\epsilon - \epsilon_{k'} \pm \omega_q) \ .$$

The quasi-elastic approximation drops the phonon-energy in the electronic delta-function, because that scale is usually far below the electronic scales. This also removes the $\pm$ in the probabilities $\alpha^2 F_k^\pm \approx \alpha^2 F_k$ with

$$\alpha^2 F_k(\epsilon,\omega) = \frac{1}{N_q} \sum_q \delta(\omega - \omega_q) \sum_{k'} |g_{k',k}^q|^2 \delta(\epsilon - \epsilon_{k'}) \ .$$

This can be integrated to the dimensionless coupling parameter

$$\lambda_k = 2 \int d\omega \frac{\alpha^2 F_k(\epsilon,\omega)}{\omega} \ ,$$

which can be further summed into an isotropic coupling constant

$$\lambda = \sum_k \omega_k \lambda_k \ .$$

This coupling constant can be used directly to calculate the critical temperature of the superconductivity phase transition and has been calculated for bulk materials in DFT codes fitting to those experimental values. It would probably be the most direct comparison and check for the correctness of the electron-vibration calculations in TURBOMOLE.

Appendix D

Transport through ferrocene

Parallel to the work in the main part of the thesis, some investigation was done on the electronic transport properties of ferrocene ($Fe(C_5H_5)_2$), connected to metallic gold leads through either amine or thiol sidegroups. This lead to a publication on the transport properties through ferrocene-diamine (FDA) [69] explained by a single-level model. For ferrocene-dithiol (FDT) the experiments found an interesting kink in the IV-curves [70](unpublished). Simulations of the molecule found an anti-resonance in the transmission sometimes appearing with larger distances of the contacts. Further simulations showed a change in the symmetry of the wave functions of the molecule with rotation. Theoretical investigations showed that this anti-resonance can not explain the exact structure of the experimental kink observed, since the quantum-interference can not produce the dip-peak signature of the experimental IV-curves.

The single level model as presented in chapter 13 of Ref. [3] gives an energy and voltage-dependent transmission of a single orbital of energy ϵ_0 as

$$T(E,V) = \frac{4\Gamma_L\Gamma_R}{[E-\epsilon_0(V)]^2 + [\Gamma_L+\Gamma_R]^2} \ ,$$

with $\Gamma_{L,R}$ being the coupling to the left and right lead respectively and ϵ_0 being the position of the single level. The transmission in that model is a Lorentzian peak with its width given by the strength of the couplings and its height ≤ 1 given by the ratio of the couplings. Under symmetric coupling $\Gamma = \Gamma_L = \Gamma_R$ this model gives two parameters in the level position ϵ_0 and the coupling to the leads Γ. The values of these parameters can be easily extracted from experimental measurements and simulations. The behavior of those parameters with changes of molecule and experimental setup, e.g. pull distance, can be investigated, and it is possible to show that the coupling to the leads is the primary determiner of changes in transmission values with only small changes of ϵ_0.

This approach is different from metallic contacts, where one has a many states around the Fermi energy. Most molecules have only limited number of electronic states (orbitals) around the fermi energy and quite often there exists a band gap. The conductance properties are then determined mostly be the behavior of the highest occupied and lowest unoccupied molecular orbitals (HOMO and LUMO).

Experimental questions and simulation setup

The initial data were measurements of the electronic transport properties of ferrocene $Fe(C_5H_5)_2$ in mechanically controlled break junction (MCBJ) experiments. These experiments sometimes showed an interesting feature in the transport properties - a kink in the IV curves at around 50 mV, exhibiting a dip-peak signature with increasing voltage.

This feature appeared in about 25% of measurements on FDT, and its position in voltage increases with the baseline conductance of the contact from $25 - 30\,\mathrm{mV}$ in the $0.5\,G_0$-ranges to 120 mV at $0.1\,G_0$ [70](unpublished). The feature did not appear for FDA. The amine ($-NH_2$) and thiol (-SH) groups are the anchoring groups binding the ferrocene to the metals. The thiol-metal bonds are considerably stronger than the amine-metal bonds.

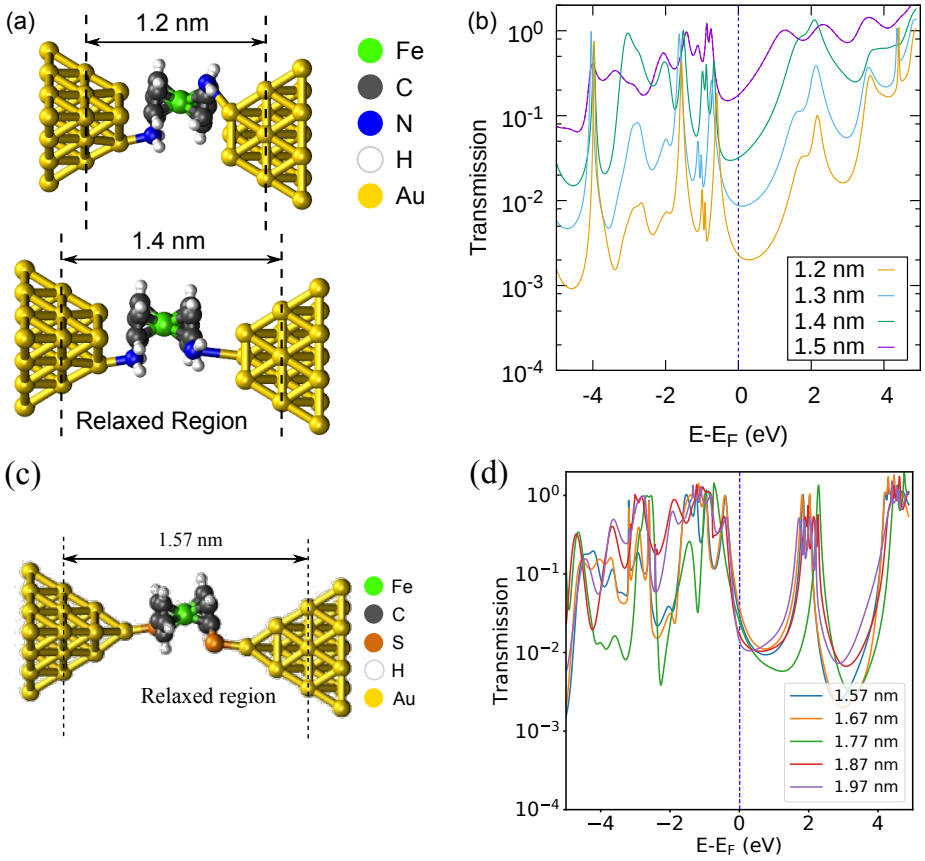

Figure D.1: This figure shows sample geometries (a+c) and transmission curves (b+d) for the investigated ferrocene-diamine (a+b) [69] and ferrocene-dithiol molecules (c+d) [70](unpublished). The transmission of FDT is less dependent on distance and generally higher.

To investigate the measured *IV* curves, FDA and FDT molecules in between gold leads of different structure and distance were simulated and the electric transmission was calculated. Some samples of that are shown in Fig.

D.1. FDA is very well behaved and fits well to the single-level model [69] with slight changes in level position and strong changes in coupling with distance (b). In comparison, the transmission at the Fermi energy for FDT has a reduced dependence on distance (d). For the example in Fig. D.1(c+d) the coupling is nearly independent of distance and the level positions change only slightly. Additionally, for some configurations of FDT a weak anti-resonance feature in the transport was found in simulations, see Fig. D.2.

Quantum interference

For an anti-resonance feature in the transmission two transmitting electron wave functions of a contact have to interfere destructively. Such an effect can sometimes be seen in molecular conductors, where the standard picture is investigating the symmetry and signs of the wave-functions (molecular orbitals) at the contacting end-points, which would be the sulfur or nitrogen in our example. The sign alone is not enough however, the local orbitals also need to have a significant overlap to interfere either constructively or destructively.

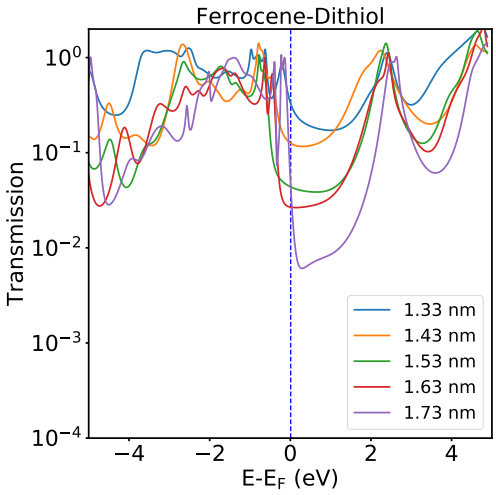

Figure D.2: Shown are the transmissions for an FDT contact exhibiting an anti-resonance for a distance of 1.73 nm.

Antiresonance in FDT

The anti-resonance appears only in very few simulation setups, e.g. Fig. D.2, typically connected with large distances of the leads. This larger distance is also connected with a rotation of the C_5 rings against each other. The anti-resonance analysis with respect to the orbitals proved not illuminating. To investigate this in depth a smaller version of that molecule in contact with only one gold atom on each side was set up.

Simple model

Since a contact with only one gold atom is too small to investigate in transport calculations, only the position and form of the molecular orbitals could be investigated in simulation. The behavior of the molecular orbitals with respect to angle is shown in Fig. D.3(a) and some examples of the form of the molecular orbitals are shown in (b) and (c). The highest occupied molecular orbital changes the symmetry of its wave-function between 90 and 180°, same as in the larger contact.

The transmission heat map in fig. D.3(a) is calculated in a toy model showing the possible effect of such a change of parity. In the toy model the true

overlap of the orbitals is neglected, i.e. the orbitals in D.3(b+c) would be orthogonal on the sulfur, so no interference would be expected. Ignoring that, a change of sign with angle of the HOMO alone at 135° can produce an antiresonance in the toy model. The position of the antiresonance is dependent on the respective coupling strength of the orbitals involved. For ferrocene the conducting unoccupied orbitals are coupled more strongly than the occupied orbitals with a broader transmission peak.

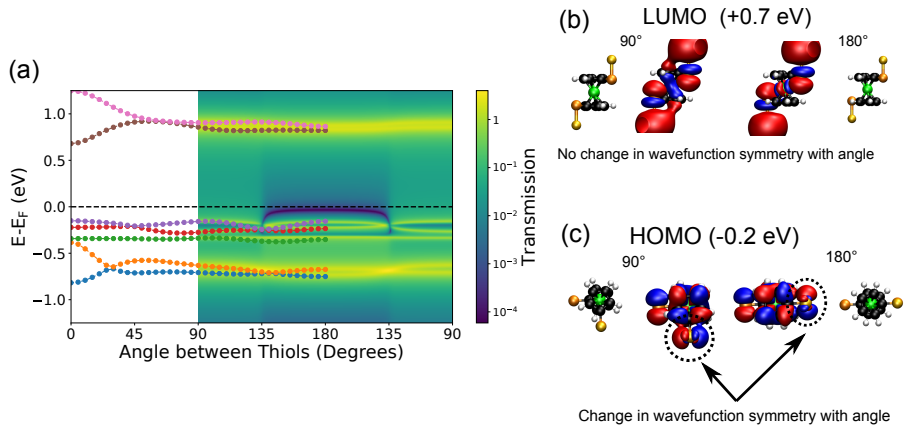

Figure D.3: This figure shows investigations of the anti-resonance in ferrocene-dithiol connected to a single gold atom. The lines in subfigure (a) shows molecular orbitals HOMO-4 through LUMO+1 over the angle between thiols. Further shown in (a) are transmissions calculated in a toy model, where an anti-resonance appears in the HOMO-LUMO gap by changing the sign of the HOMO. In (b+c) the wave functions for the LUMO and HOMO are shown for angles 90 and 180 degrees.

According to the supplementary material of [71] the antiresonance due to quantum-interference is explained this way: The transmission through a molecule is

$$\tau(E) = \frac{(2\pi\gamma^2)^2}{2} G^+(E) G^-(E) \rho_L(E) \rho_R(E) \ ,$$

with γ being the transfer integral between the endpoints of the molecule and the metals. $\rho_{L/R}(E)$ are the local densities of states for the leads and $G^{+/-}(E)$ the retarded/advanced Green's functions of the molecule. The zeroth order Green's functions of the molecule are given by

$$G^{(0)\pm}(E) = \sum_k \frac{|\phi_k\rangle \langle\phi_k|}{E - \epsilon_k \pm i\eta}$$

in the appropriate basis set ϕ_k of the electronic states of energy ϵ_k for the molecule. Now the transmission is gained in a first order inclusion of the coupling of the endpoints. For this we project on the endpoints l and r that couple to the leads with $\gamma \approx \Gamma_{L/R}$ and calculate the overlap of the overall basis with the local function $\langle l/r|$ of the endpoints

$$c_{l/r,k} = \langle l/r|\phi_k\rangle$$

in order to get the zeroth order Green's function in the local basis of the end points

$$G_{LR}^{(0)+} = \sum_k \frac{c_{L,k} c_{k,R}}{E - \epsilon_k + i\eta} \, .$$

Now the Green's function between two niveaus $\epsilon_1 < \epsilon_2$ is dominated by the terms

$$\frac{c_{L,1} c_{R,1}^*}{E - \epsilon_1 + i\eta} + \frac{c_{L,2} c_{R,2}^*}{E - \epsilon_2 + i\eta} \, .$$

At energies $\epsilon_1 < E < \epsilon_2$ the denominators have opposing signs. If the products in the numerators have the same sign, there is an energy E between the two levels at which the terms cancel each other out. This is seen as an anti resonance in the transmission through the molecule

$$T = |G_{LR}^{(0)+}|^2 \, .$$

For the toy-model we just calculate that transmission with parameters extracted from the simulations in fig. D.3(a). The coupling parameters are set in the order of $\eta \approx |c_{L,k} c_{R,k}^*| \approx 20\,\mathrm{meV}$ to fit approximately to the transmission values of the contact calculations. The sign of the product $c_{L,k} c_{R,k}^*$ as well as the energy position were set to change with the angle θ as a broadened step-function around $90^\circ = \pi/2$ through

$$c_{L,k} c_{R,k}^* = \frac{2}{\pi} \mathrm{arctan}(b(\theta - \pi/2)) \, ,$$

which is a shifted arcus tangens with a scaling factor b. In the transmissions calculated in the toy model, an anti-resonance appears in the HOMO-LUMO gap by changing the sign of the HOMO. Integrating this anti-resonance does not give rise to an IV feature as observed in experiment, because the peaking back of the transmission is missing and because the anti-resonance is very likely to be lost in thermal excitation.

Discussion

The investigation of transport through ferrocene in the single level model is straightforward and showed success and applicability as well as good agreement of simulations and experiments for most situations. The feature of interest on the other hand, the kink in the IV curve of FDT, remained elusive.

Although something resembling an anti-resonance was found for the transmission curves gained from simulations of FDT, they could not be pinned to certain molecular orbitals. Even if that connection would be made, the explanation of the kink with its dip-peak structure is still missing. In typical Fano resonance situations a resonance and an anti-resonance are paired [3]. This could explain a dip-peak structure. Other investigations [72] indicate that the Fano resonance is often dominated by the resonance part, which would prevent seeing a feature. A problem connected to that is also the high temperature of 300 K used in experiment compared to the width of the measured feature of less than 30 meV. This similarity of energy scales washes out hypothetical Fano resonance features, in which case the resonance should dominate the behavior. Furthermore, no localized orbital was found in simulations, only the

anti-resonance as presented in the last section. Also missing is an explanation why this feature appears in the dithiol case and not in the diamine one.

Overall, neither the feature, nor an explanation of it, could be found in the simulations done. For future work these simulations should be checked again and redone. Especially an in-depth investigation of the effect of rotation on the electronic structure of ferrocene-dithiol seems promising.

Bibliography

[1]R. Hoffmann-Vogel, "Electromigration and the structure of metallic nanocontacts", Applied Physics Reviews **4**, 031302 (2017).

[2]R. S. Sorbello, "Theory of Electromigration", in *Solid State Physics: Advances in Research and Applications*, Vol. 51, edited by H. Ehrenreich and F. Spaepen, Solid State Physics (Academic Press, 1998), pp. 159–231.

[3]J. C. Cuevas and E. Scheer, *Molecular Electronics: An Introduction to Theory and Experiment* (World Scientific, 2012) Chap. Coherent transport through molecular junctions I: Basic concepts, pp. 357–390.

[4]M. Bürkle, J. K. Viljas, T. J. Hellmuth, E. Scheer, F. Weigend, G. Schön, and F. Pauly, "Influence of vibrations on electron transport through nanoscale contacts", Phys. Status Solidi B **250**, 2468–2480 (2013).

[5]J.-T. Lü, M. Brandbyge, and P. Hedegård, "Blowing the Fuse: Berry's Phase and Runaway Vibrations in Molecular Conductors", Nano Letters **10**, 1657–1663 (2010).

[6]T. N. Todorov, D. Dundas, J.-T. Lü, M. Brandbyge, and P. Hedegård, "Current-induced forces: a simple derivation", European Journal of Physics **35**, 065004 (2014).

[7]J.-T. Lü, B.-Z. Hu, P. Hedegård, and M. Brandbyge, "Semi-classical generalized Langevin equation for equilibrium and nonequilibrium molecular dynamics simulation", Progress in Surface Science **94**, 21–40 (2019).

[8]M. Ring, D. Weber, P. Haiber, F. Pauly, P. Nielaba, and E. Scheer, "Voltage-Induced Rearrangements in Atomic-Size Contacts", Nano Letters **20**, 5773–5778 (2020).

[9]C. J. Muller, J. M. van Ruitenbeek, and L. J. de Jongh, "Experimental Observation of the Transition from Weak Link to Tunnel Junction", Physica C: Superconductivity **191**, 485–504 (1992).

[10]J. M. Krans, C. J. Muller, I. K. Yanson, T. C. M. Govaert, R. Hesper, and J. van Ruitenbeek, "One-Atom Point Contacts", Physical Review B **48**, 14721–14724 (1993).

[11]P. S. Ho and T. Kwok, "Electromigration in metals", Reports on Progress in Physics **52**, 301–348 (1989).

[12]D. G. Pierce and D. G. Brusius, "Electromigration: A review", Microelectronics Reliability **37**, 1053–1072 (1997).

[13]C. Schirm, "Einfluss hoher Ströme auf atomare Kontakte", PhD thesis (Universität Konstanz, Konstanz, 2009).

[14]M. Aono and T. Hasegawa, "The Atomic Switch", Proceedings of the IEEE **98**, 2228–2236 (2010).

[15]M. Matt, "Theoretical study of the charge and energy transport in metallic atomic-size contacts", PhD thesis (Universität Konstanz, Konstanz, 2017).

[16]T. Frederiksen, M. Paulsson, M. Brandbyge, and A.-P. Jauho, "Inelastic transport theory from first principles: Methodology and application to nanoscale devices", Physical Review B **75**, 205413 (2007).

[17]L. Cui, W. Jeong, S. Hur, M. Matt, J. C. Klöckner, F. Pauly, P. Nielaba, J. C. Cuevas, E. Meyhofer, and P. Reddy, "Quantized thermal transport in single-atom junctions", Science **355**, 1192–1195 (2017).

[18]J. C. Klöckner, M. Matt, P. Nielaba, F. Pauly, and J. C. Cuevas, "Thermal conductance of metallic atomic-size contacts: Phonon transport and Wiedemann-Franz law", Phys. Rev. B **96**, 205405 (2017).

[19]D. Dundas, E. J. McEniry, and T. N. Todorov, "Current-driven atomic waterwheels", Nature Nanotechnology **4**, 99–102 (2009).

[20]J.-T. Lü, R. B. Christensen, J.-S. Wang, P. Hedegård, and M. Brandbyge, "Current-Induced Forces and Hot Spots in Biased Nanojunctions", Physical Review Letters **114**, 096801 (2015).

[21]J. M. van Ruitenbeek, A. Alvarez, I. Piñeyro, C. Grahmann, P. Joyez, M. H. Devoret, D. Esteve, and C. Urbina, "Adjustable Nanofabricated Atomic Size Contacts", Review of Scientific Instruments **67**, 108–111 (1996).

[22]N. Agraït, J. G. Rodrigo, and S. Vieira, "Conductance Steps and Quantization in Atomic-Size Contacts", Physical Review B **47**, 12345–12348 (1993).

[23]N. Agraït, A. L. Yeyati, and J. M. van Ruitenbeek, "Quantum properties of atomic-sized conductors", Physics Reports **377**, 81–279 (2003).

[24]R. Landauer, "Spatial Variation of Currents and Fields Due to Localized Scatterers in Metallic Conduction", IBM Journal of Research and Development **1**, 223–231 (1957).

[25]G. Binnig, H. Rohrer, C. Gerber, and E. Weibel, "Surface Studies by Scanning Tunneling Microscopy", Physical Review Letters **49**, 57–61 (1982).

[26]C. Schirm, M. Matt, F. Pauly, J. C. Cuevas, P. Nielaba, and E. Scheer, "A current-driven single-atom memory", Nature Nanotechnology **8**, 645–648 (2013).

[27]D. Weber, "Current-Induced Switching in Superconducting Break Junctions", PhD thesis (Universität Konstanz, Konstanz, 2018).

[28]G. Binnig and H. Rohrer, "In touch with atoms", Reviews of Modern Physics **71**, 324–330 (1999).

[29]N. Bode, S. V. Kusminskiy, R. Egger, and F. von Oppen, "Scattering Theory of Current-Induced Forces in Mesoscopic Systems", Physical Review Letters **107**, 036804 (2011).

[30]N. Bode, S. V. Kusminskiy, R. Egger, and F. von Oppen, "Current-induced forces in mesoscopic systems: A scattering-matrix approach", Beilstein Journal of Nanotechnology **3**, 144–162 (2012).

[31]W. Dou and J. E. Subotnik, "Perspective: How to understand electronic friction", The Journal of Chemical Physics **148**, 230901 (2018).

[32]M. Head-Gordon and J. C. Tully, "Molecular dynamics with electronic frictions", The Journal of Chemical Physics **103**, 10137–10145 (1995).

[33]M. Bai, C. S. Cucinotta, Z. Jiang, H. Wang, Y. Wang, I. Rungger, S. Sanvito, and S. Hou, "Current-induced phonon renormalization in molecular junctions", Physical Review B **94**, 035411 (2016).

[34]M. Di Ventra, *Electrical Transport in Nanoscale Systems* (Cambridge University Press, 2008).

[35]R. Kubo, "The fluctuation-dissipation theorem", Reports on Progress in Physics **29**, 255–284 (1966).

[36]F. Tisseur and K. Meerbergen, "The Quadratic Eigenvalue Problem", SIAM Review **43**, 235–286 (2001).

[37]E. Scheer, P. Joyez, D. Esteve, C. Urbina, and M. H. Devoret, "Conduction Channel Transmissions of Atomic-Size Aluminum Contacts", Physical Review Letters **78**, 3535–3538 (1997).

[38]E. Scheer, J. C. Cuevas, A. Levy Yeyati, A. Martín-Rodero, P. Joyez, M. H. Devoret, D. Esteve, and C. Urbina, "Conduction channels of superconducting quantum point contacts", Physica B: Condensed Matter **280**, 425–431 (2000).

[39]E. Scheer, N. Agraït, J. C. Cuevas, A. Levy Yeyati, B. Ludoph, A. Martín-Rodero, G. Rubio Bollinger, J. M. van Ruitenbeek, and C. Urbina, "The Signature of Chemical Valence in the Electrical Conduction through a Single-Atom Contact", Nature **394**, 154–157 (1998).

[40]E. Scheer, W. Belzig, Y. Naveh, M. H. Devoret, D. Esteve, and C. Urbina, "Proximity Effect and Multiple Andreev Reflections in Gold Atomic Contacts", en, Physical Review Letters **86**, 284–287 (2001).

[41]F. Pauly, "Phase-coherent electron transport thorugh metallic atomic-sized contacts and organic molecules", PhD thesis (TH Karlsruhe, 2007).

[42]S. Plimpton, "Fast Parallel Algorithms for Short-Range Molecular Dynamics", Journal of Computational Physics **117**, 1–19 (1995).

[43]M. S. Daw and M. I. Baskes, "Embedded-atom method: Derivation and application to impurities, surfaces, and other defects in metals", Physical Review B **29**, 6443–6453 (1984).

[44]H. W. Sheng, M. J. Kramer, A. Cadien, T. Fujita, and M. W. Chen, "Highly optimized embedded-atom-method potentials for fourteen fcc metals", Physical Review B **83**, 134118 (2011).

[45]*TURBOMOLE V7.0 2015, a development of University of Karlsruhe and Forschungszentrum Karlsruhe GmbH, 1989-2007, TURBOMOLE GmbH, since 2007; available from*
`http://www.turbomole.com`.

[46]J. P. Perdew, M. Ernzerhof, and K. Burke, "Rationale for mixing exact exchange with density functional approximations", The Journal of Chemical Physics **105**, 9982–9985 (1996).

[47]A. Schäfer, H. Horn, and R. Ahlrichs, "Fully optimized contracted Gaussian basis sets for atoms Li to Kr", The Journal of Chemical Physics **97**, 2571–2577 (1992).

[48]A. Schäfer, C. Huber, and R. Ahlrichs, "Fully optimized contracted Gaussian basis sets of triple zeta valence quality for atoms Li to Kr", The Journal of Chemical Physics **100**, 5829–5835 (1994).

[49]M. Frei, S. V. Aradhya, M. Koentopp, M. S. Hybertsen, and L. Venkataraman, "Mechanics and Chemistry: Single Molecule Bond Rupture Forces Correlate with Molecular Backbone Structure", Nano Letters **11**, 1518–1523 (2011).

[50]D. Weber and E. Scheer, "Superconducting Properties of Lithographic Lead Break Junctions", Nanotechnology **29**, 045703 (2017).

[51]A. I. Yanson and J. M. van Ruitenbeek, "Do Histograms Constitute a Proof for Conductance Quantization?", Physical Review Letters **79**, 2157–2157 (1997).

[52]I. K. Yanson, O. I. Shklyarevskii, S. Csonka, H. van Kempen, S. Speller, A. I. Yanson, and J. M. van Ruitenbeek, "Atomic-Size Oscillations in Conductance Histograms for Gold Nanowires and the Influence of Work Hardening", Physical Review Letters **95**, 256806 (2005).

[53]I. K. Yanson, O. I. Shklyarevskii, J. M. van Ruitenbeek, and S. Speller, "Aluminum Nanowires: Influence of Work Hardening on Conductance Histograms", Physical Review B **77**, 033411 (2008).

[54]A. I. Yanson, G. R. Bollinger, H. E. van den Brom, N. Agraït, and J. M. van Ruitenbeek, "Formation and Manipulation of a Metallic Wire of Single Gold Atoms", en, Nature **395**, 783–785 (1998).

[55]G. Rubio Bollinger, C. de las Heras, E. Bascones, N. Agraït, F. Guinea, and S. Vieira, "Single-Channel Transmission in Gold One-Atom Contacts and Chains", Physical Review B **67**, 121407 (2003).

[56]R. Landauer, "The noise is the signal", Nature **392**, 658–659 (1998).

[57]D. Weber, M. Ring, F. Pauly, P. Nielaba, and E. Scheer, "Current-induced rearrangements in single-atomic contacts", 2019.

[58]E. Y. Wilner, H. Wang, G. Cohen, M. Thoss, and E. Rabani, "Bistability in a nonequilibrium quantum system with electron-phonon interactions", Physical Review B **88**, 045137 (2013).

[59]D. Weckbecker, P. B. Coto, and M. Thoss, "Controlling the Conductance of a Graphene–Molecule Nanojunction by Proton Transfer", Nano Letters **17**, 3341–3346 (2017).

[60]C. Hofmeister, P. B. Coto, and M. Thoss, "Controlling the conductance of molecular junctions using proton transfer reactions: A theoretical model study", The Journal of Chemical Physics **146**, 092317 (2017).

[61]A. Erpenbeck, C. Schinabeck, U. Peskin, and M. Thoss, "Current-induced bond rupture in single-molecule junctions", Physical Review B **97**, 235452 (2018).

[62]M. Thoss and F. Evers, "Perspective: Theory of quantum transport in molecular junctions", The Journal of Chemical Physics **148**, 030901 (2018).

[63]G. Kresse and J. Furthmüller, "Efficiency of ab-initio total energy calculations for metals and semiconductors using a plane-wave basis set", Computational Materials Science **6**, 15–50 (1996).

[64]F. Weigend and R. Ahlrichs, "Balanced basis sets of split valence, triple zeta valence and quadruple zeta valence quality for H to Rn: Design and assessment of accuracy", Physical Chemistry Chemical Physics **7**, 3297–3305 (2005).

[65]F. Weigend, "Accurate Coulomb-fitting basis sets for H to Rn", Physical Chemistry Chemical Physics **8**, 1057–1065 (2006).

[66]R. Bjornsson, T. Kraemer, M. Sparta, I. Schapiro, J. Barilone, and B. D. Rose, *Orca Input Library*, (Sept. 30, 2019) `https://sites.google.com/site/orcainputlibrary/basis-sets`.

[67]T. Ahmet, *The Specific Heat Of Matter At Low Temperatures* (Imperial College Press, London, UK, Jan. 13, 2003), 348 pp.

[68]R. Heid, "Electron-Phonon Coupling", in *The Physics of Correlated Insulators, Metals, and Superconductors*, Vol. 7, edited by E. Pavarini, E. Koch, R. Scalettar, and R. Martin, Schriften des Forschungszentrums Jülich Reihe Modeling and Simulation (Forschungszentrum Jülich GmbH, Jülich, Sept. 25, 2017).

[69]K. Kanthasamy, M. Ring, D. Nettelroth, C. Tegenkamp, H. Butenschön, F. Pauly, and H. Pfnür, "Charge Transport through Ferrocene 1,1'-Diamine Single-Molecule Junctions", Small **12**, 4849–4856 (2016).

[70]K. Kanthasamy, M. Ring, C. Tegenkamp, H. Butenschön, F. Pauly, and H. Pfnür, "Charge transport through ferrocene-1,1'-dithiol molecular junctions", unpublished.

[71]D. Stefani, K. J. Weiland, M. Skripnik, C. Hsu, M. L. Perrin, M. Mayor, F. Pauly, and H. S. J. van der Zant, "Large Conductance Variations in a Mechanosensitive Single-Molecule Junction", Nano Letters **18**, 5981–5988 (2018).

[72]C. J. Lambert, "Basic concepts of quantum interference and electron transport in single-molecule electronics", Chemical Society Reviews **44**, 875–888 (2015).

[73]D. Krause and P. Thörnig, "JURECA: Modular supercomputer at Jülich Supercomputing Centre", Journal of large-scale research facilities JLSRF **4**, `10.17815/jlsrf-4-121-1` (2018).

[74]Jülich Supercomputing Support, "JUWELS: Modular Tier-0/1 Supercomputer at the Jülich Supercomputing Centre", Journal of large-scale research facilities JLSRF **5**, `10.17815/jlsrf-5-171` (2019).

Acknowledgements

Finally I thank (in no particular order):

- Fabian Pauly and Peter Nielaba for the possibility to work on this topic.
- Manuel Matt and Fabian Müller for long years of sharing my office and listening to a fair share of my frustrations.
- David Weber and Elke Scheer for discussions and experimental data.
- Thomas Hellmuth, Jan Klöckner, Safa Golrokh Bahoosh and Werner Schosser for the transport code, samples and discussions and support regarding the extensions used in this thesis.
- Stefan Gerlach for technical support and keeping the computing cluster and my workstation running.
- For computing resources the SCC in Konstanz, JUSTUS in Ulm and JURECA [73] as well as JUWELS [74] in Jülich.
- The people of the Nielaba, Nowak and Pauly groups for putting up with me and my restless wandering and sudden desires for discussions and distractions.
- Andreas Donges, Fabian Müller and Simone Reinke for reading and correcting the many drafts of this thesis.
- My family for raising and supporting me.
- Simone Reinke, not just for being there - although that is already enough reason for thanks - but simply for everything.